THE AXONAL TRANSCRIPTOME OF HUMAN EMBRYONIC STEM CELL DERIVED NEURONS AND THE CELL AUTONOMOUS TRANSCRIPTIONAL RESPONSE TO AXON INJURY

Rebecca Lea Bigler

A dissertation submitted to the faculty at the University of North Carolina at Chapel Hill in partial fulfillment of the requirements for the degree of Doctor of Philosophy in the Curriculum in Genetics and Molecular Biology in the School of Medicine

Chapel Hill
2017

Approved by:

Stephen F. Crews

Todd J. Cohen

C. Ryan Miller

Patrick F. Sullivan

Anne M. Taylor

ABSTRACT

REBECCA LEA BIGLER: The Axonal Transcriptome of Human Embryonic Stem Cell Derived Neurons and the Cell Autonomous Transcriptional Response to Axon Injury
(Under the direction of Anne Marion Taylor)

During development and adulthood neurons rapidly react to isolated events sensed by and affecting the most distal portion of the neuron, the axon. Prompt local responses at axons to extracellular signaling molecules and mechanical contacts suggest limited immediate involvement of the neuron cell body. The delayed response of the cell bodies may include altered gene expression and mRNA trafficking, which may influence the availability of mRNA at distal axons. The primed axonal transcriptome is critical for the rapid and local responses influenced by local protein synthesis.

To establish the presence of mRNA within human axons and quantify the axonal transcriptome I evaluated human embryonic stem cell derived neurons (hESC-neurons) grown in axon-isolating microfluidic chambers. The hESC-neuron axonal transcriptome was significantly different from the somatic transcriptome suggesting functions within the axons that depend on local translation. The enriched functional categories within the axonal transcriptome of hESC-neurons were similar to those of primary rodent neurons demonstrating conservation of translation-dependent axonal functions, while features unique to hESC-neurons are also present. This evidence supports the use of hESC-neurons as a model system to further investigate mechanisms establishing and modifying the human axonal transcriptome and the function of local translation within human axons.

The axonal transcriptome encodes locally translated proteins required for axon injury signaling. Axon injury initiates a multi-phased injury response that begins locally at the injury site, is transmitted to the somata and eventually expands to other regions of the neural network. The structural and functional changes of the delayed injury response have been investigated *in vivo* but the molecular signaling of this response is poorly understood. I evaluated the effect of sparse direct axotomy to cultured primary rat neurons grown in two-compartment axon-isolating microfluidic chambers. Directly injured axons regenerated *in vitro* and axotomy did not affect culture viability but

did induce a delayed, persistent synaptic function change in the *in vitro* neural network, consistent with previously reported *in vivo* findings. This functional change was dependent on a transcriptional response generated within the first hour after injury. Gene expression 24 hours after axotomy in this model system showed similarities to gene expression 24 hours after *in vivo* injury and suggested expression of proteins that function at the synapse might mediate the synaptic changes. Our *in vitro* axotomy model system demonstrates significant similarities to *in vivo* model systems but greatly enhances our ability to investigate the transcription-dependent mechanisms of injury signaling within neurons.

This dissertation is dedicated in memory of Terra Bigler, January 11, 2002 - October 9, 2016, and Ellen Marianne Proctor, September 13, 1979 – April 13, 2017. They lived without being held back by fear. I miss you both more than words can convey. Thank you for welcoming me into your lives and I will forever be grateful for the love and support you gave me.

ACKNOWLEDGEMENTS

My thesis mentor, Dr. Anne M. Taylor, supported my interested and pursuits while guiding and focusing my efforts. As a scientist, businesswoman, wife, mother, daughter and sister she demonstrated balancing these diverse and sometimes conflicting aspects of a full life. She was deeply understanding when challenges in my life took me away from the lab and I will forever be grateful.

My colleagues in the lab, Dr. Tharkika Nagendran, Dr. Mark Niedringhaus, Dr. Kent Gordon and Dr. Joyce Kamande, engaged me in daily discussion to streamline our work, understand new topics and bring a little entertainment into the workplace. As a small group we frequently relied on a cooperative environment and it was a pleasure working with them

My many friends shared the ups and downs of graduated school and the last seven years with me. I would like to particularly acknowledge the support of Dr .Aleksandra Skrajna, Dr. Joy Meserve, Dr. Diana Chong, Dr. Esteban Terzo and Dr. Anna Cliffe.

I would like to thank my in-laws, Roy C. Bigler, III and Diana M. Bigler, who are always there when needed. To my brother-in-law, Rhett C. Bigler, thank you for making sure I didn't lose faith in the final dark hours.

My mother, Beatrice J. Baldwin, never made me stop asking 'Why?' She fostered my curiosity and made troubleshooting a game, which made work in the lab seem familiar. My dear sisters, Heather J. Ford and Ellen M. Proctor, helped mold me from my earliest days. They made sure I wasn't a delicate, proper little lady so I have a little streak of stubborn from Heather and a little streak of tough from Ellen, giving me a bit of what I needed to finish this degree.

My beloved 'T-dog', Terra Bigler, talked me into spending time outside each day to enjoy the fresh air, decompress and see the forest and the trees.

My daughter, Alexandra C. Bigler, challenges me to slow down and shows me that some of the greatest joys are in the simple moments of daily life.

My best friend and husband, Roy C. Bigler, IV, has supported me daily since we met. Without him by my side I would not have had the confidence to begin this degree. He has shared my many failures and eventual successes and his contributions to the completion of this body of work equal mine.

PREFACE

The majority of the work in Chapter 2 was previously published as a research article. The study was initiated by a former post-doctoral researcher Dr. Mark Niedringhaus who created an early version of Figure 2.1A, published in Niedringhaus *et al* (2015). He also performed the immunofluorescent staining and imaging presented in Figure 2.2D. Former post-doctoral researcher Dr. Joyce Kamande performed the work presented in Figures 2.2A, B, C and E. Dr. Raluca Dumitru, formerly of the University of North Carolina Human Pluripotent Stem Cell Core Facility, performed all maintenance, differentiation and maturation of human embryonic stem cells. Dr. Anne M. Taylor selected the samples for RNA collection and performed the RNA isolation. I performed the remaining immunofluorescence, RNA-FISH, imaging and all bioinformatics processing and analysis of the microarray data. All figures are previously published except Figure 2.3C, 2.4A and 2.7A-B. Reproduced figures are used with permission under the Creative Commons CC-BY license.

> **Bigler, R.L., Kamande, J.W., Dumitru, R., Niedringhaus, M., Taylor, A.M.** (2017) Messenger RNAs localized to distal projections of human stem cell derived neurons. Sci. Rep. 7(1):611. doi: 10.1038/s41598-017-00676-w.

Portions of the work described in Chapter 3 has been published on the web in a prepublication journal and is accepted for publications by *Nature Communications*. The study was done in collaboration with a post-doctoral researcher Dr. Tharkika Nagendran who initially observed the change in synaptic function following *in vitro* axotomy. The following figures are based on the work of Dr. Nagendran: 3.2C-D, 3.6A-E and 3.7A-B. I performed all remaining experiments. Previously published figures include: 3.1A-B, 3.2A (Somata before and after axotomy), 3.2C-D, 3.3A, 3.6A-E, 3.7A-B, and 3.8A-E. Reproduced figures are used with permission under the Creative Commons CC-BY-NC-ND license.

> **Nagendran, T., Larsen, R.S., Bigler, R.L., Frost, S.B., Philpot, B.D., Nudo, R.J., Taylor, A.M.** (2017) Distal axotomy enhances retrograde presynaptic excitability onto injured pyramidal neurons via trans-synaptic signaling. bioRxiv, doi: 10.1101/065391.

For this dissertation I created all figures and wrote the text.

TABLE OF CONTENTS

LIST OF TABLES xiii

LIST OF FIGURES xiv

LIST OF ABBREVIATIONS xvi

CHAPTER ONE: INTRODUCTION 1

Overview 1

Neurons 2

The Mammalian Nervous System 4

Compartmentalized Analysis of Neurons *in vitro* 7

Campenot chamber 7

Modified Boyden chamber 8

Microfluidic chamber 9

Axonal Capacity for Translation 10

Axonal Ribosomes 10

Axonal protein secretion machinery 11

Glia to axon transfer of RNA 12

Axonal transcriptomes 15

In vitro sensory neurons 16

In vitro sympathetic neurons 23

In vitro CNS neurons 24

In vivo CNS neurons 27

Conserved axonal transcriptome functions 29

Intra-axonal translation 30

Cell viability and axon maintenance 30

Axonal translation in synaptic plasticity 33

Axonal translation in injury signaling 39

Dissertation goals 42

CHAPTER TWO: MESSENGER RNAS LOCALIZED TO DISTAL PROJECTIONS OF HUMAN STEM CELL DERIVED NEURONS 44

INTRODUCTION 44

MATERIALS AND METHODS 45

Microfluidic chambers 45

Maintenance and differentiation of hESC-neurons 45

Maturation of hESC-neurons in microfluidic chambers 45

Immunocytochemistry 46

RNA-FISH 48

Modified rabies virus infection 49

Confocal imaging 50

Image analysis 50

Determination of differentiation efficiency 50

RNA isolation 51

RNA amplification and microarray 51

Data analysis 52

Data availability 53

RESULTS 53

Differentiation of human embryonic stem cell derived neurons in microfluidic chambers 53

Differential gene expression between axons and neurons derived from hESCs 57

Abundant transcripts within axons of hESC-neurons functionally resemble axonal transcripts localized to rat cortical neurons 65

RNA-FISH verification of specific mRNAs within hESC-neuron distal projections 68

DISCUSSION 71

Significance 71

Possible improvements 73

CHAPTER THREE: DIFFERENTIAL GENE EXPRESSION FOLLOWING IN VITRO AXON INJURY OF RAT HIPPOCAMPAL NEURONS 75

INTRODUCTION 75

MATERIALS AND METHODS 76

Hippocampal cultures 76

Microfluidic chambers 76

Cell viability assay 77

Retrograde labeling 77

Immunocytochemistry 78

Microgroove length analysis 78

RNA isolation 78

Microarray analysis 79

FM dye experiments and analysis 80

Drug treatments 81

Microscopy 81

Statistics 82

Data availability 82

RESULTS 82

Fluidically isolated axons of embryonic rat hippocampal neurons can be injured without affecting cell viability 82

Neurons with axons extending into the isolated compartment are typically close to the microgrooves....88

Transcription is necessary for axotomy-induced functional changes....92

Microarray analysis suggests possible mechanisms of injury-induced plasticity....96

Differential gene expression following in vitro axotomy resembles that of young rats 24 hours after spinal cord injury....100

DISCUSSION....103

Significance....103

Possible improvements....105

CHAPTER FOUR: FUTURE DIRECTIONS....107

Novel microfluidic chamber to increase axon yield....107

Zooming in on the axonal transcriptome....109

Stimulus driven changes in local translation....110

Axon-glia communication....111

Secondary axon injury signaling....112

Human stem cell derived neurons and axon function....113

Closing thoughts....114

APPENDIX A: hESC-NEURON EXPRESSION OF CELL TYPE SPECIFIC MARKERS....115

REFERENCES....117

LIST OF TABLES

Table 1.1 Functional analysis of the axonal transcriptome in multiple models 16

Table 2.1 Primary antibody concentrations 46

Table 2.2 Secondary antibody concentrations 48

Table 2.3 ViewRNA ISH Cell Assay procedure 48

Table 2.4 Evaluation of differentiation efficiency and glutamatergic enrichment 56

Table 2.5 Calculated RNA yield from axonal compartment 58

LIST OF FIGURES

Figure. 1.1. Scale representation of an adult vertebrate neuron. 2

Figure. 1.2. Schematic representations of compartmentalized neuron culture chambers for isolation of axons. 9

Figure. 1.3. Glia-to-axon transport of the large ribosome subunit to degenerating and regenerating axons in the sciatic nerve of the PNS. 14

Figure. 2.1. Human embryonic stem cell derived neurons (hESC-neurons) matured in axon-isolating microfluidic chambers. 55

Figure. 2.2. hESC-neurons demonstrate common neuronal features. 57

Figure. 2.3. Evaluation of the quality of Affymetrix microarray results generated from mRNA from hESC-neurons. 60

Figure. 2.4. hESC-neuron gene expression profile is enriched for markers of mature neurons. 62

Figure. 2.5. Differential gene expression between the transcriptome of distal projections and the neuronal transcriptome of hESC-neurons. 64

Figure. 2.6. Enriched gene ontology categories were similar between the transcriptomes of isolated hESC-neuron axons and axons of embryonic rat cortical neurons. 66

Figure. 2.7. Conserved orthologous transcripts within the axons of hESC-neurons and embryonic rat cortical neurons are enriched for synaptic proteins. 68

Figure. 2.8. Multiplexed RNA-FISH verification of mRNA within the distal projections of hESC-neurons. 70

Figure. 3.1. Long projecting axons of rat hippocampal neurons grown in axon-isolating microfluidic chambers can be injured. 84

Figure. 3.2. Axons regenerated after axotomy and cell viability was unaffected. 86

Figure. 3.3. Rabies virus carrying a fluorescent protein gene administered to the isolated axons allowed monitoring of the somatodendritic arbor and axons. 88

Figure. 3.4. The number of cells with isolated axons depended on microgroove length. 90

Figure. 3.5. The distribution of cells with isolated axons depended on microgroove length. 92

Figure. 3.6. Axotomy-induced hyper-excitability was present 48 hours after axotomy and persisted to 4 days after axotomy. 94

Figure. 3.7. Hyper-excitability is dependent on transcription not action potentials

at the time of axotomy. 96

Figure. 3.8. RNA quality assessment and verification of microarray quality controls. 98

Figure. 3.9. Differential gene expression 24 hours after axotomy. 100

Figure. 3.10. Comparison of ranked gene expression fold change from in vitro axotomy model and published in vivo corticospinal tract injury model. 102

Figure. 4.1. A novel asymmetric microfluidic chamber design to maximize axon growth. 109

LIST OF ABBREVIATIONS

°C	degrees Celsius
3H	tritium
ACTB	β-actin
AKT	Protein kinase B
AMPAR	α-amino-3-hydroxy-5-methyl-4-isoxazolepropionic acid receptor
ANOVA	analysis of variance
ARC	activity-regulated cytoskeleton-associated protein
ATF4	activating transcription factor 4
βtub	neuron-specific class III β-tubulin
β-tubulin III	neuron-specific class III β-tubulin
BDNF	brain derived neurotrophic factor
CA1	cornu ammonis 1
CA3	cornu ammonis 3
CA3-CA1	cornu ammonis 3 to cornu ammonis 1 hippocampal synapse
CAMK2A	calcium/calmodulin-dependent protein kinase type II alpha chain
cAMP	cyclic adenosine monophosphate
Cdk5	cyclin-dependent kinase 5
cDNA	complementary deoxyribonucleic acid
CMV	cytomegalovirus
CNQX	6-cyano-7-nitroquinoxaline-2,3-dione disodium
CNS	central nervous system
COXIV	cytochrome C oxidase subunit IV
CREB	cAMP response element binding protein
CST	corticospinal tract
d	day
D-AP5	D-(-)-2-amino-5-phosphonopentanoic acid
DAPI	4’,6-diamidino-2-phenylindole

DAVID	Database of Annotation, Visualization and Integrated Discovery
DIC	differential contrast
DIV	days *in vitro*
DMSO	dimethyl sulfoxide
DPO	days post operation
DRB	5,6-dichloro-1-β-D-ribofuranosyl-1H-benzimidazole
DRG	dorsal root ganglion
E	embryonic day
eCB	endocannabinoid
eCB-LTP	endocannabinoid-dependent long-term depression
eGFP	enhanced green fluorescent protein
EM	electron microscopy
ER	endoplasmic reticulum
FACS	fluorescence activated cell sorting
FITC	fluorescein
GABA	gamma-aminobutyric acid
GAD67	glutamate decarboxylase, 67 kDa
GAP43	growth associated protein 43
GFAP	glial fibrillary acidic protein
GO	Gene Ontology
h	hour
HA	human influenza hemagglutinin
HBS	Hank's balanced salt solution
hESC-neuron	human embryonic stem cell derived neuron
Hz	Hertz
IF	immunofluorescence
IMPA1	inositol monophosphatase 1
IPA	Ingenuity Pathway Analysis

JAK	Janus kinase
kDa	kilodaltons
L4-eGFP	ribosomal protein L4 fused to enhanced green fluorescent protein
LB2	Beta type nuclear lamin, protein
LCM	laser capture microdissection
lmnb2	Beta type nuclear lamin, gene *X. laevis*
LTD	long-term depression
LTP	long-term potentiation
M7	7-methyl-guanosine-5’-triphosphate-5’-guanosine
MAG	myelin-associated glycoprotein
MAP2	Microtubule-associated protein 2
MAPK	mitogen-activated protein kinases
MBP	myelin basic protein
microRNA	micro ribonucleic acid
µA	microampere
µg	micrograms
µl	microliter
µm	micrometer
µM	micromolar
mJ	millijoules
mm	millimeter
mRNA	messenger ribonucleic acid
ms	milliseconds
mtDNA	mitochondrial genome
mTOR	mammalian target of rapamycin
mt-rRNA	mitochondrial rRNA
mW	milliwatt

N2B27	media supplement N-2 with B-27
ng	nanogram
NGF	nerve growth factor
NLS	nuclear localization sequence
nm	nanometer
NMDAR	N-methyl-D-aspartate receptor
NPC	neural progenitor cell
nt	nucleotide
NT-3	neurotrophin-3
oligo(dT)	oligomer of deoxythymine
OXT	oxytocin
p35	Cyclin-dependent kinase 5 activator 1
$p75^{NTR}$	low-affinity neurotrophin receptor
PBS	phosphate buffered saline
pCREB	phosphorylated CREB
PDMS	poly(dimethylsiloxane)
PET	polyethylene tetraphthalate
PFA	paraformaldehyde
PGMEA	propylene glycol methyl ether acetate
PGMEA	picogram
PI3K	phosphatidyl inositol-3 kinase
PNS	peripheral nervous system
polyA	polyadenylate
rAAV	recombinant adeno-associated viral
RGC	retinal ganglion cell
RINe	RNA integrity number equivalent
RIP	RNA immunoprecipitation
RMA	Robust Multichip Analysis

RNA	ribonucleic acid
RNA-FISH	ribonucleic acid fluorescent *in situ* hybridization
RNA-seq	RNA sequencing
ROS	reactive oxygen species
rpm	revolutions per minute
rRNA	ribosomal ribonucleic acid
RT	room temperature
RT-PCR	reverse transcription-polymerase chain reaction
SAGE	serial analysis of gene expression
SC	superior colliculus of the midbrain
SCG	superior cervical ganglion
SEM	standard error of the mean
Sema3A	semaphorin 3A
STAT	signal transducer and activator of transcription
SynCAM	Cell adhesion molecule 1
Trk	tropomyosine receptor kinase
TrkA	tropomyosine receptor kinase A
TrkB	tropomyosine receptor kinase B
tRNA	transfer ribonucleic acid
TTX	Tetrodotoxin citrate
UTR	untranslated region
UV	ultraviolet light
vGLUT1	vesicular glutamate transporter 1

CHAPTER ONE: INTRODUCTION

Overview

Neurons are unique among all the cells of the body in that a single cell can span up to half the length of the organism (Fig.1.1A). Throughout development and adulthood they must rapidly respond to isolated local events, such as extracellular signaling molecules or mechanical contacts. Some of these events are only sensed by and affect the most distal portions of the neuron, the dendrites and/or axon. Prompt local responses suggest a high degree of independence from the neuron cell body, the soma. Rapid quantitative and qualitative changes in the local proteome, that do not require somatic transcription or translation, demonstrate that the most distal regions are semi-autonomous. The autonomy of the axon is of particular interest as the furthest location from the soma.

There is a wide diversity of neurons, morphologically and functionally, within each organism. A broad description of the variety of neurons and components of the mammalian nervous system will be given in the first two sections of this chapter as reference for the similarities and differences between common model systems.

Historically, the dogma of axon function stated that the axon was solely dependent on the neuron cell body for all necessary protein components. This theory has been overturned within the last few decades with a growing body of evidence definitively identifying translational machinery and the organelles necessary for protein trafficking within axons. Further, the transcriptome within axons is diverse and translation-dependent axonal functions have been determined from development through adulthood. This body of work will be covered in detail in this introduction. An intriguing, still controversial topic related to axon independence from the somata is glia-to-axon transport of RNA. Current evidence supporting this theory will also be discussed.

Figure 1.1

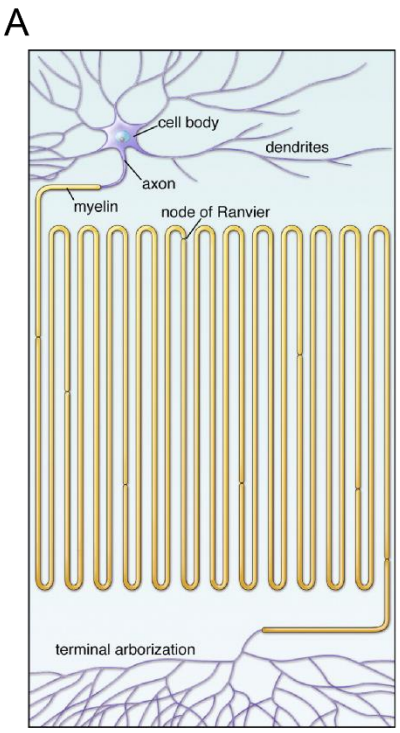

Figure. 1.1. Scale representation of an adult vertebrate neuron.
A. The axon depicted corresponds to a length of approximately 1 cm. Several neurons have axons longer than 1 m and may form thousands of synapses in their terminal arborization. [Modified with permission from Giuditta *et al* (2008)].

While much seminal work has been performed in invertebrate and non-mammalian systems, such as the squid giant axon, goldfish, *Aplysia californica*, *C. elegans*, *X. laevis* and *D. melanogaster*, my focus will be mammalian systems. Significant nervous system differences exist between the branches of the animal kingdom, this includes anatomical, dendritic-axon polarity, axon myelination and chemical or electrical synaptic signaling. Literature from the body of mammalian work is more relevant to the data contained herein though I will mention seminal work in other systems for historic reference.

Neurons

Together neurons form a cellular information conductance network throughout the body, the nervous system. It is an extremely complex and dynamic network with component parts that have

significant similarities and differences. The information transfer is bidirectional within and between neurons.

Neurons are polar cells, they have unique and unequal traits at different subcellular locations within the cell. They are morphologically polar, functionally polar and the local proteome is polarized. A key morphological and functional feature of neurons are the long projections emanating from the cell body (Fig. 1.1A). These projections can be classified as dendrites, which typically extend a few millimeters to centimeters from the cell body, and axons, which can extend meters from the cell body. This polarity facilitates information transfer between neural networks through maintenance of subcellular regions with segregated functions, this polarity also imposes significant biological constraints. The functional polarity of neurons resides within these projections, the dendrites receive information, the cell body consolidates the input and regulates whether the axon transmits information to the synaptic terminals. The local proteome is polar with many unique proteins in dendrites and axons. The polarity of the local proteome is maintained through protein transport and local protein translation (Holt and Schuman, 2013).

When an axon and dendrite are in close proximity they can form a synapse, the site of information transfer between neurons. The presynapse is formed along the axon and the postsynapse is formed along the dendrite. Each axon and dendrite can form hundreds of synapses leading to an extremely complex network of connections. In each synapse the postsynaptic component and dendrite are many times larger than the presynaptic component and axon, creating unique technical challenges when investigating the axon and presynapse.

Rapid anterograde transmission from the soma to the synapse occurs through a well-established actively propagated wave of ions, an action potential, generated through changes in membrane potential. The result is presynaptic neurotransmitter release to the extracellular environment of the synapse where postsynaptic neurotransmitter receptors are activated, initiating an intradendritic response to this brief chemical change. The postsynaptic cell is also capable of releasing signaling molecules to modulate the function and stability of the presynaptic structure. These signaling mechanisms are the basis of all neural network communication from autonomic processes, such as

controlling and responding to internal organ function, to the highest level brain function processes, including memory, thought and consciousness.

Retrograde signaling, from the axon to the soma, is less well established. There is evidence that some signaling occurs through active transport of protein complexes from the distal axon to the soma. In addition, there might be mechanisms of back-propagating ionic waves or biophysical methods conducted through the cytoskeleton.

Neurons can have many different dendrite and axon configurations, which provide unique signaling capabilities to each type of neuron. Multipolar neurons have many dendrites extending in multiple directions and a single axon. The broad dendritic arbor allows them to synapse with and receive information from many neurons. Bipolar neurons have clustered dendrites extending in a single direction from the soma, a more focused source of input, and a single axon. Unipolar neurons have a bifurcated single projection, one branch is the dendritic arbor and the other branch is the axon such that information bypasses the cell body. Pseudo-unipolar neurons also have a bifurcated projections but in these cells it is only axonal in nature, with the distal branch receiving stimulation and transmitting it directly to the proximal branch.

The Mammalian Nervous System

The mammalian nervous system is classified into many branches based on function and anatomy. The neurons and support cells of each have unique features that result in significant biological differences between branches of the nervous system.

The central nervous system (CNS) includes the brain and spinal cord and functions to integrate information across the nervous system, regulate motor function and control “higher” brain function. Many of the neurons in the CNS have a multipolar structure. Notable exceptions are the retinal ganglion cells (RGC) and olfactory receptor neurons which have a bipolar neuron structure. These two neuron types are also unique in the CNS as the only neurons that are directly activated by environmental stimuli and have axons that project to the brain, directly converting environmental stimuli into synaptic activity in the brain. Substructures of the brain are differentially enriched for neurons that release and respond to more than 13 different neurotransmitters. A neuron, and even an

individual postsynapse, can be capable of responding to information transmitted by more than one neurotransmitter but each neuron only releases one type of neurotransmitter. Canonically axons of CNS neurons *in vivo* have limited capacity to regenerate and re-establish proper synaptic connections. This might be the combined effect of an inhospitable *in vivo* cellular milieu for regeneration, the inability of the target neurons to release neurotrophic factors or the inability of the injured axon stump to respond to cues.

Neurons from the CNS can be cultured *in vitro* by a number of methods that all require special surface coatings to provide an extracellular matrix mimetic environment. Retinal ganglion can be dissected and directly cultured as an explant culture preserving the anatomical structure; the axons naturally grow out from the tissue to the cell culture substrate and are easy to visually isolate. Glutamatergic and GABAergic neurons are common CNS model neurons because they function in many 'higher' brain function pathways. They release the neurotransmitters glutamate and gamma-aminobutyric acid (GABA), respectively. Glutamate is an excitatory neurotransmitter, meaning a dendrite that receives the neurotransmitter signal is more likely to initiate an action potential signal to the soma, while GABA is an inhibitory neurotransmitter, reducing the probability that an action potential signal will initiate in the dendrite. The hippocampus and cerebral cortex brain substructures are common sources for glutamatergic and GABAergic neurons. The cerebral cortex plays a key role in a number of higher brain functions, such as memory, attention, perception, awareness, thought, language and consciousness. The hippocampus functions in long-term memory and spatial navigation and is located directly below the cortex. Neurons of the hippocampus and cortex can be cultured in a number of ways. Organotypic slices, prepared from coronal sections of microdissected tissue, can be derived from embryonic, neonatal, young or adult animals. They preserve much of the unique cellular structure and neuro-circuitry established during brain development. Alternatively, microdissected cortical and hippocampal tissue can be enzymatically dissociated and cultured for approximately a month, either with an astrocyte feeder layer or with media supplements (Kaech and Banker, 2006; Vicario-Abejon, 2004). The enzymatic digestion damages the dendrites and axons and destroys the *in vivo* neurocircuitry but the axons and dendrites regenerate and new synaptic connections are made *in vitro* demonstrating that CNS neurons are capable of reactivating mechanisms of projection

development and synaptogenesis. These preparations have been used for many studies, including axon guidance and synaptic plasticity.

The nerves and ganglia, clusters of nerve cell bodies, outside the brain and spinal cord are part of the peripheral nervous system (PNS). The PNS is divided into the somatic nervous system, which transmits sensory signals, such as taste and touch, to the CNS, and the autonomic nervous system, which controls the function of internal organs. Neurons derived from the dorsal root ganglion (DRG) of the somatic nervous system, responsible for relaying sensory information to the CNS, are a common *in vitro* model system. DRG neurons are pseudo-unipolar neurons, they have a single, very long axon with two functionally distinct branches, the 'distal process' performs dendrite-like functions while the 'proximal process' operates as the axon. The distal process projects to the sensing organ in the animal periphery while the proximal process projects to the spinal cord making it possible for an action potential that originated in the distal process to bypass the soma and propagate directly to the synaptic terminal with the spinal cord. The axons within the sciatic nerve are a common *in vivo* model system. The sciatic nerves emanate from DRGs in the lower back and innervate the legs/ hind legs, providing most of the somatic nervous system connections for the whole leg and foot. They are large and easy to identify making them an experimentally tractable system.

The autonomic nervous system is further differentiated into the sympathetic nervous system, activated during "fight or flight" situations, and the parasympathetic nervous system, functioning in "rest and digest". Norepinephrine and epinephrine are the dominant signaling molecules of the sympathetic nervous system while acetylcholine is the primary neurotransmitter of the parasympathetic nervous system. The superior cervical ganglion (SCG), of the sympathetic nervous system, is a common *in vitro* research model. These neurons are pseudo-unipolar, similar to DRGs, allowing signaling to quickly occur over long distances from the distal process to the proximal process. Axons of the SCG innervate the head and neck, including the blood vessels of the facial muscles and brain, salivary glands and thyroid gland.

Dissected DRGs and SCGs can be cultured directly as explants or dissociated and cultured, both methods require special surface coatings to provide an extracellular matrix mimetic environment and exogenous addition of neurotrophic factors for *in vitro* viability. Sympathetic and sensory neurons

have significant regenerative capability, *in vivo* and *in vitro*, such that proper functional re-innervation can occur following injury. Because of their biologically relevant regenerative mechanisms they are commonly used in to study axon injury signaling, axon-to-soma survival signaling, axon regeneration and guidance.

Compartmentalized Analysis of Neurons *in vitro*

The distinctive morphological and functional polarity of neurons has necessitated the development of custom cell culture environments to facilitate isolating long axons from the somata once the tissue is dissected or neurons are dissociated.

Campenot chamber

The Campenot chamber (Campenot, 1977) is a three-chamber system developed to investigate the biology of nerve growth factor (NGF) signaling in sympathetic neurons but has been applied to sensory neurons and other signaling molecules. The chamber is constructed from a collagen coated surface with multiple parallel microscratches in the coating, a three compartment Teflon piece is sealed to the surface with silicon grease. Dissociated neurons or whole tissue explants, derived from the SCG of neonatal rodents or DRG of rodents, are plated in one chamber. Guided by the microscratches as barriers the axons penetrate the fluid-impermeable barrier of silicon grease to access a separate fluidically-isolated compartment (Fig. 1.2A). If the neurons are plated in the center chamber the axons can extend into the left and right chambers (Fig. 1.2B), with a minimum axon length of about 1 mm. If the neurons are plated in a side chamber the axons can extend into the middle then the far opposite chamber allowing the manipulation of distal axons with a minimum axon length of over 3 mm (Fig. 1.2C). The fluidic environments of the three compartments can be independently manipulated to evaluate the local effects of neurotrophic or guidance factors. Also, the cellular material within each compartment can be collected without contamination from the other compartments for downstream analysis. Optical properties of the Teflon piece and silicon grease restrict live imaging of neurons and axons but low resolution fixed imaging is possible. These chambers are prone to leakage and not all cells are biocompatible with silicon grease. Further, due to

the chamber dimensions these are only appropriate for use with peripheral neurons that have very long axons, not neurons from the central nervous system.

Modified Boyden chamber

The Boyden chamber was originally developed for chemotaxis assays and has been modified to physically isolate DRG and SCG axons in explant and dissociated cell culture (Fig. 1.2D) (Zheng et al., 2001). The chamber is composed of a cell culture well with a removable insert well. The polyethylene tetraphthalate (PET) insert well has micropores of sufficiently small size to only allow axons, but not somata, to grow through and cover the bottom surface of the insert. The surface of the insert can be directly coated with the necessary coatings or glass coverslips can be coated and placed on the inserts. Media is added to the culture well, the insert is placed in the well and the cells or explant are added to the upper chamber with media. Fluid exchange occurs between the upper and lower compartments occurs through the micropores, so media must be changed regularly if differential treatment of the somata and axons is desired. Because the cell bodies or explants are grown on the other side of the insert membrane from the axons this culture method cannot be used to visually evaluate the neurons by immunocytochemistry unless the cells are cultures on coverslips. Modified Boyden chambers allow biochemical isolation of pure axons for downstream biochemical analysis.

Figure 1.2

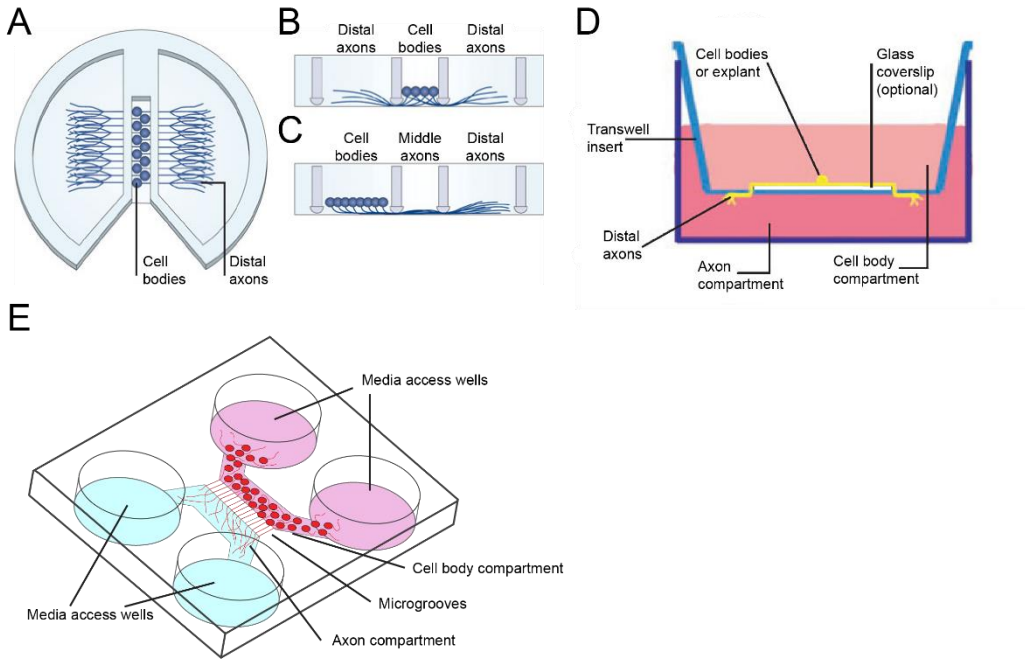

Figure. 1.2. Schematic representations of compartmentalized neuron culture chambers for isolation of axons.
A. Top view of sympathetic or sensory neurons/ explants cultured in a Campenot chamber. A thin layer of vacuum grease seals the Teflon divider to the prepared culture surface. [Modified with permission from (Zweifel et al., 2005)]
B. Side view of a Campenot chamber with dissociated cells or ganglion explants plated in the center compartment. [Modified with permission from (Zweifel et al., 2005)]
C. Side view of a Campenot chamber with dissociated cells or ganglion explants plated in the side compartment. [Modified with permission from (Zweifel et al., 2005)]
D. Boyden chamber schematic. Dissociated cells or explants are cultured on the upper surface of a microporous membrane, with or without a glass coverslip between the neurons and membrane. Elongating axons pass through the micropores. The cell body compartment and the axon compartment are not fluidically isolated due to diffusion but a gradient can be maintained with regular media changes. [Modified with permission from (Cox et al., 2008)]
E. The molded PDMS microfluidic chamber is affixed to a glass coverslip creating two symmetrical, fluidically isolated compartments connected by over 150 microgrooves, each compartment has two media access wells. Dissociated CNS neurons are plated in one compartment, growing axons enter the microgrooves and emerge in the parallel compartment.

Microfluidic chamber

The microfabricated multicompartment microfluidic chamber was developed for optimal growth and isolation of long projections from hippocampal and cortical neurons (Fig. 1.2E) (Taylor et al., 2003). There are two symmetrical, parallel fluidically isolated compartments measuring 2 mm by 7 mm by 100 µm tall connected by over 150 microgrooves 10 µm wide by 3 µm tall, which fill by capillary action when media is added to one of the compartments. Commercially available microfluidic

chambers have various microgroove lengths, which regulates the minimum length necessary for an axon to reach the isolated compartment. There are two large media access points, wells, for each compartment which minimize the effect of evaporation. Sterile, replica molded poly(dimethylsiloxane) (PDMS) microfluidic chambers are placed on coated glass coverslips to create the microfluidic chamber, dissociated neurons are directly added to one of the compartments followed by media. Astrocyte feeder co-culture is not used in this culture platform, instead B-27 neuron culture supplement (Invitrogen) is added to the media. These chambers have been optimized for visual and biochemical axon isolation and can be used for fixed or live imaging and biochemical analysis.

Axonal Capacity for Translation

For many decades dogma held that the axon of mature neurons depended exclusively on transport of proteins from the soma yet a large body of work has overturned this view and informed the establishment of a 'local synthesis model' of axon function (Alvarez et al., 2000). In this model a portion of the local proteome is locally synthesized from mRNA and ribosomes within the axon. Early work investigating RNA in neurons detected RNA in the adult rabbit optic nerve derived from the soma following *in vivo* intraocular injection of tritium labeled nucleoside, ([3H]uridine) (Gambetti et al., 1973). This study was not able to differentiate between the many different classes of RNA including, rRNA, mRNA, tRNA and microRNA, but suggested the hunt for axonal ribosomes and mRNA would be successful. Since then translational machinery has been identified within axons of many species. Further, cellular components necessary for protein trafficking and secretion, the endoplasmic reticulum and Golgi apparatus, are present in axons. Recent, controversial, work proposes transport of ribosomes from glia to axons in the PNS.

Axonal Ribosomes

Historically the presence of ribosomes within mature axons was discounted due to the inability to find them by electron microscopy (EM) but technological advances have facilitated detecting ribosome and the proteins of translation initiation and elongation within mature axons. In the rodent peripheral nervous system ribosomes have been detected by immunofluorescence (IF) in cultured

DRGs from neonatal and adult rats (Bisbal et al., 2009; Calliari et al., 2014) and *in vivo* by EM in adult sciatic nerves (Zheng et al., 2001). Within the central nervous system ribosomes have been demonstrated by IF in adult rat medullary roots projecting to the spinal cord (Calliari et al., 2014), myelinated axons of spinal nerve roots from adult rabbits and rats (Koenig et al., 2000) and by EM in the axons of retinal ganglion cells within the mouse brain from embryonic, young and adult animals (Shigeoka et al., 2016). Axonally localized ribosomes have been identified within cultured hippocampal neuron by IF and EM (Taylor et al., 2013; Tcherkezian et al., 2010) and adult rat and mouse GABAergic hippocampal neurons as well as at the presynapse, as detected by super-resolution STORM microscopy (Younts et al., 2016). Evidence suggests mechanisms to regulate the supply of axonal translational machinery to meet the local demand. Translational machinery was detected in regenerating adult rat spinal cord axons but decreased after recovery. Subsequent injury reactivated the axonal enrichment of these proteins suggesting a dynamic intra-axonal environment (Sachdeva et al., 2016). Additionally, proteomic analysis of extracted axioplasm from *in vivo* regenerating adult rat sciatic nerves also demonstrated in increase in translational machinery following injury (Michaelevski et al., 2010).

Axonal protein secretion machinery

Proper trafficking of membrane and secreted proteins involves the rough endoplasmic reticulum (ER) and Golgi apparatus. Transcripts encoding membrane and secreted proteins have been identified repeatedly as enriched in axons. ER and Golgi components have been detected in rat DRG and *X. laevis* RGC cultures (Merianda et al., 2009) and *in vivo* in rat DRG (Merianda and Twiss, 2013). Pharmacological inhibition of Golgi function of cultured *X. laevis* RGC blocked growth cone turning, a process known to require protein synthesis (Merianda et al., 2009). Mechanical injury of axons increases intra-axonal calcium levels, and the calcium stores of the axon localized ER is a major source for this increase in adult rat DRG axons (Villegas et al., 2014). Additionally, ER and Golgi components were enriched in regenerating axons following *in vivo* axon injury consistent with an increased demand for protein synthesis during reinnervation (Merianda and Twiss, 2013).

Glia to axon transfer of RNA

There is a growing body of evidence demonstrating glia to axon transport of RNA. Early work investigating RNA in neurons used the peripheral nerve of the adult newt, *Triturus viridescens* (Singer and Green, 1968). Newts have high tissue regenerative capacity with the ability to regenerate whole functional limbs following amputation. To investigate the RNA content of axon fragments detached from the somata they locally injected [3H]uridine immediately after severing peripheral nerves. They found radioactivity in the distal peripheral nerve portions 24 h later despite the fact that these axons were severed from the somata and destined to degenerate (Fig. 1.3A and 1.3B). They concluded that the most likely source of this RNA signal was the associated Schwann cell (Singer and Green, 1968). The unusual regenerative capacity of the newt made it unclear whether this was a species specific phenomenon. Similar work identified [3H]uridine labeled RNA grains in the severed axon stump of adult rat sciatic nerves (Benech et al., 1982) suggesting transfer of RNA from glia to degenerating axon fragments occurs in mammals. Glia-to-axon RNA transfer has been definitively demonstrated in the squid giant axon *in vitro*. It is strongly stimulated by axon depolarization or activation of glial glutamate and acetylcholine receptors (Eyman et al., 2007) suggesting the neurotransmitters for communication between neurons might also signal to surrounding glia.

Interest in the possibility of glia-to-axon transport in mammals was fueled by a unique spontaneous mutant mouse, Wallerian degeneration slow (*Wld*^{s}), that has delayed peripheral nerve degeneration following injury. Typically a distal desomatized axon (Fig. 1.3A), begins to degenerate within 24 to 36 h by a process known as Wallerian degeneration that takes roughly 24 h (Fig. 1.3B). In the *Wld*^{s} mouse, desomatized axon degeneration is delayed by 2 -3 weeks facilitating studies of the severed axon fragment (Lunn et al., 1989). Court and Alvarez (2005) noticed that axon fragments following sciatic nerve crush in adult *Wld*^{s} mice contained more ribosomes than their uninjured axon counterparts. Since the distal axon was severed from the neuron soma it was highly unlikely that the ribosomes originated there (Court and Alvarez, 2005). To study this more closely they created a DNA lentivirus encoding enhanced green fluorescent protein (eGFP) fused to the ribosomal protein L4 (L4-eGFP) and injected the lentivirus into the distal segment of the desomatized nerve. Nerves were dissected 7 d later and evaluated for co-localization of ribosome antibody staining and L4-eGFP

protein within glia and axons (Fig. 1.3B). All axons that demonstrated L4-eGFP signal were enveloped by L4-eGFP positive Schwann cells and uninfected Schwann cells enveloped L4-eGFP negative axons (Court et al., 2008). They showed that this transfer was relatively specific as Schwann cell cytoplasmic protein S100 was not detected in axons and neither was eGFP from a control lentivirus lacking the L4 protein. Small protrusions of the Schwann cells appeared to pierce the myelin sheath and enter the axon suggesting a model of axonal entry for the glial derived ribosomes (Court et al., 2008).

To investigate glia-to-axon ribosome transfer in the context of axon regeneration they performed similar experiments on wild-type adult mice. Degeneration of the severed axon portion is complete by day 3 after injury and regeneration begins around day 4. Seven days after injury co-localization of L4-eGFP and ribosome staining was detected in 12% ± 1% of the regenerating axons (Fig. 1.3C) (Court et al., 2011). They also investigated this phenomenon in the regenerative context of rat sciatic nerve grafts. Instead of administering the L4-eGFP lentivirus *in vivo* they cultured and infected Schwann cells *in vitro*, enriching for eGFP positive Schwann cells by fluorescence activated cell sorting (FACS). Rats received a 13 mm sciatic nerve graft then 5 x 10^5 transduced Schwann cells were injected into the graft. Regeneration through the length of the graft was seen 16 days after surgery and co-localized L4-eGFP and ribosome staining was observed in these axons (Fig. 1.3C). There were also L4-eGFP negative ribosomes in axons potentially from the neuron soma or non-transduced Schwann cells. Co-localized L4-eGFP and ribosome staining was detected in a subpopulation of axons at 3, 6 and 8 weeks after surgery (Court et al., 2011). These long term observations could mean that the glial derived ribosomes have a very long half-life in the axon or the glial transfer of ribosomes continues after regeneration, potentially to support axon maintenance. Evidence using rat sciatic nerve explants collected 18 h after nerve injury suggests the mechanism of glia-to-axon transport of ribosomal RNA and non-ribosomal RNA molecules requires actin polymerization and the actin-based motor protein myosin-Va (Sotelo et al., 2013). In mouse myosin-Va is necessary for survival beyond 19-21 days (Searle, 1952) and has been associated with axonal transport of diverse cargo including synaptic vesicles and axonal mRNA (Calliari et al., 2014; Kisiel et al., 2014).

Figure 1.3

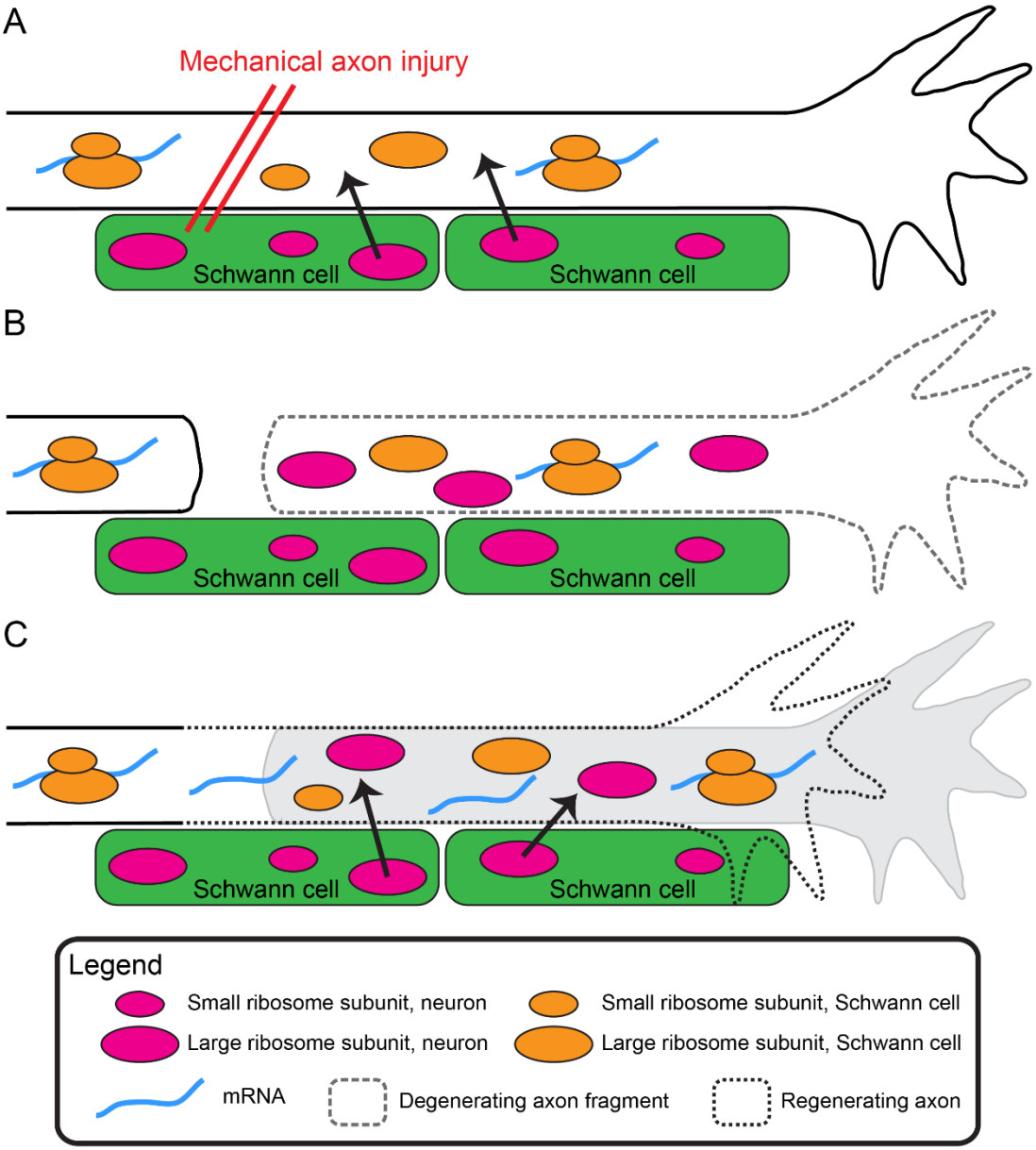

Figure. 1.3. Glia-to-axon transport of the large ribosome subunit to degenerating and regenerating axons in the sciatic nerve of the PNS.
A. Mechanical injury to the sciatic nerve severs the distal portions of the axons from the somata, inhibiting soma-to-axon transport.
B. Large ribosome subunits derived from the surrounding Schwann cells can be detected in the degenerating axon fragments of the sciatic nerve after injury.
C. Large ribosome subunits derived from the surrounding Schwann cells can be detected in regenerating axons of the sciatic nerve.

The theory of glia-to-axon transport challenges the doctrine of an autonomous neuron, holding that the soma is the only source of protein and mRNA for the axon. It has only been observed

following axotomy of PNS neurons and might be limited to this context. The fact that highly enriched populations of dissociated neurons, lacking significant numbers of glial cells, can be cultured *in vitro* for weeks demonstrates that neurons have the capacity for autonomous growth. In addition, culturing CNS neurons with glial feeder cells, compared to media supplements, does not significantly improve viability or the length of time cells can be cultured *ex vivo* but these feeder layers are rarely in direct contact with the neurons (Kaech and Banker, 2006; Vicario-Abejon, 2004). A deeper understanding of bidirectional communication between glia and axon, together with our understanding of axon-to-soma communication, could alter the way we approach axon biology.

Axonal transcriptomes

A critical element for axonal protein synthesis is axonally localized protein-coding mRNA. High resolution polyA mRNA *in situ* hybridization of cultured cortical neurons demonstrated mRNA throughout the somata, dendrites and proximal axons after 4 d in culture (Bassell et al., 1994). With the necessary components for translation identified within axons the next logical questions were: what mRNAs are present in axons and what axonal functions are translation dependent? Unbiased methods to evaluate large scale gene expression within the axons of a variety of neurons have revealed many conserved Gene Ontology (GO) functional groups. These include proteins involved in translation (ribosomal proteins as well as translation initiation and elongation factors), nuclear-encoded mitochondrial proteins, cytoskeletal proteins, transmembrane and secreted proteins (Table 1.1).

There are a few special technical considerations when performing an analysis of axonal RNA. First, the RNA content of axons and somata is quantitatively different by many fold, this must be controlled and corrected for to compare relative gene expression. Secondly, *in vitro* methods to evaluate axons necessitates that the *in vivo* axons are injured and regenerate *in vitro* prior to analysis. Mechanisms of axon regeneration are dependent on intra-axonal translation and, as described below, active regeneration alters the axonal transcriptome.

Table 1.1 Functional analysis of the axonal transcriptome in multiple models

	Functional categories				
Sample	Translation	Mitochondrial	Cytoskeleton	Transmembrane/ Secreted	Reference
Injury-conditioned adult DRG, rat	Yes	Yes	Yes	Yes	(Willis et al., 2007)
Embryonic DRG, rat	Yes	Yes	Yes	Yes	(Gumy et al., 2011)
Adult DRG, rat	Yes	Yes			(Gumy et al., 2011)
Embryonic DRG, mouse	Yes	Yes		Yes	(Minis et al., 2014)
Neonatal SCG, rat		Yes			(Andreassi et al., 2010)
Naïve CNS, rat	Yes	Yes	Yes		(Taylor et al., 2009)
Regenerating CNS, rat	Yes			Yes	(Taylor et al., 2009)
Embryonic RGC, frog	Yes	Yes	Yes	Yes	(Zivraj et al., 2010)
Adult hippocampal neuropil, rat	Yes			Yes	(Cajigas et al., 2012)
In vivo RGC, mouse		Yes	Yes	Yes	(Shigeoka et al., 2016)

In vitro sensory neurons

One of the earliest axonal transcriptome datasets used adult rat 'injury-conditioned' DRGs grown in modified Boyden chambers (Willis et al., 2007). Previous *in vivo* injury of the DRG unipolar axon distal branch conditions them to regenerate axons more rapidly following subsequent injury, such as dissociation prior to *in vitro* culturing (Lankford et al., 1998). This axon regeneration is transcription-independent but translation-dependent over 24 h in culture suggesting important features of the

axonal transcriptome facilitate regeneration (Twiss et al., 2000). Animals underwent sciatic nerve crush injury 7 d before primary DRGs were dissected, dissociated and cultured on Boyden chamber inserts with 8 µm diameter pores. Both the injured distal axon branch and the uninjured proximal branch of the DRG axon likely regenerated but this was not differentiated in this system. After 20 – 22 h in culture the lower surface of the membrane, coated with isolated axons, was scraped and processed for hybridization to Atlas cDNA arrays (approximately 4000 cDNAs represented). They identified more than 200 protein encoding mRNAs, including 'transmembrane proteins', 'translational machinery', 'cytoskeleton', and nuclear encoded 'mitochondrial proteins'.

To investigate the effects of axon growth-promoting and growth-inhibiting factors on the axonal transcriptome they selected a representative panel of 50 mRNAs evaluate following growth factor treatment. The growth-promoting factors selected were NGF, neurotrophin-3 (NT3) and brain derived neurotrophic factor (BDNF) which all signal through members of the tropomyosine receptor kinase (Trk) family of tyrosine receptor kinases. The growth-inhibiting factors were semaphorin 3A (Sema3A) and myelin-associated glycoprotein (MAG), selected because they induce retraction or repulsion of rat DRG axons. To prevent diffusion to the upper chamber growth factors were covalently coupled to 15 µm diameter polystyrene microspheres and the inserts were placed directly in contact with the microspheres for 4 h. An additional pharmacological manipulation in these experiments was the addition of the reversible transcription blocker, 5,6-dichloro-1-β-D-ribofuranosyl-1H-benzimidazole (DRB), to prevent any transcriptional effect of the growth factors. The ability to rule out transcription as the driving force behind changes in the axonal transcriptome allowed them to focus on targeted, stimulated trafficking of mRNA to axons though it did not rule out changes in mRNA stability. Since this form of injury-conditioned axon regeneration is transcription-independent blocking transcription did not negatively affect axon growth. Each of the 5 treatments resulted in significant increases and decreases in specific axonal mRNAs as well as identification of transcripts that did not change (Willis et al., 2007).

They found that NGF and BDNF broadly had similar effects on the transcripts tested while the effect of NT3 was unique. With only one exception the growth-inhibiting factors had distinct effects on transcripts compared to the growth-stimulating factors. Some of the most interesting single transcript

response patterns included the very well characterized axonally translated β-actin mRNA; all three neurotrophins significantly increased axonal localization of this mRNA while both inhibitory factors significantly decreased its localization. Localization of growth associated protein 43 (GAP43) mRNA was increased only by NGF and remained unchanged in the presence of the other growth factors. Subsequently, this group demonstrated that the balance between axonal translation of GAP43 and β-actin regulated axon branching and axon length in this model system (Donnelly et al., 2013). In addition, vimentin mRNA had a unique response pattern, it was unchanged following NT-3 exposure but increased greater than 3.5 fold with the other growth-stimulating factors and the growth-inhibiting factors. Vimentin is a type III intermediate filament protein of the intermediate filament protein family the cytoskeleton and has a role in anchoring ER and mitochondria within the cytosol (Katsumoto et al., 1990). They showed that changes in the axonal and somatic transcriptomes were inversely related supporting the hypothesis that, in at least some cases, individual transcript changes in the axon draw from the pre-existing somatic transcriptome. Further, bath application of NGF did not stimulate the same axonal transcriptome changes as isolated axon NGF treatment suggesting the importance of the local extracellular environment in altering the local axonal transcriptome.

To determine the mechanism behind this NGF-stimulated transcriptome plasticity they demonstrated functional microtubules were critical while functional microfilaments were important but not necessary. Trk kinase activity was necessary for the NGF-stimulated increases and blocking it lead to axonal increases in the transcripts typically decreased following NGF. Lastly, individual transcripts responded differently to pharmacological inhibition of phosphatidyl inositol-3 kinase (PI3K) and mitogen-activated protein kinase (MAPK) signaling pathways downstream of Trk activation. Taken together their data suggest that the plasticity and diversity of the adult rat DRG axonal transcriptome in the integrated effect of multiple local mechanisms (Willis et al., 2007).

Axon regeneration in the PNS system is dependent on local translation and the axons of neurons from younger animals have a higher capacity for regeneration than those from older animals (Chierzi et al., 2005). The axonal transcriptomes of DRGs from young and old animals might reveal axon-intrinsic regeneration mechanisms. To investigate this, whole DRG explants were dissected from embryonic (E16) and adult (3 – 5 month old) rats and cultured without dissociation in Campenot

chambers with NGF-supplemented media for 4 d (Gumy et al., 2011). Microarray analysis of axonal mRNA revealed 2627 transcripts localized to embryonic axons and 2924 transcripts within adult axons, 1445 of these localized transcripts (55.0% and 49.4% of the embryonic and adult transcriptomes, respectively) were present in both age samples while the remainder were age specific. The common transcripts were enriched for nuclear encoded 'mitochondrial protein's, proteins involved in 'translation', and 'neurite development and growth'. The embryonic specific transcripts were enriched for 'cytoskeleton' proteins and 'transport/trafficking' related proteins, such as microtubule associated motor proteins, 'vesicle' proteins involved in membrane trafficking and synaptotagmins, synaptic vesicle proteins necessary for Ca^{2+}-induced exocytosis. They were also exclusively enriched for 'cell cycle' proteins. In the adult derived DRG axons mRNAs encoding 'inflammatory' and 'immune-related' functions were enriched, specifically cytokine-cytokine receptor interactions, Toll-like receptor signaling and antigen presenting and processing functions. The enriched functions in the axonal transcriptome point toward axon growth and maintenance while those of the adult transcriptome highlight pathways that have been implicated in chronic and neuropathic pain (Gumy et al., 2011).

There are a few noteworthy details of the pharmacological manipulations in this work. First, the potent DNA cross-linker mitomycin C was included in their cultures to block the proliferation of mitotic, non-neuronal cells, such as fibroblasts and Schwann cells, present in DRG explants. This served to isolate the neuron intrinsic differences between embryonic and adult DRG axons without the potentially confounding contribution of non-neuronal cells. Secondly, as previously demonstrated by Willis *et al* (2007), the necessary inclusion of NGF in this culture system likely had an effect on the axonal transcriptome. This might recapitulate the *in vivo* environment since NGF is one of the neurotrophic factors secreted by DRG innervated tissues.

Microarrays have a reduced quantitative range and finite coverage of the genome as compared to RNA sequencing (RNA-seq). Minis et al (2014) applied Solexa sequencing to total RNA derived from the distal axon branch of embryonic mouse DRGs. They used cultured explants of embryonic mouse DRGs still attached to the spinal cord in Boyden chambers; because the proximal axon branch was still attached to the spinal cord it was not able to grow through the membrane pores (Minis et al., 2014). Explants were cultured in the presence of NGF for 48 h prior to purifying RNA. The

‘explant’ RNA samples contained the whole DRG-spinal cord explant. Using ranked differential expression they evaluated enriched GO categories within differential expression bins spanning the expression profile from ‘absent in axons but present in explants’ to ‘highly enriched in axons’. The transcripts highly depleted in axons clustered into one functional category while the transcript highly enriched in axons clustered into 4 categories. They focused their analysis on the mRNAs that were within the extremes of differential expression (Minis et al., 2014).

The axonally depleted fraction was best represented by the GO category ‘membrane fraction’ (GO:0005624). They interpreted this as support for somatic synthesis of membrane proteins followed by transport to axonal sites. This GO term was based on experimental results of biochemical cell fractionation not a *bona fide* cellular compartment and was made obsolete in the EMBL-EBI database in mid-2012. They specifically look at 20 transcripts encoding receptors for neurotrophins and axon guidance cues within their RNA-seq data and found that 9 were depleted from axons, 5 were not differentially expressed and 6 were enriched in axons. While they stated this supported their conclusions I find this diverse transcript specific localization more suggestive of a variety of mechanisms regulating receptor localization.

The 4 axonally enriched categories included ‘secreted proteins’, ‘sequence specific DNA binding’, proteins involved in ‘translation’ and ‘immune response’. Beyond this broad characterization they made three unique discoveries. First, a closer analysis of the transcript encoding ‘secreted proteins’ revealed that, in particular, mRNAs encoding proteins with an N-terminal signal peptide amino acid sequence were axonally enriched. The signal peptide sequence is rapidly bound during protein translation by the signal-recognition particle which stalls translation and facilitates transport of the ribosome complex to the ER for secretion of the new protein. Another sub-category of note within ‘secreted proteins’ were related to collagen of the extracellular matrix. Transcripts encoding many collagen chain subunits and enzymes of the collagen biosynthesis pathway were highly enriched in axons. Taken together these results suggest local translation and ER-dependent protein secretion within sensory axons facilitates modification of the local extracellular environment.

Secondly, taking advantage of the unique genome coverage of their RNA-seq data evaluated the axonal expression of all mitochondrial genes. Mitochondrial function requires coordinated

expression of the 37 genes of the mitochondrial genome (mtDNA) and more than 1000 nuclear encoded mitochondrial genes (Garesse and Vallejo, 2001), events that are separated by a long physical distance in axons. Proteins encoded in both genomes form the complexes of the electron transport chain, but the enzymes of the citric acid cycle and the mitochondrial transcription machinery are all nuclear encoded. Mitochondrial translation requires mtDNA encoded tRNAs and rRNA and nuclear encoded accessory ribosomal proteins and translation factors. Mitochondrial encoded genes were within the highest expressed RNAs in both axons and explants. More than 20% of the total axonal RNAs aligned to mtDNA, while approximately 2% of the explant RNA aligned to mtDNA; mitochondrial rRNA (mt-rRNA) was extremely enriched in the axons. Transcripts from the nuclear encoded mitochondrial genes were equal expressed between the two compartments, consistent with the finding that the GO category 'mitochondria' was not an enriched cluster in the axons. The relative expression, not enrichment, of mtDNA genes was 1 to 2 orders of magnitude higher than the expression of nuclear encoded genes in the axons. This novel finding of extreme differential expression of mitochondrial genes could be a result of the smaller size of the axonal transcriptome, in terms of how many genes are represented, as compared to the explant transcriptome. Alternatively, it could point to unknown post-transcriptional events coordinating mitochondrial gene expression and function.

The ability to deeply evaluate splice variants in their RNA-seq data allowed them to identify short sequence motifs enriched in axonal mRNAs. They identified 4169 differentially expressed splice variants, from 1556 genes, where at least one splice variant was preferentially found in axons and at least one different splice variant was found in the whole explant but absent from the axon, 1888 were preferentially axonal and 2281 were absent from axons. This is the first large scale evidence for alternative splicing associated with mRNA axonal localization. Using only unique sequences contained within each splice variant, 7743 axonally present elements and 6202 axonally devoid elements, they used a published 'Feature Motif Model' algorithm to find elements enriched in the axonal sequences versus the axonally devoid sequences. They identified 5 short sequence elements enriched in the axonally localized splice variants and 2 sequence elements in the axonally absent splice variants. Messenger RNA localization sequence elements are canonically found in the 3' untranslated region

(UTR) of the mRNA between the stop codon and the polyA tail. They evaluated the distribution of the 5 short sequence elements within the 1888 preferentially axonal transcripts finding that the elements were equally distributed across the 5' UTR, protein coding sequence, and 3' UTR, after controlling for the length of each of these elements (Minis et al., 2014).

It is important to point out that proliferation of non-neuronal cells in explant tissue was not blocked in this work. Mitotic cells, particularly Schwann cells, were clearly detected in the explant cultures by immunocytochemistry. These non-neuronal cells also contributed to the quantitative gene expression profile of their explant samples to an unknown degree. Additionally, the presence of NGF in the axonal media, to stimulate axon regeneration, could affect the transcriptome (Willis et al., 2007), the methods do not specify whether the explants were also in NGF supplemented media which could have an effect on transcription.

The mitochondrial mRNA and mt-rRNA results raise a few questions. They did not consider that the extremely high mitochondrial rRNA expression could be a technical or bioinformatic artifact. Nuclear-encoded rRNA typically makes up more than 80% of the total RNA isolated from whole cell lysate and *in vitro* RNA amplification methods might be slightly biased toward amplifying rRNA over mRNA. Specifically, amplification methods use a pool of primers including random hexamer sequence primers and 12 – 18 nt oligo(dT) primers, the random primers equivalently amplify the whole transcript while the oligo(dT) primers amplify sequences upstream of a poly-adenylate track, such as the polyA tail. Most mRNAs have a polyA tail, co-transcriptionally added by factors associated with RNA polymerase II, regulating mRNA translation and degradation. Ribosomal RNA units are transcribed by RNA polymerases I and III, they do not have polyA tails but they do contain multiple poly-adenylate tracks that are genetically encoded; these sequences can be amplified by oligo(dT) primers. Taken together this creates an *in vitro* reaction where each mRNA is primed once from the polyA tail and multiple times, roughly proportional to the length of the mRNA, throughout the length of the transcript. The rRNAs can be amplified from each polyA track and multiple times from random locations by the random hexamer primers. It would have been helpful if they reported on the relative quantity of cellular rRNA within axons in relation to mt-rRNA, but the rRNA RNA-seq data is typically discarded during the RNA-seq data genome mapping process.

In vitro sympathetic neurons

Sympathetic and sensory neurons are functionally unique so the axonal transcriptome of neonatal rat SCGs were quantified by serial analysis of gene expression (SAGE) (Andreassi et al., 2010). The SAGE technique produces one short, less than 20 base pair, cDNA 'tag' from each RNA molecule. The library of cDNA tags are enzymatically concatenated, cloned and sequenced by traditional Sanger sequencing (Gowda et al., 2004). Theoretically the transcript to tag ratio is 1:1 so the number of unique tags mapping to a gene is a direct measure of the number of transcripts. Dissociated SCG cells from neonatal rats were plated in Campenot chambers supplemented with NGF. Regenerating axons were grown for 3 – 4 weeks. Total RNA was purified from the cell bodies and isolated axons and amplified with SAGE primers incorporating sequence elements to facilitate preparation of the SAGE library and deconvolution of the sequencing results. They sequenced 1440 clones from each library, obtaining 20082 tags from the axonal library and 20420 tags from the cell body library which they mapped to the rat UNiGene build 166 reference database. They found the somatic transcriptome contained transcripts related to 'cytoskeletal', 'synaptic', and 'nuclear' functions. The axonal library was enriched for transcripts of nuclear encoded 'mitochondrial' and 'signal transduction' proteins (Andreassi et al., 2010).

The greatest difference between their somatic library and axonal library was the percentage of tags that that could not be mapped to their reference database. The UNiGene databases contain only transcribed sequences, not intergenic DNA sequences, and are filtered to omit RNAs with repeated or low-complexity sequences, RNAs derived from ribosomal RNA genes, and mtDNA genes. Tags mapping to uncharacterized but annotated genes represented 11.25% of the somatic library and 4.7% of the axonal library but tags that couldn't be mapped comprised 30.05% of the somatic library and 39.9% of the axonal library. Comparing these unannotated axonally derived tags to a database of known noncoding RNAs suggested that approximately 1% of the total axonal transcriptome could be noncoding RNAs.

Two cell culture pharmacological manipulations they used created a unique and potentially more homogeneous cell body population. First, similar to Gumy *et al* (2011), they prevented the proliferation of mitotic cells using a deoxyribonucleotide analogue to disrupt DNA synthesis enriching

for neurons in the cell body compartment. Second, they remove NGF from the somatic compartment after a week causing cells without axons in the isolated compartment to activate programmed cell death pathways leaving a neuronal population that only had axons extending into the isolated culture compartment.

Regarding the 'unmappable' tags, it would be informative if these tag sequences could be mined for ribosomal RNA, mtDNA encoded proteins and mt-rRNA. This analysis could support the mitochondrial RNA findings of Minis *et al* (2014) in a different species and neuron type.

In vitro CNS neurons

RNA within the axons of CNS neurons is more controversial than within the axons of PNS neurons. The axonal transcriptome of CNS neurons grown in axon-isolating microfluidic chambers was evaluated in uninjured and injured regenerating axons (Taylor et al., 2009). Dissociated cortical and hippocampal neurons from embryonic rats were grown in microfluidic chambers with 450 µm microgrooves separating the somatic compartment from the axonal compartment. While these neurons have an embryonic origin they are fully differentiated 'mature' neurons. The media did not contain serum, limiting the proliferation of rare non-neuronal cells, or exogenous growth or guidance cues for axon elongation through the microgrooves but the media supplement B-27 (Gibco) was used.

Axonal and somatic RNA was collected on days *in vitro* (DIV) 13 and evaluated by microarray. Microarray data was thresholded for expression resulting in 6702 microarray probe sets in the somatic dataset and 2051 probe sets in the axonal dataset. All of the axonal probes were detected in the somatic dataset. A second threshold was set for the axonal dataset to generate a list of transcripts reliably localized to axons, 308 genes. GO categories enriched in the axonal mRNAs encoded 'translation', 'mitochondrion', 'intracellular transport', and 'cytoskeleton' proteins (Taylor et al., 2009).

Next they investigated how *in vitro* axon injury affected the axonal transcriptome of regenerating axons. On DIV11 fluidically-isolated axons were destroyed by physical disruption and the transcriptome of regenerating axons was evaluated 48 h later, on DIV13. The somatic RNA following this manipulation was not collected. Comparing the transcriptome of regenerating axons to naïve axons revealed 866 transcripts that changed in axonal expression by more than 20% in regenerating

axons, 480 transcripts increased and 386 transcripts decreased. Surprisingly, all but 8 of the increased transcripts had not been detected as reliably localized to axons in their initial axonal transcriptome analysis. Functional classification of the differentially expressed mRNAs suggested that the increased transcripts in regenerating axons were enriched for 'cell-cell signaling' molecules, 'cell differentiation', and 'secreted' proteins. The decreased transcripts were enriched for 'mitochondrial' and 'cytoskeletal' proteins and 'intracellular transport' proteins. Many of the enriched 'cell differentiation' proteins are required for nervous system development and those of the 'cell-cell signaling' and 'secretion' groups are involved in synaptogenesis, neurotransmitter release and synaptic plasticity suggesting that these regenerating axons might have an increased capacity for axon targeting and synapse formation and function. The decreased categories in regenerating axons suggests that the dynamic cytoskeleton and intracellular transport along the cytoskeleton might be unique in regenerating axons. Also, the balance between oxidative phosphorylation and glycolysis might be different in regenerating axons or transport of new mitochondria during axon outgrowth reduces the local need for mitochondrial protein synthesis. They pointed out that axonal localization of proteins involved in translation, such as ribosomal proteins and initiation and elongation factors, were not significantly changed during regeneration suggesting the local capacity for translation was not significantly altered (Taylor et al., 2009).

Growth cone turning in response to guidance cues is unequivocally dependent on local translation and the attractive or repulsive response to cues changes during the course of development (Jung et al., 2011; Jung and Holt, 2011). To determine whether this change in responsiveness was dependent on changes in the growth cone transcriptome Zivraj *et al* (2010) used laser capture microdissection (LCM) to isolate mRNA within growth cones. Whole-eye primordia from late stage *X. laevis* embryos were cultures and growth cone RNA was collected 24 h later. Microarray analysis identified 444 transcripts with known functions in the growth cones. Ingenuity Pathway Analysis (IPA) for enriched functions and signaling pathways revealed that 31% of the encoded proteins functioned in 'protein synthesis and translation', this included translation initiation and elongation factors, mRNA processing proteins, protein folding chaperones and 69 0f the 80 ribosomal proteins. The second largest functional category was 'metabolic/glycolytic' and included proteins of oxidative phosphorylation and metal-binding proteins. Functional categories with fewer transcripts represented

included ‘cytoskeletal/motor’, ‘signaling’, ‘transmembrane/cell surface receptor’, and ‘transcription factor’. They then evaluated the mRNA within growth cones derived from earlier stage embryos grown in culture for 17 h, resulting in growth cones that were approximately 24 h younger than the ones previously evaluated. Significantly fewer mRNAs were detected in these younger growth cones, 171 genes with known function. The young growth cone transcriptome was significantly less diverse than that of the older growth cones. The majority of these transcripts could be functionally classified as involved in ‘protein synthesis’ and the major enriched pathway was ‘oxidative phosphorylation’. Of the transcripts in young growth cones 66% were also present in old growth cones, only 60 transcripts were exclusively detected in the young growth cones (Zivraj et al., 2010).

The growth cone is a unique functional subcellular compartment as compared to the axon but whether the growth cone transcriptome was distinct or reflected that of the axonal transcriptome was the next question they asked. Since the older growth cones had a more diverse transcriptome they used LCM to capture axons of similarly cultured older RCGs. They identified 5105 axonally localized mRNAs. Functionally there were many similarities between the axonal and growth cone transcriptomes, including functional enrichment for ‘protein synthesis’, ‘metabolic/glycolytic’, and ‘cytoskeleton/motor’, as well as the ‘oxidative phosphorylation’. Categories unique to the axons included ‘protein trafficking’, ‘protein folding’ and ‘cell-mediated immune response’. They then turned to evaluate the transcripts enriched in growth cones as compared to the axons. Twenty-eight genes were enriched in the growth cones, the majority had cytoskeleton-associated functions or were involved in protein synthesis. The 523 transcripts enriched in the axons over the growth cones included the ‘metabolic/glycolytic’ functional group and ‘transcription factors’ (Zivraj et al., 2010).

To compare the RGC growth cone transcriptome across species they collected embryonic mouse RGC growth cones by LCM after 24 h in culture. They identified 1800 annotated transcripts. They found moderate conservation between species of specific transcripts within growth cones which was enriched for ‘oxidative phosphorylation’ and ‘protein synthesis’, in particular ribosomal proteins, yet the mouse growth cones included several nuclear-encoded proteins of the mitochondrial ribosome.

Taken together their work suggests a dynamic transcriptome in the RGC growth cone that has age specific and species specific unique features with a moderate sized pool of potentially constitutive

mRNAs. The finding that young growth cones have a smaller transcriptome than older growth cones suggests that as growth cones mature they require an increase in the diversity of the locally synthesized proteins, potentially protein transport from the somata cannot produce a sufficiently rapid change in the local proteome of longer axons. Their work was somewhat restricted due to the limited annotation of the *X. laevis* genome at the time of the study. Notwithstanding, the similarities found between the *X. laevis* and mouse grown cone transcriptomes are consistent with previous findings.

In vivo CNS neurons

As previously pointed out cultured neurons must recover from the stress and injury associated with techniques to isolate them. Whether this has long term effects on the somatic or axonal transcriptome is unknown making it valuable to evaluate the axonal transcriptome *in vivo*. The ability to collect pure axonal RNA *in vivo* is significantly hindered by the extreme size differential between axons and the surrounding cells. Extensive brain mapping data can suggest areas that are enriched for axons but the ability to physically isolate axons from dendrites *in vivo* has not been developed, though some genetic tools exist to isolate the presynapse from the postsynapse. Intra-axonal translation in mature, uninjured neurons of the adult CNS has been difficult to unequivocally prove; dendrites rely on local translation and easily mask any contribution of axonal translation. Regions enriched for dendrites, axons and glial filaments are referred to as ‘neuropil’ and provide the best physical sites to enrich for axonal and dendritic transcripts *in vivo*.

Many forms of synaptic plasticity in the CA1 region of the hippocampus are translation dependent so deep sequencing was used to determine the transcripts within the neuropil of the adult rat CA1 area (Cajigas et al., 2012). The microdissected neuropil contained dendrites, axons, glia, a sparse population of interneurons and some blood vessels. They detected 8379 unique mRNAs enriched for genes classified in ‘synaptic function’, ‘myelin’ and ‘translation’. To enrich for transcripts within axons and dendrites they bioinformatically subtracted mRNAs identified in astrocytes, oligodendrocytes, interneurons, blood vessels, mitochondria and transcripts encoding nuclear proteins. The resulting list of 2550 transcripts represents the combined axonal and dendritic transcriptome of the adult rat hippocampal neuropil. These transcripts broadly represented most of the

biological functions known to occur in dendrites and axons. Specific to axons they found many mRNAs encoding canonical presynaptic proteins including proteins that function to structurally organize the presynapse and regulate presynaptic vesicle release.

This work was not able to quantify or differentiate the relative contribution of transcripts localized to the axons versus the dendrites so questions regarding the differences between the transcriptomes of these subcellular compartments remain. I suspect that there is a significant amount of overlap between these transcriptomes since both regions rely on local translation for cytoskeleton dynamics, ribosomal protein expression, and mitochondrial function. Differences might include neurotrophic and endocannabinoid receptors, implicated in modulating presynaptic function, or the protein subunits of post-synaptic glutamate and GABA receptors, the major neurotransmitters in this brain region.

Recently, a group developed a method to sequence the ribosome-bound mRNAs from the axons of mouse RGCs *in vivo* (Shigeoka et al., 2016). The RiboTag knock-in mouse (Sanz et al., 2009) uses cre-mediated recombination to replace the endogenous ribosomal protein L22 (*Rpl22*) allele to a human influenza hemagglutinin (HA) tagged allele. Shigeoka *et al* (2016) permanently labelled RGCs by mating RiboTag mice with Pax6-alpha-Cre mice to transiently express *cre* in neural progenitors of the peripheral retinal primordium. The axons of these cells terminate in the superior colliculus of the midbrain (SC) so dissection of this region followed by RNA immunoprecipitation (RIP) significantly enriched for ribosome bound mRNAs within the distal axons. They also prepared samples from the retinal ganglion somata. Electron microscopy demonstrated HA-tagged ribosomes in RGC axons and presynaptic terminals of embryonic (E17.5), neonatal (P0.5), young (P7.5) and adult animals so they evaluated axonally localized mRNA at these stages. They estimated that the optimized protocol captured approximately 40% of the total HA-tagged ribosome population. They confirmed, using an *in vitro* ribosome run-off protocol, that 85% of these purified ribosome-mRNA complexes were actively translating so they refer to their data as capturing the ‘axonal translatome’ (Shigeoka et al., 2016).

The landscape of the translatome was developmentally regulated. There was clear evidence of axonal translation within adult axons but the number of axonally translated mRNAs was highest in

neonatal axons and decreased with age. Axon enriched categories included ‘neuron projection’, the actin and microtubule ‘cytoskeleton’, ‘axon’, ‘synapse’, and ‘vesicle’, ‘oxidative phosphorylation’ and neurodegenerative disease pathways. Developmental changes in the translatome included categories associated with ‘morphogenesis’, ‘development’, ‘organization’, and transport at the embryonic and neonatal time points and at the young and adult time points ‘neuron remodeling’, ‘synaptic transmission’ and ‘plasticity’, and ‘metabolic’ processes.

An interesting finding of this work was evidence in younger axons of active translation to regulate axon pruning that was absent from adult axons. This suggesting that in mature, properly targeted, uninjured RGCs axon pruning mechanisms are locally silenced through mRNA trafficking or storage in ribonucleoprotein complexes that do not contain ribosomes. Secondly, they found evidence for differential translation of isoform-specific splice variants between the somata and axon such that one variant is axonally translated while the other was only detected in the RGCs. In fact, some of these axonal splice variants contained alternative amino acid sequences, absent from the somatic isoform, potentially pointing to altered protein function in axons. Lastly, they found evidence of ribosome-bound circular RNAs derived from three genes (*Rhobt3*, *Ubn2*, and *Ankrd12*) and were able to confirm this using RT-PCR without additional RNA amplification techniques.

The RiboTag mouse provides a unique genetic tool to capture and enrich for ribosome-bound mRNAs within heterogeneous material. The novel application of this allele in isolating axonally localized ribosomes and the associated mRNAs by Shigeoka *et al* (2016) support existing functions for axonal translation and suggest that differential trafficking of mRNA splice variants might mechanistically regulate some mRNA trafficking and axonal protein function. It is important to note that if glia-to-axon ribosome transport occurs in RGC axons astrocyte delivered ribosomes would not contain the HA-tagged RLP22 protein and would not be captured.

Conserved axonal transcriptome functions

Taken together these datasets clearly demonstrate the conserved enrichment for mRNAs encoding ribosomal proteins and factors regulating translation, nuclear encoded mitochondrial

proteins, cytoskeleton components, transport proteins and their regulators, as well as secreted proteins.

Intra-axonal translation

A large body of evidence from a number of *in vitro* model systems implicates intra-axonal translation in mechanisms during all stages of life. Local translation within the growth cone, a unique subcellular compartment at the tip of the axon, during axon guidance is well established. The related topic of local translation during axon growth and extension, in the context of development and regeneration following injury, is well accepted. Local translation during these processes, guidance and extension, have been thoroughly reviewed (Doron-Mandel et al., 2015; Jung and Holt, 2011; Jung et al., 2011; Wang et al., 2007). These topics will not be specifically covered in this review. I will focus on axonal translation in the context of the long term health of the neuronal cell body and axon, synaptic plasticity and axon-to-soma signaling following axon injury.

Nerve growth factor (NGF) was discovered in the late 1940's for its ability to regulate the survival, maturation and guidance of embryonic neurons in the chick PNS (Levi-Montalcini and Hamburger, 1951; Levi-Montalcini et al., 1954). Study of this prototypical neurotrophic factor and others led to the 'neurotrophic factor hypothesis' (Levi-Montalcini, 1987). It states: developing neurons compete with each other for a limited supply of neurotrophic factors secreted from target tissues; successful neurons survive while unsuccessful neurons die. The tenets of this hypothesis place the developmentally regulated mechanisms of neuron survival, axon guidance, axon maintenance/ pruning, as well as axon regeneration and reinnervation on the opposite side of the coin from the disease and disability of neurodevelopmental disorders, age related neurodegeneration and axon injury.

Cell viability and axon maintenance

Neuron cell death and axon pruning are necessary during the highly orchestrated process of neurodevelopment. The predictable neuroanatomical circuitry necessary for normal nervous system

function relies on removing unnecessary components but dysregulated cell death or axon degeneration can have a significant effect on health.

CREB-mediated pro-survival gene expression profile

DRG sensory neuron survival *in vitro* is dependent on axonal NGF signaling (Cox et al., 2008). There are two known NGF receptors, tropomyosine receptor kinase A (TrkA) and low-affinity neurotrophin receptor ($p75^{NTR}$) (Levi-Montalcini, 1987), both are tyrosine receptor kinases. Locally applied NGF stimulated intra-axonal translation of cyclic adenosine monophosphate (cAMP) response element binding protein (CREB) and this locally synthesized CREB was retrogradely transported to the nucleus, likely via microtubule motor-dependent active transport, to maintain a pro-survival gene expression profile. Further, this axonally synthesized CREB seemed to be the predominant source of transcriptionally active phosphorylated CREB (pCREB) required for the transcriptional profile (Cox et al., 2008).

NGF-stimulated local translation of IMPA1 has been implicated in SCG axon maintenance (Andreassi et al., 2010). *Impa1* encodes the protein inositol monophosphatase 1, a key enzyme in regulating the cellular availability of inositol which is a basic component or precursor to many intracellular messengers and membrane phospholipids. Interestingly a downstream of TrkA phosphatidyl inositol-3 kinase (PI3K)/ Protein kinase B (AKT) signaling is implicated in the translational response. The authors speculate that axonal IMPA1 might locally regulate membrane phosphoinositides and therefore have a role in lipid biosynthesis required for axon membrane stability, growth, vesicle trafficking and endocytosis. Predicting that axonally applied *Impa1* siRNA would negatively affect endocytosis and vesicle trafficking by disrupting lipid biosynthesis they evaluated nuclear pCREB which depends on NGF-TrkA internalization and retrograde transport; pCREB was significantly reduced (Andreassi et al., 2010).

In stark contrast to the axons of rodent sensory neurons from the DRG (Cox et al., 2008), *Creb* mRNA was not detected in SCG axons (Andreassi et al., 2010), suggesting significantly different mechanisms of NGF-stimulated pCREB nuclear accumulation in DRGs and SCGs. The pro-survival gene expression profile maintained through axonal NGF signaling has not been characterized.

Axonally translated mitochondrial proteins

Local protein synthesis is required for SCG axon maintenance *in vitro* (Hillefors et al., 2007). A 24 h blockade of axonal translation using three functionally distinct translation inhibitors (the cytosolic translation inhibitor cycloheximide; mitochondrial translation inhibitor chloramphenicol; cytosolic and mitochondrial translation inhibitor emetine) resulted in axon retraction with no detectable change in the fluidically isolated somata. Further, blocking local translation for 3 h was sufficient to reduce mitochondrial function as measured by the renewal of ATP stores following chemical axon depolarization. Blocking axonal mitochondrial protein transport, the mechanisms by which nuclear-encoded mitochondrial proteins are imported, reduced mitochondrial function. They verified the axonal localization of mRNA for three nuclear-encoded mitochondrial genes, including that of cytochrome C oxidase subunit IV (*Coxiv*) (Hillefors et al., 2007). In a follow up study they verified that local synthesis of COXIV is directly proportional to mitochondria function within the axon. Increased COXIV protein was associated with increased ATP levels and decreased COXIV protein was associated with reduced ATP levels. Further, axonal levels of *Coxiv* mRNA, protein and mitochondrial function could be regulated by axonal miR-338 (Aschrafi et al., 2008). Transport of *Coxiv* mRNA to the axon could be prevented with a competitive transgene carrying the *Coxiv* localization sequence resulting in decreased local ATP levels and increases in reactive oxygen species (ROS). Transgenic mice expressing the competitor in the forebrain had increased ROS in the forebrain and behavioral testing revealed an “anxiety-like” and “depression-like” phenotype (Kar et al., 2014).

Lamin B2 (LB2, gene *lmnb2*) was identified, using proteomic techniques, as axonally translated in *X. laevis* retinal ganglion cells (RGC) following stimulation by the guidance cue Engrailed-1 (Yoon et al., 2012). Beta type nuclear lamin (LB2) is one of three class V intermediate filament proteins that comprise the nuclear lamina inside the inner nuclear membrane with functions in nuclear stability and chromatin structure. It has also been identified in proteomic studies of mitochondria (Rezaul et al., 2005). Local synthesis of LB2 was required and sufficient for *in vivo* axonal maintenance of the retinal ganglion cell pathway. Axonal knockdown of LB2 resulted in axon degeneration without activating apoptotic signaling in the RGCs, suggesting the nuclear lamina was undisturbed. Further, an LB2 construct lacking the nuclear localization sequence was able to rescue

axon degeneration following local LB2 knockdown, further suggesting axonally synthesized LB2 did not primarily function in the nucleus. Axonal mitochondria morphology was altered and membrane potential was reduced following local Lamin B2 knockdown suggesting axonal LB2 is involved in mitochondrial function necessary for axon maintenance (Yoon et al., 2012).

Taken together this work demonstrates that neuron viability can depend on distal neurotrophic signals detected by the axon and converted to somatic signals through local protein synthesis. Further, axon maintenance relies on local translation-dependent mitochondrial function and implicates axonal microRNA mediated gene regulation. Reduced local mitochondrial function and compromised axon health might contribute to some neuropsychiatric diseases.

Axonal translation in synaptic plasticity

The current theory for the molecular basis of memory is synaptic plasticity, the strengthening or weakening of synaptic function. Synaptic plasticity includes changes in presynaptic neurotransmitter release, changes in postsynaptic responsiveness to neurotransmitter, synaptogenesis and synapse elimination. The requirement for protein translation to form memories, a process called memory consolidation, has been demonstrated *in vivo* for many memory pathways but not all. In rodents fear-condition context memory (Barrientos et al., 2002), spatial memory (Meiri and Rosenblum, 1998) and incentive-based behavioral modification (Wang et al., 2005) depend on new protein synthesis. Synaptic plasticity mechanisms involving changes in the postsynaptic neuron response to neurotransmitter have been shown to depend on local dendritic translation. One of the major obstacles to definitively demonstrating presynaptic translation in synaptic plasticity is isolating the presynapse from the postsynapse visually, pharmacologically and biochemically.

Long-term depression of synaptic activity

Indirect evidence of intra-axonal translation in long-term depression (LTD), a form of synaptic plasticity characterized by long term reduction in synaptic signaling, was demonstrated using *in vitro* slice preparation of the striatum brain substructure (Yin et al., 2006). Glutamatergic axons from the cerebral cortex synapse with GABAergic striatal neurons in the striatum. LTD can be induced *in vitro*

at these synapses by a high-frequency sequence of individual stimulations combined with postsynaptic depolarization (Calabresi et al., 1992). Through retrograde endocannabinoid (eCB) signaling the postsynaptic neuron induces a change in the presynaptic neuron resulting in reduced glutamate release (Choi and Lovinger, 1997), known as endocannabinoid-dependent LTD (eCB-LTD). The distance between the cortex and striatum allows the striatum to be definitively dissected removing the presynaptic soma while maintaining the glutamatergic axon to GABAergic neuron circuitry. Using adult rat striatum brain slice preparations they were able to induce LTD in the absence of the presynaptic somata. This *in vitro* LTD was blocked when the whole slice preparation was pretreated with the eukaryotic translation inhibitors cycloheximide or anisomycin, but not when cycloheximide was added after the LTD-inducing stimulus. To functionally isolate postsynaptic translation they intracellularly delivered cycloheximide or an mRNA-cap analog that blocks translation by competing for translation initiation factors. LTD was induced when only postsynaptic translation was blocked suggesting the presynapse was the site for critical translation. This effect was specific since blocking transcription in the whole slice preparation or the isolated postsynaptic neuron had no effect on LTD (Yin et al., 2006). Taken together their results implicate presynaptic protein translation to alter glutamate release following endocannabinoid signaling. Alternatively, the surrounding glial cells could be a key intermediary to the plasticity since they are known to express components of the endocannabinoid signaling pathway (Stella, 2009) and can function in synaptic plasticity (Todd et al., 2006).

In the non-mammalian leech, *Hirudo verbena*, the adult nociceptive ganglia exhibit eCB-LTD (Yuan and Burrell, 2013). The intact presynaptic and postsynaptic cells can be individually manipulated pharmacologically. Bath application of transcription and translation inhibitors implicated both mechanisms in this eCB-LTD system. Specifically evaluating the individual requirements of the postsynaptic and presynaptic cells they found that transcription and translation were required within the postsynaptic cell but only translation was required in the presynaptic cell. The rapid onset of synaptic plasticity and quantitative measurements of axonal protein transport makes it highly unlikely that somatic translation was sufficient. The authors suggested that presynaptic translation occurs locally within the axon or presynaptic component itself but were not able to demonstrate this (Yuan and Burrell, 2013).

The involvement of local axonal translation versus somatic translation was evaluated in endocannabinoid-dependent LTD in the rodent hippocampus (Younts et al., 2016). At GABAergic to glutamatergic synapses translation was only required during the induction of eCB-LTD. Once eCB-LTD was established it could be maintained long-term without the need for protein synthesis, suggesting stable changes to the synaptic proteome. Mechanistically, the mammalian target of rapamycin (mTOR) pathway was required for LTD. While mTOR signaling regulates a variety of downstream functions, including translation, ribosome biogenesis, metabolism, autophagy, the requirement for translation and mTOR signaling suggested mTOR activated protein synthesis. Using long-term paired electrophysiological recordings coupled with single cell pharmacological manipulation they ruled out involvement of postsynaptic translation. Turning to the presynaptic cell they compared the effect of the large molecule translation inhibitor gelonin, which has limited diffusion to axons, with the small molecule translation inhibitor 7-methyl-guanosine-5'-triphosphate-5'-guanosine (M7), an mRNA cap analog predicted to freely diffuse through the axon. M7 completely blocked LTD when loaded to the presynaptic cell for more than 60 min but gelonin loading for over 100 min had no effect on LTD. This supports a model of presynaptic endocannabinoid receptor activation followed by local axonal translation involving mTOR signaling (Younts et al., 2016).

These three systems all demonstrate a role of presynaptic translation in eCB-LTD suggesting that presynaptic endocannabinoid signaling might active translation across species and synapse types.

Long-term potentiation of synaptic activity

BDNF, a neurotrophin related to NGF, is required for long-term potentiation (LTP) within the adult hippocampus, specifically at the synapse between cells of the cornu ammonis 3 (CA3) region and cornu ammonis 1 (CA1) region (CA3-CA1 synapses). LTP, a persistent increase in the synaptic signal transmission between neurons, can be induced with electrical stimulation patterns or pharmacologically with BDNF. In hippocampal slice preparations extracellular bath application of BDNF enhanced CA3-CA1 synaptic transmission by a transcription-independent, translation-dependent mechanism (Kang and Schuman, 1996). Further, the translation-dependent effect on

synaptic transmission was maintained when either the presynaptic axons or the postsynaptic dendrites were severed from their somata. When both the presynaptic and postsynaptic somata were severed, completely insulating the synapse from somatic protein translation, synaptic transmission was still enhanced suggesting a completely local origin for the effect (Kang and Schuman, 1996). Many *in vitro* stimulation protocols that result in hippocampal LTP also induce BDNF secretion (Kang et al., 1997). BDNF signals through two receptors tropomyosine receptor kinase B (TrkB) and $p75^{NTR}$ and TrkB mutant mice have significantly dampened LTP response (Minichiello et al., 1999; Minichiello et al., 2002). BDNF mutant mice also have significantly reduced CA3-CA1 LTP, that can be rescued with bath application of recombinant BDNF (Patterson et al., 1996) or re-expression of BDNF via a virally delivered BDNF gene (Korte et al., 1996a; Korte et al., 1996b).

To investigate the relative contribution of presynaptic and postsynaptic BDNF-TrkB signaling cultured rat hippocampal neurons were genetically manipulated with a dominant-negative truncated TrkB gene delivered by adenovirus also carrying a GFP gene (Li et al., 1998). In this system a 3 minute BDNF treatment is sufficient to induce potentiation of synaptic signaling including greater stimulus-evoked synaptic transmission and frequency of spontaneous synaptic currents in the culture. The BDNF effect was absent from synapses where the presynaptic and postsynaptic cells expressed the mutant TrkB (GFP-positive). When the postsynaptic cell was transduced and the presynaptic cell was wild type synaptic signaling was potentiated but when the presynaptic cell expressed the mutant TrkB the BDNF effect was blocked (Li et al., 1998). This *in vitro* synapse model suggested presynaptic BDNF-TrkB signaling in LTP, whether it truly reflected mature neurocircuitry synaptic plasticity was unclear.

To evaluate *in vivo* TrkB signaling in organotypic slice circuits a TrkB mutant mouse with reduced TrkB protein was genetically manipulated to remove the TrkB gene from the CA1 (postsynaptic) neurons in the CA3-CA1 pathway (Xu et al., 2000). *In vitro* stimulated LTP could be induced in adult hippocampal slices but the magnitude of the persistent increase was reduced. The presynaptic CA3 neuron still expressed TrkB so they added a scavenger antibody to globally reduce TrkB signaling in the preparations, significantly reducing LTP, implicating TrkB signaling within the presynaptic CA3 neuron. They evaluated presynaptic function following LTP induction in the TrkB

mutant and the CA1 knockout mouse and found no significant difference between them, though both were reduced compared to wild type mice (Xu et al., 2000). This suggest that presynaptic BDNF-TrkB signaling in the CA3-CA1 synapse contributes to a sustained change in neurotransmitter release.

Having established that LTP following BDNF is presynaptically expressed and translation dependent the question turned to the cellular source of BDNF. CA3-CA1 BDNF induced LTP was evaluated in mutant mice with the *Bdnf* gene deleted from both the presynaptic and postsynaptic neurons were compared to CA1 only BDNF deletion mice (Zakharenko et al., 2003). LTP could not be established in adult hippocampal slice preparations using two different LTP-inducing stimulation protocols. The CA1 mutants demonstrated LTP following both stimulation protocols implicating presynaptic release of BDNF required for BDNF-LTP. *In vivo* stereotaxic microinjection of a Sindbis virus carrying the *Bdnf* gene when targeted to the CA3 somata but not the CA1 somata.

Taken together this body of work demonstrates that BDNF-LTP at the CA3-CA1 hippocampal synapse is modulated by presynaptic release of BDNF which functions in an autocrine manner to activate presynaptic TrkB signaling. Further, this rapid form of synaptic plasticity does not require transcription or the somata but does require local protein synthesis. A potential critical role of glial cells and a small population of GABAergic interneurons in BDNF-LTP cannot be completely ruled out though. While BDNF-TrkB induced protein synthesis within the presynapse or axon in BDNF-LTP was not been explicitly demonstrated in this work BDNF activates translational machinery and stimulates global protein synthesis in dissociated embryonic mouse cortical neurons through MAP kinase-interacting kinases (Genheden et al., 2015).

Synaptogenesis

There is only a small amount of direct evidence implicating presynaptic translation in synaptogenesis due to technical complications isolating the presynaptic component. There is a body of evidence demonstrating BDNF-induced synaptogenesis in hippocampal neurons where presynaptic translation is necessary for BDNF-induced LTP.

Hippocampal neurons from early embryonic rats (E16) cultured for 2 weeks rarely form functional synaptic connections, as measured by spontaneous and evoked synaptic activity, unlike

neurons derived from E18 rats which exhibit strong synaptic activity. Treatment with either BDNF or NT-3 for 24 h, 72 h or 2 weeks significantly increased the number of mature functional synapses in E16 cultures only. BDNF stimulated excitatory and inhibitory synaptogenesis while NT-3 was specific for excitatory synapses (Vicario-Abejon et al., 1998). In follow up work they evaluated the presynapse and postsynapse individually. BDNF and NT-3 significantly increased the number of synaptic vesicle within presynaptic terminals, detected by fluorescent microscopy and EM. Postsynaptic activity of E16 cultures could only be detected after drug treatment. Pharmacological blockade of postsynaptic neurotransmitter receptors or action potentials did not affect synaptogenesis suggesting key synaptogenic signaling occurred presynaptically (Collin et al., 2001). This work demonstrates that BDNF can increase the number of mature, functional glutamatergic synapses, and therefore synaptic transmission, through a presynaptic mechanism.

One mechanism by which BDNF increases the density of mature synapses is by destabilizing the presynaptic cadherin-β-catenin scaffold that organizes synaptic vesicles in pre-existing synapses possibly allowing mobilization of vesicles for capture during subsequent synaptogenesis (Bamji et al., 2006). In mature *in vitro* synapses BDNF lead to phosphorylation of β-catenin, transient disruption of the cadherin-β-catenin interaction and synaptic vesicle pool splitting. The result was a significant increase in the number of stable mature synapses and mobile synaptic vesicle clusters (Bamji et al., 2006). These results are consistent with aspects of the BDNF-LTP model, namely a presynaptic driven mechanism that has the potential to alter synaptic signaling long term.

There are many potential axonally synthesized proteins that could mediate BDNF-induced synaptogenesis and long-term potentiation. One potential target is β-catenin. Evidence suggests that presynaptic translation of β-catenin is necessary during the early stages of synaptogenesis, potentially to provide the increased demand for local β-catenin to stabilize synaptic vesicles at maturing synapses (Taylor et al., 2013). Secondly, β-actin and actin dynamics play a role in synaptogenesis (Dillon and Goda, 2005) and neurotransmitter release (Wolf et al., 2015) and local translational control of this pathway is well established in growth cones and dendrites (Jung et al., 2011; Jung and Holt, 2011; Shirao and Gonzalez-Billault, 2013). An additional target for consideration is growth associated protein 43 (GAP43). It is translated within DRG axons to regulate axon extension and branching (Donnelly et

al., 2013) and increased GAP43 phosphorylation following hippocampal LTP is directly correlated with the increase in synaptic function (Biewenga et al., 1996). Lastly, inhibition of intra-axonal translation, using a genetically-encoded constitutively-active translation inhibitor increased the size of synaptic vesicle clusters and increased synaptic vesicle release. Cyclin-dependent kinase 5 activator 1 (p35), a necessary activator of cyclin-dependent kinase 5 (Cdk5), was identified as axonally synthesized and critical for regulating synaptic vesicle dynamics, implicating axonal Cdk5 signaling in moderating synaptic vesicle clustering and release (Hsiao et al., 2014).

There is clear evidence for presynaptic translation in synaptic plasticity induced by presynaptic TrkB and endocannabinoid signaling and suggestive evidence for presynaptic translation in synaptogenesis. Techniques to visually, genetically or biochemically isolate the axon and presynapse from the postsynapse will facilitate investigating these mechanisms and identify relevant locally synthesized mRNA.

Axonal translation in injury signaling

Axon-to-soma signaling following axon injury likely employs multiple mechanisms, including a back-propagating action potential, cytoskeletal biophysical fluctuations and changes in retrograde transported molecules. Post-translational modification of transported proteins and complexes could change following injury or there could be quantitative differences in the molecules due to catabolic and anabolic axonal mechanisms. The relative contributions and integration of these signaling mechanisms might be different following different insults, including toxic events, metabolic changes or mechanical axon injury, called axotomy. A common model system for axon injury is sciatic nerve crush, which injures sensory neurons of the DRG.

While the role of axonal translation in axon regeneration following injury is well understood, and the translation of many specific mRNA targets have been described and functionally characterized, less is known about the axonally translated proteins involved in signaling to the soma following distal injury of the axon.

Peripheral nerve injury

Nuclear proteins have an amino acid encoded ‘nuclear localization sequence’ (NLS) to traffic the protein to the nucleus following translation. The importin protein family are a group of proteins that bind the NLS to ensure nuclear import. Importin α/β heterodimers have high affinity for the NLS and facilitate transport of NLS-containing proteins through the nuclear pore complex (Cautain et al., 2015). Many importin-α family members were detected in dissected sciatic nerves but importin-β protein was only detectable after mechanical crush injury (Hanz et al., 2003). Importin-β mRNA was detected in uninjured axons and the injury-induced increase in importin-β protein was dependent on local protein synthesis. This locally synthesized importin-β was implicated in axon-to-soma transport of NLS-containing axonal proteins which was critical for axon regeneration *in vitro* and *in vivo* (Hanz et al., 2003). Further, a conditional knockout mouse missing the axonal localization sequences within the importin-β mRNA had reduced importin-β protein in the sciatic nerve. These animals demonstrated a significant change in the DRG transcriptional response following sciatic nerve crush and had a significant delay in rehabilitation after injury (Perry et al., 2012). Additionally, axon injury of cultured DRGs induced calcium-dependent local translation of RanBP1, an effector of Ran GTPase. Axonal RanBP1 was implicated in activating Importin-β mediated, dynein-driven axon-to-soma signaling necessary at the time of injury to stimulate axon outgrowth hours and days later (Yudin et al., 2008).

This body of work demonstrates a critical role for local translation of components and regulators of importin-mediated axon-to-soma transport of NLS-containing proteins following axotomy. This raises the question: what cargo is transported by this mechanism after injury? The demonstration that the injury-induced transcriptional response was altered in the importin-β knockout mouse suggests axonally localized transcription factors could be responsible.

The signal transducer and activator of transcription (STAT) family of transcription factors was bioinformatically identified as a likely to participate in retrograde injury signaling in DRGs (Ben-Yaakov et al., 2012). STAT transcription factors are canonically activated by receptor-associated Janus kinase (JAK) phosphorylation. Three STAT family members were identified in axons but only STAT1 and STAT3 were phosphorylated following injury. Phosphorylated STAT1 was only detected in axons while phosphorylated STAT3 was in axons and somata, suggesting that only STAT3 was transported to the

nucleus. STAT3 was locally translated within injured axons by a calcium-dependent mechanism and phosphorylated STAT3 interacted with dynein. Activated STAT3 axon-to-soma transport appeared to promote DRG neuron survival *in vivo* following sciatic nerve crush (Ben-Yaakov et al., 2012).

CNS injury

There are few models to study axonal injury signaling in mammalian CNS neurons. *In vivo* models are not optimal for investigating the immediate axonal events so relevant *in vitro* models are necessary. A recently developed *in vitro* mechanical axon injury model of microfluidically isolated axons (Taylor et al., 2005) has been used to investigate the axonal transcriptome of regenerating CNS neurons (Taylor et al., 2009). An *in vitro* model of Alzheimer's has been recently developed employing microfluidically isolated rat hippocampal neurons treated with a β-amyloid peptide (Aβ). Somatic apoptosis in this model depended on axonal translation of activating transcription factor 4 (ATF4). Axonally translated ATF4 was retrogradely transported to the somata to initiate the cell death cascade *in vitro* and *in vivo* (Baleriola et al., 2014). Interestingly, Aβ treatment significantly increased the amount of ATF4 mRNA in axons suggesting Aβ peptide injury signaling primes the axon for a robust ATF4 translational response.

Much more work is necessary to better understand pro-survival and apoptotic signaling following distal axon injury. General mechanism of injury signaling might be shared throughout the nervous system, such as calcium-stimulated local translation, importin-dynein transport complexes and local translation and/ or activation of transcription factors. The specific transcription factors transported are likely neuron and injury specific to initiate proper survival and regeneration pathways or cell death pathways. The CNS injury induced gene expression profile has been investigated *in vivo* capturing the combined transcriptional response of the heterogeneous cellular environment. The specific transcription response of neurons has not been investigated.

Axon injury work has focused on the short-term local neuronal response to the initial primary axon injury, with a therapeutic eye to axon regeneration and reinnervation. There is clear evidence of progressive long-term secondary loss of function, far from the injury site. The complex primary injury *in vivo* involves neurons, glia, and blood vessels, with immediate small scale hemorrhage and hypoxia.

Some aspects of the *in vivo* injury response are beneficial and necessary to repair cerebral circulation while other aspects lead to widespread functional changes within the brain. These primary and secondary injuries in the CNS, following stroke and blunt trauma to the brain and spine, contribute to the disability and mortality of these conditions. Currently, we do not understand the molecular events and biochemical messengers of the secondary injuries well enough to develop targeted pharmacological therapeutics specific for the detrimental aspects while minimizing interference with beneficial aspects of the injury response.

Dissertation goals

My studies establish that mRNAs are present within the axons of human embryonic stem cell derived neurons (hESC-neurons) and I investigate transcription-dependent secondary effects of mechanical axon injury using an *in vitro* axotomy model.

In Chapter Two, I demonstrate that the long projections of hESC-neurons are axon-like by immunofluorescence and contain mRNA. The hESC-neuron axonal transcriptome is significantly different from the somatic transcriptome. Enriched functional Gene Ontology categories that describe the hESC-neuron axonal transcriptome are similar to the categories that describe axonal transcriptomes of primary rodent neurons. Further, by multiplexed single molecule RNA-FISH I demonstrate the presence of β-actin, GAP43 and oxytocin mRNA within hESC-neuron axons. This evidence supports the use of hESC-neurons as a model system to further investigate mechanisms establishing and modifying the human axonal transcriptome and the function of local translation within human axons.

In Chapter Three, together with the post-doctoral researcher Dr. Tharkika Nagendran, secondary injury signaling is investigated. I evaluate the effect of sparse direct axotomy to cultured primary rat neurons grown in two-compartment axon-isolating microfluidic chambers. Directly injured axons can regenerated *in vitro* and axotomy does not affect culture viability. I demonstrate that the percentage of cells with axons entering the isolated compartment is inversely related to the length of the microgrooves and these cells are most likely to be within 500 µm of the microgrooves. Axotomy induces delayed but persistent secondary functional change in the *in vitro* neural network that is

dependent on a transcriptional response generated within the first hour after injury. Gene expression 24 hours after *in vitro* axotomy is broadly similar to gene expression 24 hours after *in vivo* injury and suggests altered expression of proteins that function at the synapse might mediate secondary injury signaling.

CHAPTER TWO: MESSENGER RNAS LOCALIZED TO DISTAL PROJECTIONS OF HUMAN STEM CELL DERIVED NEURONS

INTRODUCTION

Local translation within the axons and dendrites of neurons is involved in multiple neuronal functions, including axon maintenance, guidance, synaptogenesis, post- and presynaptic plasticity and response to injury (Donnelly et al., 2010; Holt and Schuman, 2013; Kelly et al., 2000; Lyles et al., 2006; Younts et al., 2016). Specific mRNAs implicated in these functions, distal from somata, have been experimentally identified in *Aplysia* sensory neurites, rodent peripheral and central neurons, and other model systems (Aschrafi et al., 2008; Goldman et al., 2013; Lyles et al., 2006; Merianda et al., 2015; Shigeoka et al., 2016; Taylor et al., 2013). In axons and synapses, local translation may be critical for spatially restricted and rapid responses to extracellular signals such as glutamate, brain derived neurotrophic factor, neurotrophin-3 and netrin-1 (Genheden et al., 2015; Goldman et al., 2013; Hsu et al., 2015; Kang and Schuman, 1996; Welshhans and Bassell, 2011).

Comparing axonal transcriptomes of various neuronal subtypes has the potential to highlight conserved roles of intra-axonal translation and reveal unique functions and targets within each neuron type. Direct evaluation of primary human neurons is severely restricted due to the limited ability to obtain tissue or culture isolated neurons. Human stem cell derived neurons are a biologically relevant and tractable *in vitro* system and protocols have been developed to differentiate stem cells into specific neuronal subtypes, such as motor, striatal, dopaminergic and glutamatergic neurons (Baronchelli et al., 2015; Duan et al., 2015; Hu et al., 2015; Li et al., 2009; Reddington et al., 2014; Sagal et al., 2014). Here we sought to identify the transcriptome of the distal projections of human embryonic stem cell derived neurons enriched for glutamatergic lineage (Li et al., 2009; Zeng et al., 2010) and compare this transcriptome to the axonal transcriptome of glutamatergic rodent neurons.

MATERIALS AND METHODS

Microfluidic chambers

Custom microfluidic chambers were fabricated by soft lithography using an established protocol (Taylor et al., 2005) with the following modifications. The somatic and axonal compartments of these chambers were 2 mm by 7 mm by 450 µm tall. These compartments were connected by microgrooves of 450 µm by 10 µm by 3 µm tall. The only dimension different from previously published microfluidic chambers (Taylor et al., 2009) was the compartment height, which was increased to facilitate the daily media changes necessary to meet the nutrient demands of hESC-neurons. To create the tall cell compartments a thick layer of photoresist (SU-8-2050; Microchem) was spun on the wafer in 2 coatings. Each coating was spun at 800 rpm for 45 s, the first coating was baked on a leveled 95 °C hot plate for 3 h and the second coating was baked for 5 h. Wafers were UV-exposed (1000 mJ total over 3 sessions with at least 45 s between exposures) and baked for 1 h in a leveled 95 °C oven. Finally wafers were gradually cooled to room temperature over 30 minutes and developed in propylene glycol methyl ether acetate (PGMEA).

The resulting masters were used to cast microfluidic chambers using poly(dimethylsiloxane) (PDMS) (Sylgard 184 Silicon Elastomer, Dow Corning) as described previously(Taylor et al., 2003). German glass coverslips were sterilized and coated overnight with a solution of 500-550 kDa poly-D-lysine/laminin (80 µg/ml and 10 µg/ml, respectively), washed and dried. Microfluidic chambers were assembled from PDMS devices and coated coverslips.

Maintenance and differentiation of hESC-neurons

Stem cell differentiation into neural progenitor cells (neuroepithelial cells) was performed according to previously published modifications of the original protocol (Li et al., 2009; Niedringhaus et al., 2015; Zeng et al., 2010). Days *in vitro* (DIV) numbering began when H9 human embryonic stem cells were plated in embroid body media to induce neuronal differentiation.

Maturation of hESC-neurons in microfluidic chambers

On DIV24 mitotic neural progenitor cells were manually lifted and dissociated manually or with Accutase (Life Technologies). Approximately $5x10^3$ cells were seeded into the somatic compartment of microfluidic chambers in N2B27 media supplemented with 100 ng/ml human recombinant brain derived neurotrophic factor (BDNF). Neural progenitor cells continued to divide during the differentiation period until becoming senescent neurons. Half of the media (100 µl) from each compartment was changed daily and cells were matured for at least 35 days (DIV59). This protocol has been demonstrated to generate glutamatergic neurons as early as DIV25, as verified by staining for the telencephalic transcription factor FOXG1, the transcription factor CTIP specific for subcerebral projection neurons, the glutamatergic transcription factor TBR1 and the glutamatergic marker protein VGLUT1 (Li et al., 2009; Zeng et al., 2010).

Immunocytochemistry

Human ESC-neurons grown in axon isolating microfluidic chambers were fixed with freshly prepared 4% paraformaldehyde in PBS containing 40 mg/ml sucrose, 1 µM MgCl2, and 0.1 µM CaCl2 for 45 min. Neurons were permeabilized in 0.25% Triton X-100 for 15 min then blocked in PBS containing 10% goat serum for 15 min. Staining conditions and antibodies used are summarized in Tables 2.1 and 2.2. Primary antibodies were diluted in PBS with 1% goat serum and incubation overnight at 4 °C. All Alexa Fluor conjugated secondary antibodies were raised in goat, diluted 1:1000 in PBS and incubated for one hour at room temperature. Cells were counterstained with 71.5 µM 4',6-diamidino-2-phenylindole (DAPI) in PBS.

Table 2.1 Primary antibody concentrations

Primary Antibody	Raised In	Source	Concentration
β-tub III	chicken	Aves Labs, TUJ	1:2000
β-tub III	rabbit	Abcam, ab6046	1:1000
MAP2	rabbit	Millipore, AB5622	1:1000
MAP2	mouse	Sigma, M4403	1:1000
GFAP	rabbit	Millipore, AB5804	1:1000
Nestin [10C2]	mouse	Abcam, ab22035	1:1000

VGLUT1	mouse	NeuroMab, 75-066	1:200
GAD67	chicken	Aves Labs, GAD	1:2000

Table 2.2 Secondary antibody concentrations

Species recognized	Fluorescent dye	Source
Chicken	488	Invitrogen, A11039
Mouse	488	Invitrogen, A11029
Rabbit	488	Invitrogen, A11034
Mouse	568	Invitrogen, A11031
Rabbit	568	Invitrogen, A11036
Chicken	647	Invitrogen, A21449
Rabbit	647	Invitrogen, A21245

RNA-FISH

Affymetrix ViewRNA ISH Cell Assay kit was used for multiplexed visualization of β-actin, oxytocin and growth associated protein 43 (GAP43) mRNA in human ESC-neurons grown in axon isolating microfluidic chambers. Commercially available ViewRNA Probe Sets were used to detect human β-actin mRNA (Affymetrix, VA4-10293) and GAP43 mRNA (Affymetrix, VA6-13097) and a custom probe was designed by Affymetrix to detect human oxytocin mRNA (Affymetrix, VA1-20398). The same staining procedure was used for the negative control samples, but without the RNA-FISH probes. All steps were performed in a humidified chamber protected from light and all solutions were made with DNase, RNase free molecular biology grade water (Sigma). Affymetrix ViewRNA ISH Cell Assay procedure was followed with some adjustments to preserve and fix the long projections to the coverglass, as outlined in Table 2.3.

Table 2.3 ViewRNA ISH Cell Assay procedure

Solution	Duration	Temperature	Repetition	Protocol adjustment
PBS	Brief rinse	RT	2	
4% PFA, 40 mg/ml sucrose, 1 µM $MgCl_2$, 0.1 µM $CaCl_2$ in PBS	30 minutes	RT	single	Freshly prepared, Modified for neurons
PBS	Brief rinse	RT	3	

50% Ethanol	2 minutes	RT	Single	Optional step
70% Ethanol	2 minutes	RT	Single	Optional step
100% Ethanol	2 minutes	RT	2	Optional step
70% Ethanol	2 minutes	RT	Single	Optional step
50% Ethanol	2 minutes	RT	Single	Optional step
PBS	10 minutes	RT	Single	Optional step
Detergent QC	5 minutes	RT	Single	
PBS	Brief rinse	RT	2	
Protease	10 minutes	RT	Single	1:5000, experimentally determined to be optimal
PBS	Brief rinse	RT	3	
Probe set	3 hours	40 °C	Single	Probes omitted for negative controls
Wash buffer	2 minutes	RT	3	
PreAmplifier mix	30 minutes	40 °C	Single	
Wash buffer	2 minutes	RT	3	
Amplifier mix	30 minutes	40 °C	Single	
Wash buffer	2 minutes	RT	3	
Label probe mix	30 minutes	40 °C	Single	
Wash buffer	2 minutes	RT	2	
Wash buffer	10 minutes	RT	Single	
DAPI	5 minutes	RT	Single	Increased duration
PBS	Brief rinse	RT	2	

Modified rabies virus infection

The axonal compartment of DIV61 cultures were incubated with approximately 100,000 viral units of modified rabies virus carrying the mCherry gene (Wickersham et al., 2007a) in a total of 50 µl media for 2 hours at 37 °C, washed twice with fresh media and live imaging was performed 48 hours

later. We have observed within 48 hours this viral load results in detectable mCherry expression within 80-85% of hESC-neuron axons in microfluidic chambers. Similar observations were made with primary embryonic rat hippocampal neurons grown in axon isolating microfluidic chambers.

Confocal imaging

Z-stack fluorescent images and single plane differential contrast (DIC) images were acquired using a spinning disk confocal imaging system (Revolution XD, Andor Technology) configured for an Olympus IX81 zero-drift microscope and spinning disk unit (CSU-X1, Yokogawa). Light excitation was provided by 50 mW, 488 nm; 50 mW, 561 nm; and 100 mW, 640 nm lasers. The following bandpass emission filters (BrightLine, Semrock) were used: 525/30 nm (TR-F525-030), 607/36 nm (TR-F607-036), 685/40 nm (TR-F685-040). All slides within a series were imaged during a single session in which image capture settings were identical for all fields.

Image analysis

Z-stack fluorescent images were MAX projected. 16-bit images were manually thresholded to the same values within each series of stained chambers. Montage images were stitched using the ImageJ plugin Stitching (Preibisch et al., 2009) available in the Fiji imaging processing package.

Determination of differentiation efficiency

Seven fields of hESC-neurons in monolayer from 4 independently stained chambers of at least DIV39 were used to estimate the efficiency of differentiation to mature hESC-neurons as detected by co-localization of DAPI signal with MAP2 or β-tubulin III positive staining. Three fields from two independently stained chambers of at least DIV49 were used to evaluate Nestin, GFAP, VGLUT1 and GAD67 immunofluorescence.

RNA isolation

On DIV59 RNA was isolated from microfluidic cultures using the RNAqueous-Micro Kit (Ambion) as previously described (Taylor et al., 2009). To collect RNA from the axonal compartment continuous aspiration was applied to the somatic compartment to prevent somatodendritic RNA from entering the sample. Most of the axonal media was removed and lysis buffer was added to one well, the reagent that flowed to the other axonal well through the axonal compartment was collected as the RNA of distal projections. Neuronal RNA was collected from the somatic compartment of hESC-neurons grown in microfluidic chambers not used for axonal RNA collection, this compartment contained somata, dendrites and axons which did not pass through the microgrooves. The majority of the media from the somatic compartment was removed and the same RNA isolation procedure was followed, omitting constant aspiration. Subsequent RNA purification was performed according to manufacturer's instructions and RNA was eluted in a final volume of 10 µl. Each sample was obtained from one microfluidic chamber. Samples were stored at -80°C until further processing by the UNC Lineberger Comprehensive Cancer Center Genomics Core and the UNC School of Medicine Functional Genomics Core. Three axonal and three neuronal samples were collected and analyzed.

RNA amplification and microarray

RNA of distal projections harvested from microfluidic chambers is below the detection limit of currently available technology. A fixed volume of each axonal RNA sample (5 µL) and a fixed mass of each neuronal RNA sample (250 pg) were subjected to one round of linear amplification using the Ovation One-Direct System (NuGEN). This system initiates amplification at the 3' end as well as randomly throughout the transcript and is optimized for very small biological samples such as single cell transcriptomics. The integrity and concentration of the resulting cDNA samples were quantified with an Agilent Bioanalyzer 2100 at the UNC Lineberger Comprehensive Cancer Center Genomics Core. A fixed concentration of amplified cDNA from all samples, including the 10 pg neuronal sample, were processed in parallel for microarray analysis using the Encore Biotin Module (NuGEN) at the UNC School of Medicine Functional Genomics Core.

Human Gene 2.0 ST Arrays (Affymetrix) were used and scanned with an Affymetrix GeneChip Scanner 3000 7G Plus with Autoloader. Affymetrix Expression Console v1.4 software was used to analyze microarray CEL files. Affymetrix normalization controls, built into the microarray chips and analysis software, were used for raw data normalization. The Robust Multichip Analysis (RMA) algorithm was used for global background adjustment, quantile normalization and gene expression summarization between samples. This method is sensitive to small changes between samples without negatively affecting signal variance. Affymetrix Transcriptome Analysis Console v2.0 software algorithms were used to determine differential expression and statistical analysis using one-way between-subject ANOVA of normalized intensities.

Data analysis

Microarray probe sets with fold change linear (Axon vs Neuron) greater than or equal to 1.5 and an ANOVA p-value (Axon vs Neuron) less than 0.05 were designated the enriched fraction (3943 probe sets). Probe sets with fold change linear (Axon vs Neuron) less than or equal to -1.5 and an ANOVA p-value (Axon vs Neuron) less than 0.05 were designated the depleted fraction (3631 probe sets). The fold change threshold of 1.5 was selected to counter balance the compressed calculated fold change values obtained by the RMA method. This threshold generated gene symbol lists of an appropriate size for DAVID Functional Annotation Clustering. For each subset of the data official gene symbols were extracted, duplicates were removed and gene symbol lists (3297 unique gene symbols in the enriched fraction and 3638 unique gene symbols in the depleted fraction) were submitted to DAVID Bioinformatics Resources for Gene ID Conversion and Functional Annotation Clustering with the single species Homo sapiens selected and the default human background list (Huang da et al., 2009a; Huang da et al., 2009b).

To obtain a gene symbol list of most abundant transcripts within hESC-neuron distal projections microarray probe sets with Axon bi-weight average signal (log2) equal to or greater than 6.48 were selected. This threshold excluded known dendritic transcripts and included β-actin, a well characterized axonal mRNA. These criteria were similar to those used by Taylor et al. (2009) to determine axonal mRNAs within primary rat cortical neurons. Official gene symbols were extracted,

duplicates were removed and the gene symbol list (3696 gene symbols) was submitted to DAVID Bioinformatics Resources for Gene ID Conversion and Functional Annotation Clustering with the single species Homo sapiens selected and the default human background list (Huang da et al., 2009a; Huang da et al., 2009b).

Data availability

The raw microarray data (CEL and CHP files) and gene expression data has been submitted to the NCBI Gene Expression Omnibus under accession number GSE84975.

RESULTS

Differentiation of human embryonic stem cell derived neurons in microfluidic chambers

To identify transcripts within human projections we first modified an existing microfluidic chamber design for compartmentalizing and harvesting pure axons, originally developed for murine neurons (Taylor et al., 2005). To optimize the growth of hESC-neurons, which have an increased nutrient demand compared to primary rodent neurons, we increased the height of the fluidically isolated compartments to provide a greater volume of media surrounding the cells. In these microfluidic chambers, neurons were seeded in the “somatic” compartment and stochastic neurite development and growth resulted in processes passing through the 450 µm long microgrooves to the “axonal” compartment (Fig. 1A). Similar chamber designs have been used to characterize the axonal transcriptome of primary rat cortical neurons (Taylor et al., 2009).

Differentiation of hESC-neurons (Fig. 2.1A), according to an established protocol to enrich for functionally matured glutamatergic neurons that produce action potentials after approximately 6 weeks of differentiation (Li et al., 2009; Zeng et al., 2010), began when hESC maintenance media was replaced with differentiation-inducing media, designated days in vitro (DIV) 0. On DIV24 neural progenitor cells (NPC) were transferred to our custom microfluidic chambers and matured to hESC-neurons over the next 30 day (>7 weeks in culture total, Fig. 2.1B). As early as DIV39 long neurites could be seen in the microgrooves. Microtubule-associated protein 2 (MAP2) and neuron-specific

class III β-tubulin (β-tubulin III, βtub) staining, markers for cell bodies/dendrites and neurons inclusive of axons, respectively, suggest that the majority of neurites entering the axonal compartment are axon-like (Fig. 2.1C). The dendrites of *in vitro* matured primary human neural progenitor cells cultured for 12 weeks never exceeded 80 µm in length (Stein et al., 2014) supporting our conclusion that it is unlikely these long projections are dendrites.

Figure 2.1

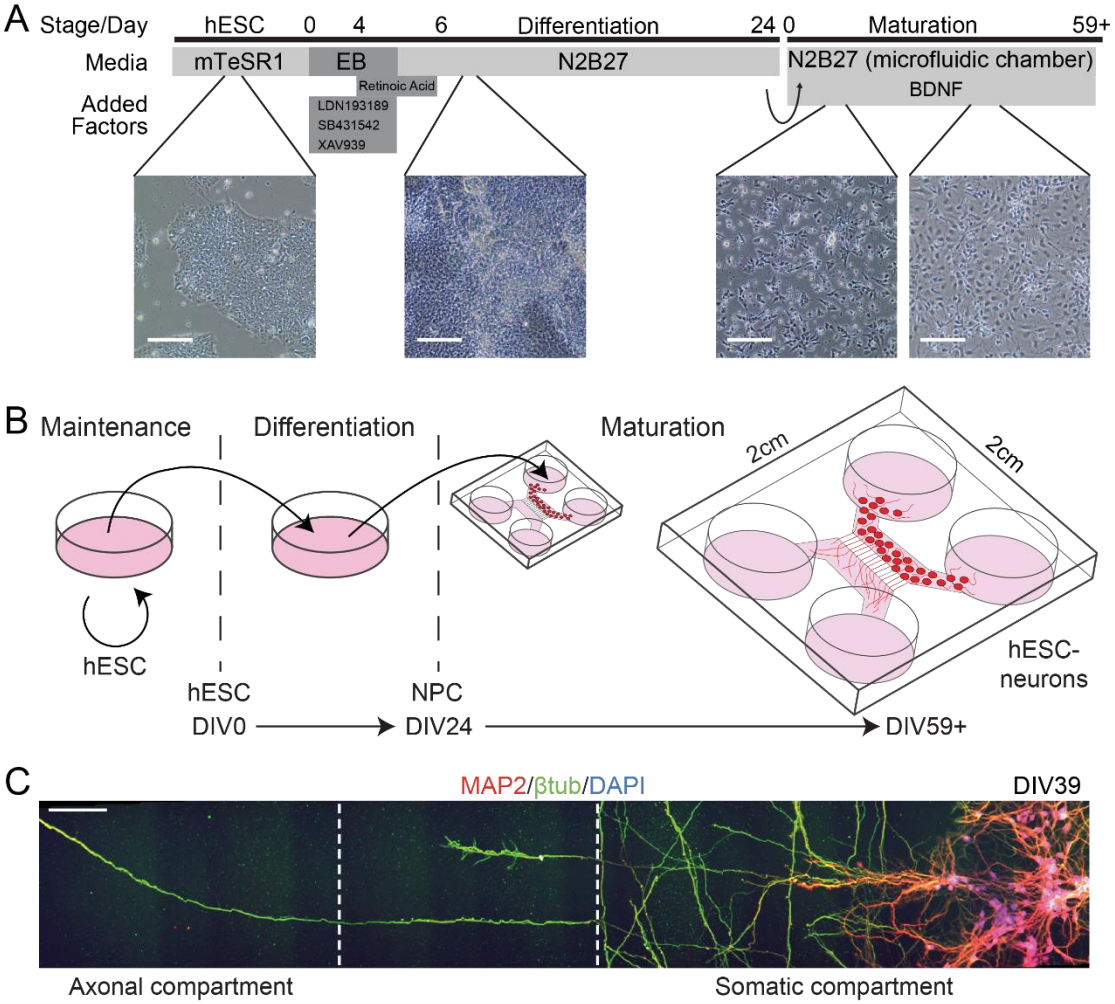

Figure. 2.1. Human embryonic stem cell derived neurons (hESC-neurons) matured in axon-isolating microfluidic chambers.
A. Schematic and timeline of the hESC-neuron differentiation and maturation protocol with images to demonstrate cell morphology at four time points, scale bars 100µm.
B. Diagram depicting the plating of neural progenitor cells (NPC) in the somatic compartment of axon-isolating microfluidic chambers and their maturation to hESC-neurons while the nascent axons extend through the microgrooves into the axonal compartment.
C. Representative montage image of MAP2 (red, dendrites), βtub (green, axons, β-tubulin III) and DAPI (blue, nuclei) immunostaining spanning the somatic and axonal compartments of DIV39 hESC-neurons cultured within a microfluidic chamber. White dashed lines delineate the boundaries of the microgroove barrier, scale bar 100µm.

β-tubulin III staining revealed extensive neurite growth within the axonal compartment at DIV59 (Fig. 2.2A) as well as healthy growth cones (Fig. 2.2B). After five weeks in culture, some clustering of somata occurred (Fig. 2.2A and Fig. 2.2E), as is common in long term cultures of hESC-neurons. Cells demonstrated neuron arborization as revealed by MAP2 staining (Fig. 2.2C). This

differentiation protocol, by DIV49, produced mainly neurons with only rare NPCs or astrocytes [nestin and glial fibrillary acidic protein (GFAP), respectively] (Table 2.4). Almost 40% of the cells expressed the glutamatergic marker vesicular glutamate transporter 1 (vGLUT1) while cells were rare that expressed the GABAergic marker glutamate decarboxylase, 67 kDa (GAD67) (Table 2.4). This differentiation efficiency and subtype enrichment were consistent with published hESC-neuron differentiation protocols (Lu et al., 2016).

Table 2.4 Evaluation of differentiation efficiency and glutamatergic enrichment

Cell identity (IF target)	Neuron (βtub and/or MAP2)	NPC (Nestin)	Astrocyte (GFAP)	Glutamatergic (vGLUT1)	GABAergic (GAD67)
n = (fields)	7	4	3	3	3
Positive cells	198	19	27	128	12
DAPI nuclei	209	501	724	333	516
%	94.74%	3.79%	3.73%	38.44%	2.33%

To further evaluate the composition of neurites extending into the axonal compartment, we tested whether a modified rabies virus incapable of trans-synaptic transmission and carrying the mCherry gene (Wickersham et al., 2007a) could infect hESC-neurons when applied exclusively to the distal neurites within the axonal compartment. Rabies virus infection requires endocytosis and retrograde transport of viral particles following attachment to one of three axonal receptors: nicotinic acetylcholine receptor, neuronal cell adhesion molecule or $p75^{NTR}$ (Lafon, 2005). The modified rabies virus was added to the axonal compartment of hESC-neuron cultures on DIV62 for 2 hours. Within 48 h fluorescent protein expression can be detected throughout the cell, including the axons and dendrites. Live imaging was performed to visualize the fine processes and fluorescent protein expression throughout hESC-neurons within the microfluidic chamber (Fig. 2.2E). Our data show that distal projections of hESC-neurons contain axonally-localized receptors sufficient for rabies viral infection. Taken together, these data support our conclusion that the vast majority of the distal projections in the isolated axonal compartment were axon-like.

Figure 2.2

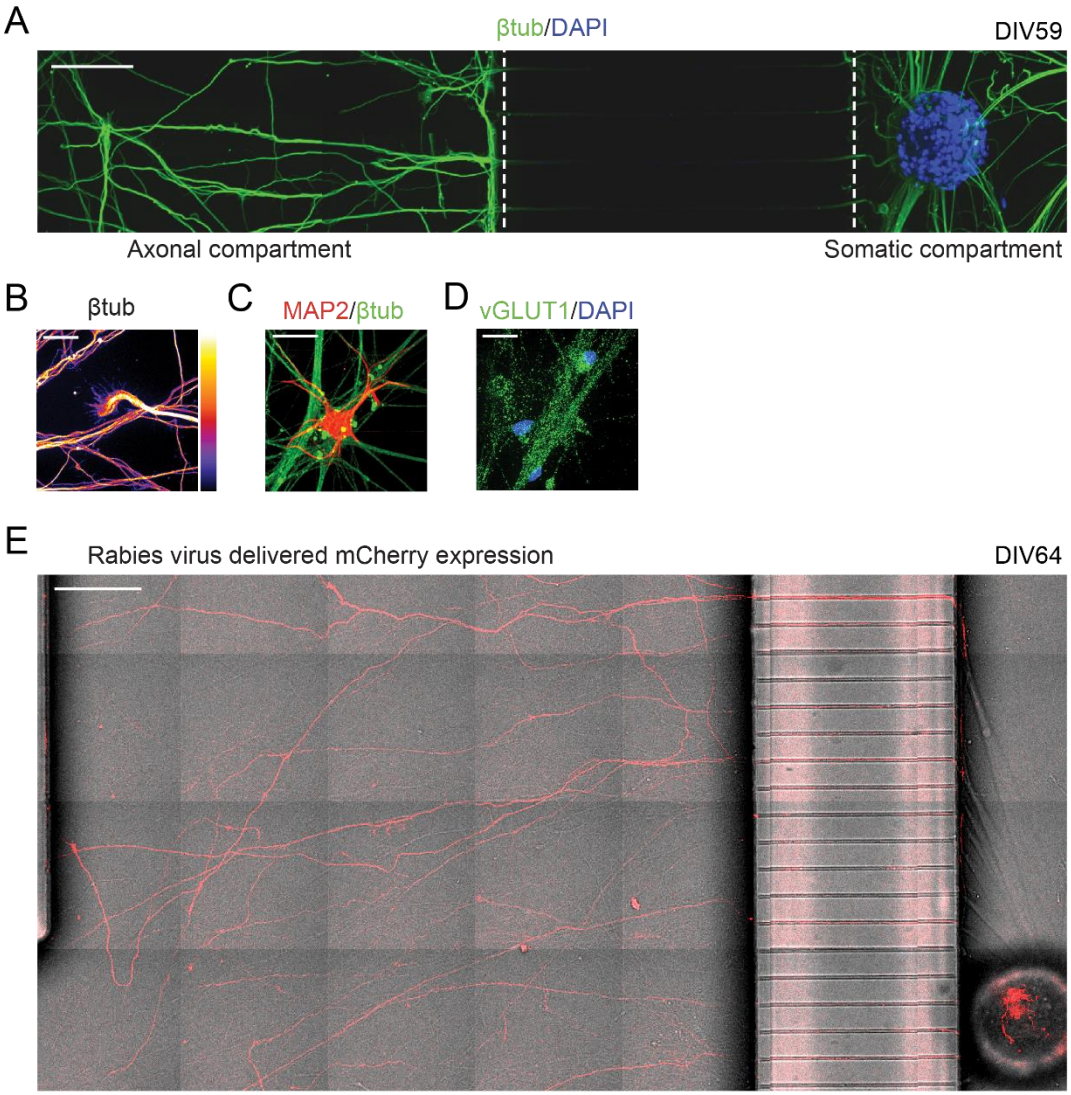

Figure. 2.2. hESC-neurons demonstrate common neuronal features.
A. Representative montage image of β-tubulin III immunostaining of distal projections in the axon compartment on DIV58. Somata demonstrate clustering as is common in long term *ex vivo* rodent neuron cultures, scale bar 100µm.
B. Image of a β-tubulin III immunostained hESC-neuron growth cone within the axon compartment, "Fire" LUT pseudocolor pixel intensity of 0 as black and 255 as white, scale bar 25µm.
C. hESC-neurons exhibited dendritic arborization revealed by MAP2 immunostaining, scale bar 25µM.
D. Matured hESC-neurons were positive for the glutamatergic marker vGLUT1, scale bar 25µm.
E. A modified rabies virus encoding the mCherry fluorescent protein was applied to the axonal compartment for 2 hr to infect neurons with axons extending into the axonal compartment and imaged 2 days after infection on DIV64, scale bar 200µm.

Differential gene expression between axons and neurons derived from hESCs

On DIV58, after more than 8 weeks in culture, we harvested total RNA from hESC-neurons and isolated neurites within the somatic and axonal compartments of microfluidic chambers (referred to as “neuron” and “axon” samples, respectively). The ‘neuron’ samples included somata, dendrite- and axon-like projections. The ‘axon’ samples were stringently scrutinized by light microscopy to ensure no somata were present in the axonal compartment. The amount of RNA harvested from the axonal compartment of an individual microfluidic chamber was below detection limits, therefore one round of linear cDNA amplification was performed on a fixed volume of RNA and a fixed mass of neuronal RNA. As a control reaction 10 pg of neuronal RNA was subjected to linear amplification in parallel. The amount of cDNA generated in this reaction suggested that the RNA yield within the axonal compartment was 1.9 ± 0.49 pg/µL (mean ± SEM, Table 2.5).

Table 2.5 Calculated RNA yield from axonal compartment

	Water (background)	**Neuronal RNA (control)**	**Axons 1**	**Axons 2**	**Axons 3**
[1] Amplification yield (ng/µl)	123.9	252.1	230.5	305.0	199.0
[2] Input (mass or volume)	0 pg	10 pg	5µl	5µl	5µl
[3] Background corrected yield (ng/µl) { = [1] – Water yield }	0	128.2	106.6	181.1	75.1
[4] Calculated amplification { = [3] / [2] }		12.82			
[5] Calculated input mass (pg) { = [3] / [4] }			8.32	14.13	5.86
[6] Calculated sample concentration (pg/µl) { = [5] / [2] }			1.66	2.83	1.17

Equivalent amounts of cDNA from all samples was processed for microarray expression profiling, including the 10 pg neuronal sample. Potential chamber-to-chamber variability as well as possible variation in sample collection led us to evaluate the specificity and robustness of our

expression profiling. Box-and-whiskers plot of the raw probe cell intensity (log2) by sample shows similarity between the dynamic range of replicates (t-test, p=0.40) (Fig. 2.3A). Pearson's correlation analysis demonstrated a high degree of correlation between replicates (correlation r value >0.8) (Fig. 2.3B). This replicability suggests little variation in the differentiation efficiency between chambers. The 10 pg neuronal sample expression profile more closely resembled the neuronal samples than the axonal samples, showing that the linear amplification step broadly preserved the gene expression profile of the low concentration samples and demonstrated that differential gene expression was not due to the amplification step. Bivariate histogram plotting of gene expression in the axonal compartment versus the neuronal compartment (Fig. 2.3C) suggested that axonal expression values (log2) clustered between values of approximately 3 to 7 while neuronal expression values (log2) clustered between values of approximately 3 to 9.

Figure 2.3

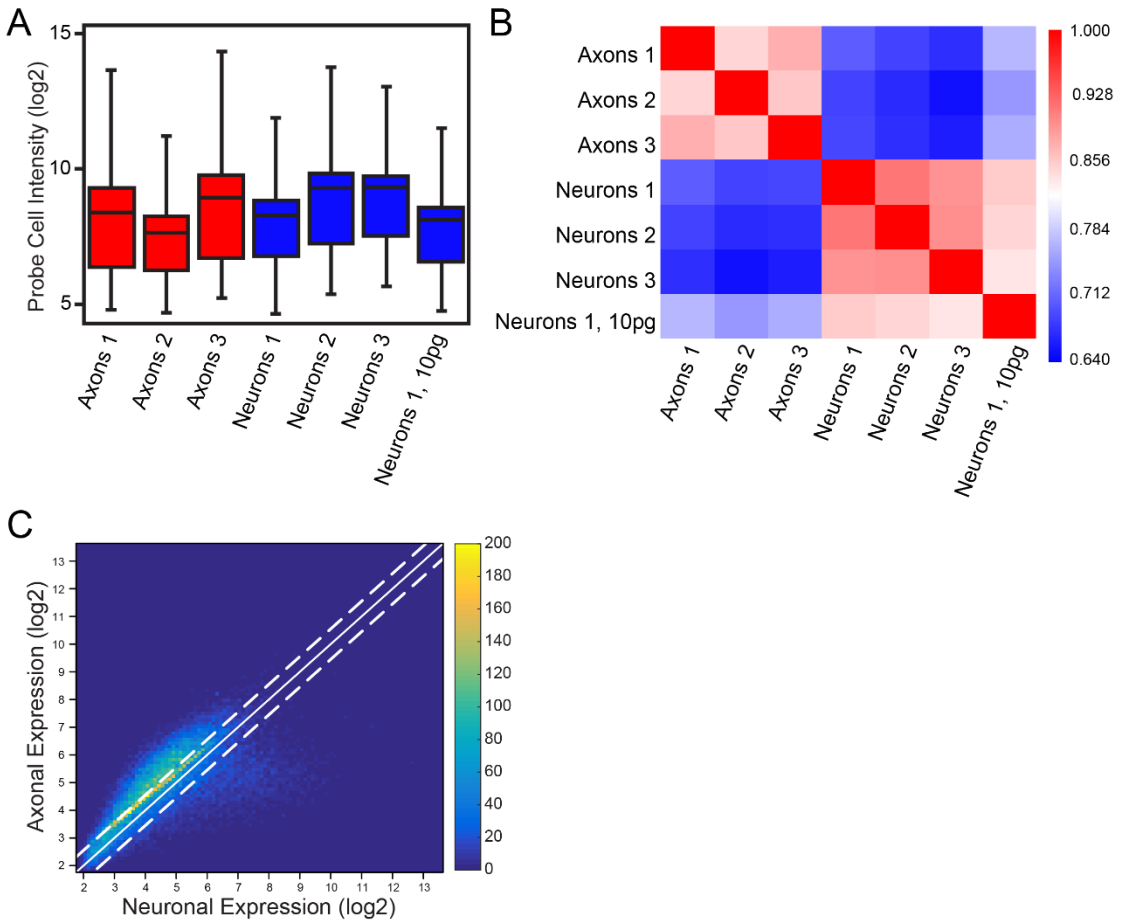

Figure. 2.3. Evaluation of the quality of Affymetrix microarray results generated from mRNA from hESC-neurons.
A. Box and whiskers plot of the Affymetrix microarray raw probe cell intensity values (log2) of samples from the axonal and somatic compartments ('Projections' and 'Neuronal' samples, respectively) in triplicate and the 10pg neuronal RNA sample.
B. Pearson correlation coefficient of microarray data from projections and neurons.
C. Bivariate histogram plot of neuronal and axonal expression (log2), solid line marks fold change of 0, upper dashed line marks fold change of 1.5, lower dashed line marks fold change of -1.5.

As an additional validation of our hESC-neuron differentiation efficiency we examined the expression of cell type specific markers in our neuronal data (Fig. 2.4A). Markers of mature neurons were significantly higher expressed in our cells than markers for neural stem cells, astrocytes and oligodendrocytes, other cell types occasionally present in stem cell derived neuron cultures (Appendix A). The neural stem cell markers were originally identified in gene expression studies across time during human fetal cortical development or *in vitro* hESC-neuron differentiation and maturation (Stein et al., 2014; van de Leemput et al., 2014). These marker genes are specific to neurogenesis and

neural differentiation. The mature neuron, astrocyte and oligodendrocyte specific marker genes were identified in dissociated adult mouse forebrain samples (Cahoy et al., 2008). This strongly supports our conclusions regarding the differentiation efficiency and neuron enrichment of our hESC-neuron protocol (Table 2.4).

Figure 2.4

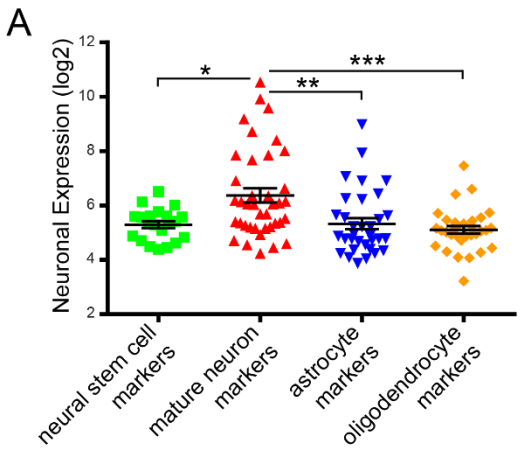

Figure. 2.4. hESC-neuron gene expression profile is enriched for markers of mature neurons. **A.** Neuronal expression (log2) values of marker proteins from: neural stem cells (Stein et al., 2014; van de Leemput et al., 2014), mature neurons, astrocytes or oligodendrocytes (Cahoy et al., 2008). Asterisks indicate one-way ANOVA with Dunnett's multiple comparison test p-value (* < 0.01, ** < 0.001, and *** < 0.0001).

The identity of transcripts within the axonal compartment that have disproportionally high expression may reveal functions reliant on local translation. We evaluated the proportionally enriched fraction of mRNAs within our axonal dataset by DAVID Gene Functional Classification (Huang da et al., 2009a; Huang da et al., 2009b). For comparison we also evaluated the proportionally depleted mRNAs within the axonal dataset. Figure 2.5A is a scatterplot of expression levels highlighting these fractions. Together these subsets encompassed approximately 15.7% of the probesets on the microarray (Fig. 2.5B). DAVID Gene Functional Classification of these genes revealed functional categories which were assigned an enrichment score (Fig. 2.5C and 2.5D, solid bars). This enrichment score measures and weighs the ratio of transcripts that fall into a given functional category. The proportionally enriched mRNAs within hESC-neuron projections were classified as 'secreted' and 'extracellular' proteins, 'DNA sequence-specific binding' proteins, 'neurofilament' proteins and 'voltage-gated' and 'cation' channels (Fig. 2.5C). This analysis suggests that translation of proteins within these classes may have a more prominent role within the specialized distal subcellular compartment than within the soma. The proportionally depleted mRNAs were associated with the terms 'intracellular' and 'nuclear" proteins and proteins that function in RNA splicing, protein degradation and maintaining genome organization and integrity (Fig 2.5D), functions representative of the identity of this dataset

inclusive of somata and dendrites. Taken together these data suggest that enriched transcripts within the distal projections of hESC-neurons have the capacity to support a repertoire of functions autonomously from the cell body.

Figure 2.5

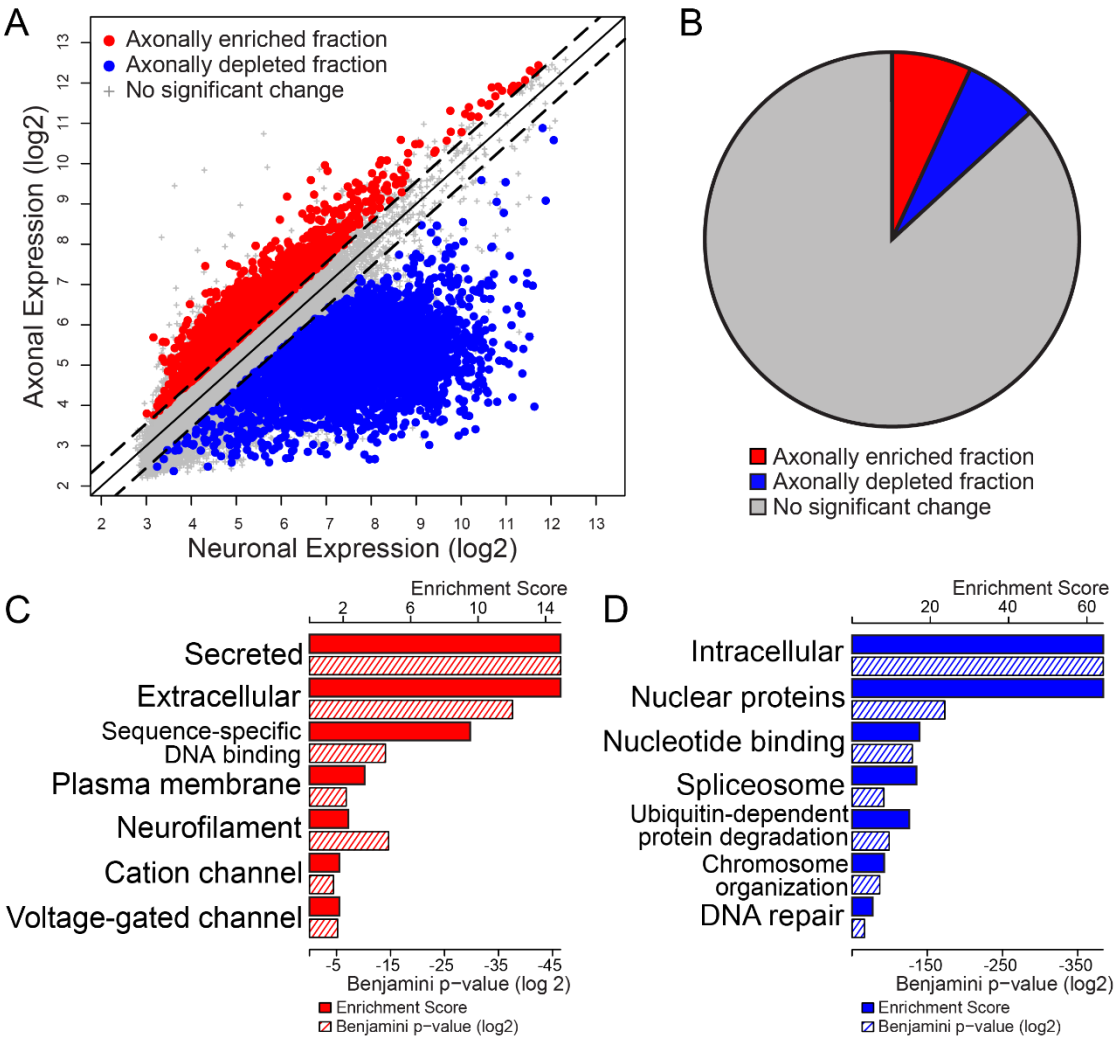

Figure. 2.5. Differential gene expression between the transcriptome of distal projections and the neuronal transcriptome of hESC-neurons.
A. Gene expression scatterplot comparing expression levels in hESC-neurons and distal projections. Threshold for proportional enrichment or depletion was set at ±1.5 fold change, ANOVA p-value < 0.05. The proportionally enriched fraction is shown in red, 3942 probe sets. The proportionally depleted fraction is shown in blue, 3630 probe sets.
B. Pie chart depicting the percentages of the total microarray probe sets that reached threshold to be considered enriched (8.17% of probe sets, red region) and depleted (7.53% of probe sets, blue region) within the axonal compartment.
C. Gene ontology (GO) enrichment scores (solid red bars, scale along the top) and Benjamini p-values (hashed red bars, scale along the bottom) of the proportionally enriched fraction as determined by DAVID Gene Functional Classification.
D. GO enrichment scores (solid blue bars, scale along the top) and Benjamini p-values (hashed blue bars, scale along the bottom) of the proportionally depleted fraction as determined by DAVID Gene Functional Classification.

Abundant transcripts within axons of hESC-neurons functionally resemble axonal transcripts localized to rat cortical neurons

Many of the mRNAs highly abundant within the axons of hESC-neurons were not enriched relative to neuronal samples, yet may perform important biological functions that depend on local translation. For example, β-actin (ACTB) is not enriched in our dataset (expression in 'axons': 6.74; expression in 'neurons': 6.86; fold change -1.09) nor in the axonal transcriptomes of rat cortical neurons (Taylor et al., 2009) or rat sympathetic neurons (Andreassi et al., 2010), yet local translation of β-actin in neurites and axons is well-established (Eng et al., 1999; Welshhans and Bassell, 2011). To assess the degree of functional similarity between the abundant transcripts within hESC-neuron axons and comparable primary rodent glutamatergic neurons we first created a subset of our expression data containing the microarray probe sets with the highest average signal intensity in our axon samples, those above the 90th percentile (expression value ≥6.48), representing the highest expressed transcripts (Fig. 2.6A) (3696 transcripts). We compared this subset of highly expressed transcripts by DAVID Gene Functional Classification with a published dataset of mRNAs reliably localized to axons of primary embryonic rat cortical neurons grown in similar microfluidic chambers (Taylor et al., 2009). Transcripts encoding proteins involved in 'translation' and ribosomal proteins were significantly over-represented in the resulting transcriptomes from both species as well as proteins of the mitochondrial 'respiratory chain' and cytoskeletal proteins ('neurofilament' in hESC-neurons and 'microtubule' and 'cell projection' in rat cortical neurons, Fig. 2.6B and 2.6C). Unique to the highly expressed mRNAs within hESC-neuron axons were transcripts encoding 'extracellular' proteins.

Figure 2.6

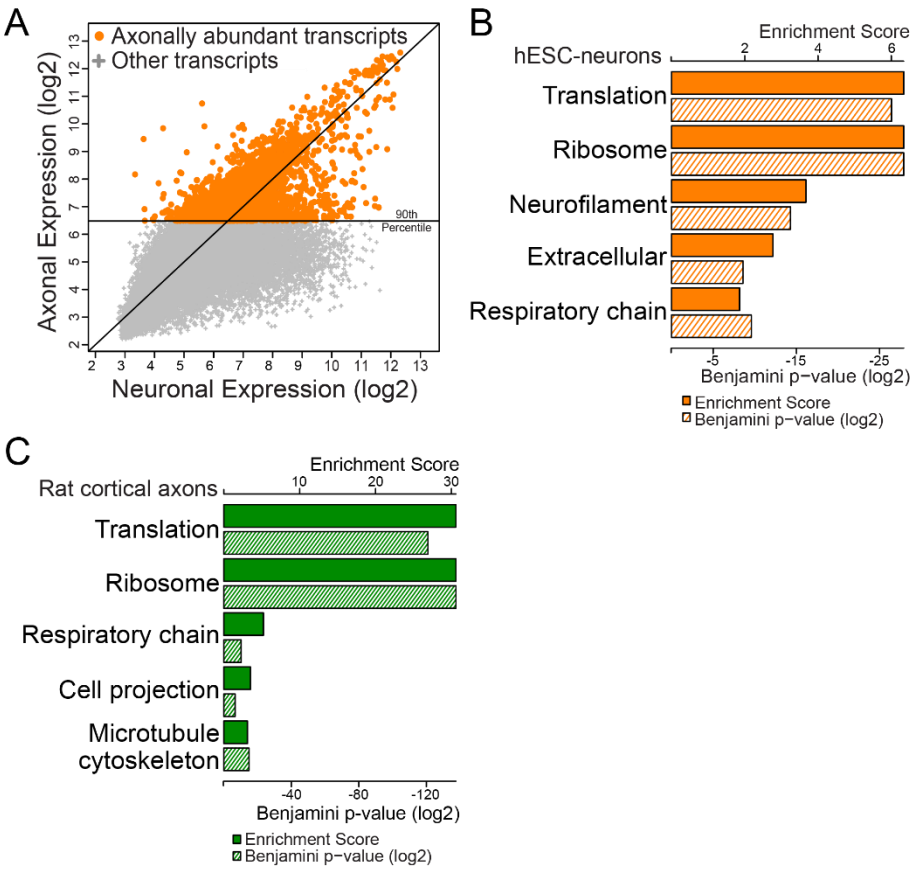

Figure. 2.6. Enriched gene ontology categories were similar between the transcriptomes of isolated hESC-neuron axons and axons of embryonic rat cortical neurons.
A. hESC-neuron gene expression scatterplot highlighting abundant transcripts within the axons, expression levels above the 90th percentile.
B. GO enrichment scores (solid orange bars, scale along the top) and p-values (hashed orange bars, scale along the bottom) of abundant transcripts from hESC-neuron axons as determined by DAVID Gene Functional Classification.
C. GO enrichment scores (solid green bars, scale along the top) and p-values (hashed green bars, scale along the bottom) of axonal transcripts from rat cortical neurons on DIV13 as determined by DAVID Gene Functional Classification.

Post hoc evaluation of this threshold revealed that it excluded known abundant dendritic transcripts, such as activity-regulated cytoskeleton-associated protein (ARC), Calcium/calmodulin-dependent protein kinase type II alpha chain (CAMK2A) and α-amino-3-hydroxy-5-methyl-4-isoxazolepropionic acid receptor (AMPAR) subunits and included the well characterized axonal transcript GAP43 (>98th percentile) and ACTB (>93rd percentile).

After determining that the axonal transcriptomes of hESC-neurons and embryonic rat cortical neurons were functionally similar we then asked if there were orthologous mRNAs within these

transcriptomes. We determined that there were 161 orthologous transcripts within the axonal transcriptomes of glutamatergic-enriched hESC-neurons and glutamatergic-enriched embryonic rat cortical neurons (Fig. 2.7A). DAVID Gene Functional Classification of these conserved transcripts revealed that they were significantly enriched for transcripts encoding proteins functioning specifically in the elongation step of translation, intracellular proteins and proteins located at the synapse (Fig. 2.7B).

Figure 2.7

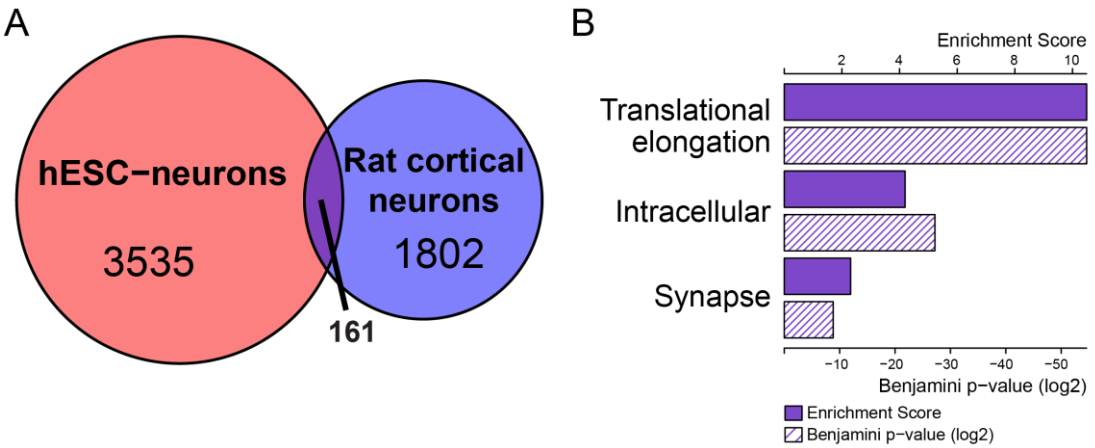

Figure. 2.7. Conserved orthologous transcripts within the axons of hESC-neurons and embryonic rat cortical neurons are enriched for synaptic proteins.
A. Venn diagram proportionally depicting the overlap of orthologous transcripts within the axons of hESC-neurons and the axons of embryonic rat cortical neurons. There are 3535 transcripts unique to hESC-neuron axons, 1802 transcripts unique to embryonic rat cortical axons and 161 orthologous transcripts present in both axonal transcriptomes.
B. GO enrichment scores (solid purple bars, scale along the top) and p-values (hashed purple bars, scale along the bottom) of conserved orthologous transcripts within the axonal transcripts from hESC-neurons and embryonic rat cortical neurons.

Overall, these data suggest that the axonal transcriptomes of hESC-neurons and primary rat cortical neurons are broadly similar, despite differences in species of origin and neuron derivation. Further, the orthologous mRNAs in common between the two axonal transcriptomes revealed further similarities.

RNA-FISH verification of specific mRNAs within hESC-neuron distal projections

To validate our microarray results, we chose to verify the presence of known axonally localized mRNA transcripts and a novel distally localized mRNA identified in our expression data using multiplexed single molecule RNA fluorescence in situ hybridization (RNA-FISH). The transcripts selected for visualization were β-actin (ACTB), growth associated protein 43 (GAP43) and oxytocin (OXT). ACTB and GAP43 mRNA are well characterized within rodent axons and are locally translated (Donnelly et al., 2013). We identified OXT mRNA as a potentially unique transcript present in these human axons as it was below the detection limit in rodent cortical axons (Taylor et al., 2009). The presence and function of OXT mRNA within distal projections has not been investigated to our knowledge. Our RNA-FISH results confirmed the presence of ACTB, GAP43, and OXT transcripts

within the long projections of hESC-neurons (Fig. 2.8A). RNA-FISH probes were omitted for negative control axons (Fig. 2.8B) and no fluorescence puncta were detected in these samples. These results confirm the hESC-neuron axonal localization of mRNAs encoding β-actin, GAP43 and oxytocin.

Figure 2.8

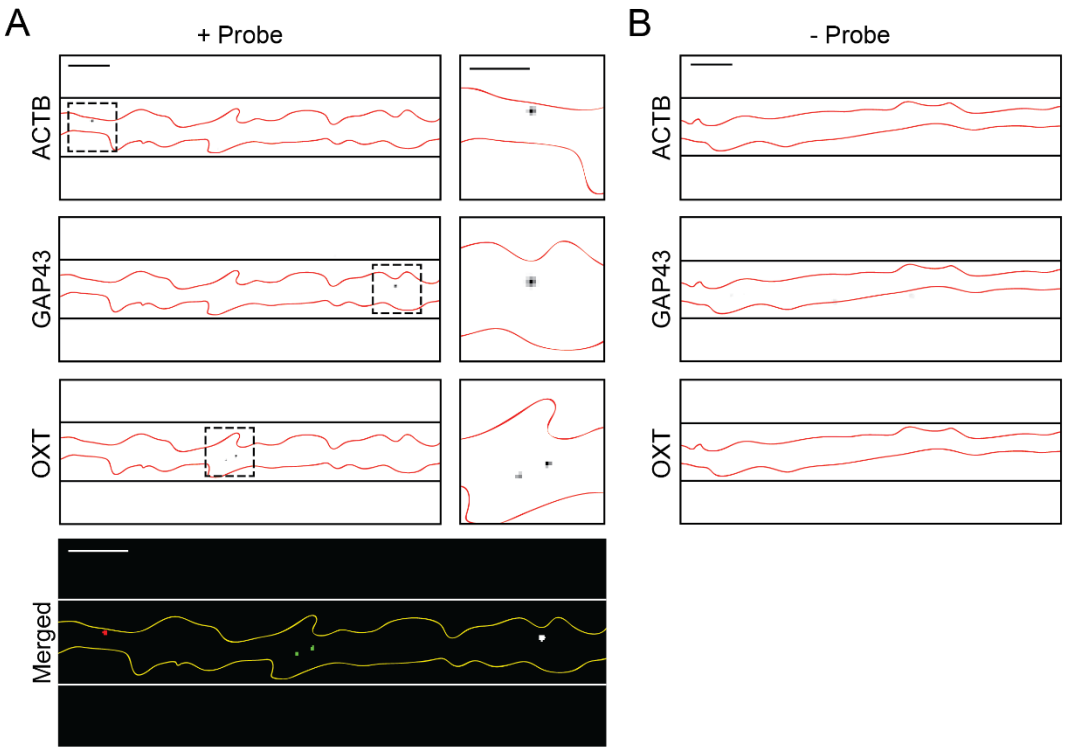

Figure. 2.8. Multiplexed RNA-FISH verification of mRNA within the distal projections of hESC-neurons.
A. Representative image of hESC-neuron projections processed for RNA-FISH with gene specific probes for β-actin (ACTB, red), Growth Associated Protein 43 (GAP43, green) and Oxytocin (OXT, white). Individual greyscale images (inverted fluorescence) for each probe and a merged color image are shown. In the greyscale images black lines delineate the microgroove walls and the neuronal projection is outlined in red. The region within the dashed box is enlarged to the right of each image, scale bar is 5 µm. In the merged image white lines delineate the microgroove walls and the neuronal projection is outlined in yellow, scale bars are 10 µm.
B. Representative portion of a negative control hESC-neuron axon processed for RNA-FISH without gene specific probes. Individual greyscale images for each probe are shown. Scale bars 10 µm.

Semi-automated quantification of RNA-FISH puncta revealed averages of 7.88 ACTB puncta/ mm axon (range 0 to 14.78), 1.58 GAP43 puncta/ mm axon (range 0 to 7.34) and 6.31 OXT puncta/ mm axon (range 0 to 18.66). A total of 1.929 mm linear axon length was evaluated. No puncta were detected when the RNA-FISH probes were omitted in 0.875 mm linear axon length evaluated. Quantification of RNA-FISH puncta is not a direct 1:1 correlate to transcript number since multiple mRNAs may appear to be a single punctum and RNA-FISH probes can have different RNA labeling efficiencies and fluorescence intensities. The short length of the oxytocin mRNA (548nt) and homology with vasopressin mRNA (AVP) our custom OXT RNA-FISH probe set pool (Affymetrix) contained 7 branched DNA sequences instead of the customary 20 sequences, which may explain the smaller size

of these fluorescent puncta. Together, these data validate our microarray data and demonstrate that these human distal projections contain mRNAs also found in axons of model organisms, yet also have mRNAs that may also be uniquely localized to human axons.

DISCUSSION

Significance

Subcellular compartments distal from the cell body, such as axons, were once thought to be devoid of mRNA and ribosomes but are proving to contain transcripts encoding thousands of proteins and the machinery for translation (Koenig and Martin, 1996; Koenig et al., 2000). Functionally, intra-axonal translation is necessary for growth cone guidance, axon maintenance, injury response and may be involved in presynaptic plasticity. Specific locally translated mRNAs involved in these cellular events have been identified (Andreassi et al., 2010; Aschrafi et al., 2008; Baleriola et al., 2014; Ben-Yaakov et al., 2012; Calliari et al., 2002; Colak et al., 2013; Eng et al., 1999; Merianda et al., 2015; Moretti et al., 2015; Perlson et al., 2005; Perry et al., 2012; Taylor et al., 2013; Welshhans and Bassell, 2011; Wu et al., 2005; Yudin et al., 2008). Discovery of axonally translated proteins in hESC-neurons has the potential to expand and deepen our knowledge of the role of local translation. While this study focuses on the proportionally enriched fraction and the abundant transcripts within distal projections local translation of moderate to low abundance axonal transcripts may also be functionally relevant.

Functional classification of differentially enriched mRNAs revealed that local, distal translation of transcription factors (Fig. 2.4C, ‘sequence-specific DNA binding’) is likely a common mechanism by which distal events trigger a transcriptional response following transport of the protein to the nucleus. Axonal translation of the transcription factors ATF4 and STAT3 are induced following injury in CNS and PNS neurons, respectively (Baleriola et al., 2014; Ben-Yaakov et al., 2012). Retrograde transport of these proteins to the soma mediate the transcriptional response to axon injury. Retrograde transport of axonally synthesized transcription factors could function in a variety of axon-to-soma signaling pathways beyond injury. Alternatively, some annotated transcription factors could have transcription-

independent roles. For example, axonally synthesized β-catenin, a Wnt signal transducer, functions at the presynapse as a scaffold protein (Bamji et al., 2003; Taylor et al., 2013).. The highly enriched categories of 'secreted' and 'extracellular' protein transcripts suggests a significant demand on distal projections to dynamically modulate the extracellular environment, likely as part of axon guidance, synaptogenesis and even synaptic plasticity. Differential expression of the proportionally enriched and proportionally depleted fractions may be the cumulative result of differential trafficking of RNA to distal subcellular compartments as well as differential mRNA stability. Messenger RNA stability can be regulated by multiple mechanisms, including microRNAs and nonsense mediated decay. MicroRNA mediated mRNA regulation is documented in axons (Hengst et al., 2006; Natera-Naranjo et al., 2010). Nonsense mediated decay (NMD) components are present in axons and growth cones and *in vivo* disruption of NMD in mouse commissural neurons alters axon guidance. Spatiotemporal cues developmentally regulate NMD of Robo3.2 mRNA in the axons of these neurons (Colak et al., 2013).

Our comparison of the most abundant distal mRNAs within hESC-neurons with that of axons of primary embryonic rat cortical neurons revealed functional similarities, specifically in mRNAs encoding proteins required for translation, ribosomal proteins and nuclear-encoded mitochondrial proteins necessary for ATP production (Fig. 2.5B and 2.5C). These axon enriched categories have been described in the adult rat neuropil, adult and embryonic rat DRGs, embryonic mouse DRGs, neonatal rat SCGs and mouse retinal ganglion cells (Andreassi et al., 2010; Gumy et al., 2011; Minis et al., 2014; Shigeoka et al., 2016; Willis et al., 2007). Axonal translation of nuclear encoded mitochondrial respiratory chain proteins has been described previously (Gioio et al., 2001; Hillefors et al., 2007). We speculate that it is more efficient to replenish critical mitochondrial proteins via *de novo* and *in situ* translation than for the neuron to support a continual cycle of soma to axon mitochondrial protein transport. The conservation of ribosomal protein transcripts in axons suggest that either the protein components of the ribosome have a shorter half-life than the RNA components or local translation of ribosomal protein is a mechanism to dynamically regulate distal ribosomes and translation. There are over 100 human ribosomal proteins but only a few are characterized as constitutive ribosome components and the function of many of these proteins are unknown. It is interesting to speculate that the unique repertoire of ribosomal proteins associated with rRNA could

confer target mRNA specificity. Ribosomes containing ribosomal protein L38 have been shown to preferentially interact with and translate the mRNA of Hox genes in mouse (Kondrashov et al., 2011). With the large number of ribosomal proteins it is possible that this is a common, under characterized, mechanism of translational regulation. Additionally, ribosomal proteins may mediate differential ribosome localization by regulating ribosome interaction with transmembrane proteins of organelles, such as the axonal endoplasmic reticulum, or growth factor receptors, such as the netrin-1 receptor Deleted in Colorectal Cancer (DCC) (Tcherkezian et al., 2010).

The enrichment of 'synaptic' protein transcripts in the conserved mRNAs between the axonal transcriptome of hESC-neurons and embryonic rat cortical neurons (Fig. 2.7B) suggests that these two glutamatergic-enriched neuron populations share the capacity for local translation of synaptic proteins, potentially functioning in synaptogenesis and synaptic plasticity. Dynamic synaptogenesis and synaptic plasticity throughout the lifespan of the organism are key features of the hippocampus and cortex, the brain regions enriched for glutamatergic neurons.

We confirmed the presence of three specific mRNAs, ACTB, GAP43 and OXT, within hESC-neuron axons using multiplexed RNA-FISH. Axonal localization of ACTB and GAP43 appears to be conserved between rodents and humans suggesting that local function and synthesis of these proteins may also be conserved. Oxytocin mRNA within the axonal compartment and intra-axonal translation of oxytocin may be unique to human neurons.

Possible improvements

In vitro differentiation and maturation of stem cell derived neurons within microfluidic chambers is a labor intensive process requiring almost daily attention for many weeks. To improve efficient use of each chamber it would be beneficial to optimize the current RNA collection method so both compartments of the same chamber can be used, maybe one compartment for RNA and the other for immunofluorescence or other downstream biochemical analysis.

The time course and identifying characteristics of human neuron polarization has not been rigorously investigated so researchers must apply what is known about neuron polarization from other species. Our immunofluorescent evaluation of the neurites within the microgrooves and the axonal

compartment demonstrated that they were β-tubulin III positive and MAP2 negative; these are canonical features of properly polarized mature axons of embryonic and adult neurons from all model species. Further, a modified rabies virus delivered to the isolated axonal compartment was able to infect the hESC-neurons and the GO functional categories were similar between this hESC-neuron axonal transcriptome and the rat cortical axon transcriptome (Taylor et al., 2009) suggesting that this was an enriched population of mature axons. The presence of mCherry negative distal projections within the axonal compartment could arise from variability in the time course of mCherry expression. In primary rat hippocampal cultures the minimum amount to time to detect fluorescent protein is 48 hours but some cells do not express detectable mCherry until 4 days after transfection. Alternatively, these mCherry negative projections could be resistant to viral infection due to lack of viral receptors suggesting an incomplete axon phenotype or, less likely, a dendritic phenotype.

Neurons derived from *in vitro* differentiated pluripotent stem cells are generally accepted as resembling fetal neurons (Stein et al., 2014). While the differentiation and maturation protocol we used has generated neurons capable of action potentials as early as DIV42 (Zeng et al., 2010), a characteristic of functionally mature neurons, these cells are not “aged” to a point of resembling adult neurons. RNA-mediated mechanisms have been implicated in both neurodegenerative and neurodevelopmental models, making “young” and “aged” neurons beneficial model systems. Researchers are working to generate appropriately aged stem cell derived neurons to model age-related neuronal function (Miller et al., 2013).

CHAPTER THREE: DIFFERENTIAL GENE EXPRESSION FOLLOWING IN VITRO AXON INJURY OF RAT HIPPOCAMPAL NEURONS

INTRODUCTION

Stroke and traumatic brain injury induce significant local synaptic reorganization as well as reorganization in distal uninjured regions isolated from the site of damage (Nudo and Milliken, 1996; Nudo, 2013; Takechi et al., 2014). This injury-induced neural plasticity supports formation of new synaptic connections and remapping of neural networks to compensate for loss of function. This is well-described in humans using neuroimaging and non-invasive stimulation techniques (Frost et al., 2003; Nudo, 2013; Oudega and Perez, 2012; Takechi et al., 2014). The cellular mechanisms of this injury-induced plasticity far from the primary injury site remain largely unknown.

Neurons of the cerebral cortex extend long axons into numerous distant areas of the CNS, including the spinal cord and the contralateral cortical hemisphere. Brain injury and disease preferentially affect these long projection neurons within the CNS (Nakatomi et al., 2002; Will et al., 2004). When remote areas are injured, long projecting axons are damaged and injury signals propagate retrogradely to the somatodendritic domains to alter the neural network. For example, spinal cord injury damages long projecting corticospinal axons with subsequent, time-dependent morphological changes to dendritic spines, protrusions that form synapses with presynaptic neurons, in the motor cortex. These changes include decreased spine density and alterations in spine length and diameter (Kim et al., 2006) which induce synaptic changes affecting neuron connectivity. Loss of local GABAergic inhibition onto injured neurons has been observed following injury, potentially unmasking preexisting excitatory connections resulting in enhanced excitability (Ding et al., 2011; Jacobs and Donoghue, 1991; Takechi et al., 2014). Further, injury signaling initiates a transcriptional response that is necessary for recovery (Rishal and Fainzilber, 2014; Urban et al., 2012). Together these findings suggest a cascade of events following distal axonal injury involving retrograde axon-to-

soma signaling, transcription and trans-synaptic signaling from the injured neuron to uninjured presynaptic neurons resulting in synaptic plasticity and enhanced excitability.

The cellular heterogeneity and structural complexity of the CNS complicates dissecting the intrinsic neuronal responses to distal axon injury *in vivo*. An *in vitro* axon injury model using embryonic rat hippocampal neurons grown in axon-isolating microfluidic chambers (Taylor et al., 2005; Taylor et al., 2009) allowed us to investigate the injury-induced synaptic and transcriptional changes.

MATERIALS AND METHODS

Hippocampal cultures

Animal procedures were carried out in accordance with the University of North Carolina at Chapel Hill Institutional Animal Care and Use Committee (IACUC). Dissociated hippocampal cultures were prepared from Sprague Dawley rat embryos (E18-E19) as previously described (Ivins et al., 1998; Taylor et al., 2003) with the following modifications. Hippocampal tissue was dissected in dissociation media containing 82 mM Na_2SO_4, 30 mM K_2SO_4, 5.8 mM $MgCl_2$, 0.25 mM $CaCl_2$, 1 mM HEPES, 20 mM Glucose and 0.001% Phenol red. For enzymatic digestion, equal volumes of TrypLE Express (Invitrogen) and dissociation media were added to the tissue and incubated at 37 °C for 8 min. Tissue was then rinsed and gently triturated in neuronal culture media consisting of Neurobasal media (Invitrogen) supplemented with 1x B-27 serum-free supplement (Gibco), 1x Antibiotic-antimycotic (Invitrogen), 1x Glutamax (Invitrogen). Dissociated cells were resuspended in neuronal culture media to yield $12x10^6$ cells per ml.

Microfluidic chambers

Poly(dimethylsiloxane) (PDMS) microfluidic chambers were replica molded from microfabricated master molds as described previously (Taylor et al., 2005). All experiments used chambers with 900µm long microgrooves to separate the somatodendritic and axonal compartments as described previously (Taylor et al., 2005; Taylor et al., 2009; Taylor et al., 2013), except the experiments associated with Figure 3.4 which used chambers with 150 µm, 450 µm and 900 µm long microgrooves. Microfluidic chambers were placed onto glass coverslips coated with 500-550 kDa poly-

D-lysine (BD Biosciences). Approximately 90,000 cells were plated into the somatodendritic compartment and axons extended into the adjacent axonal compartment after 5-7 days of culture in the absence of exogenous growth or chemotactic factors. Axotomy was performed between 11 and 15 days in vitro (DIV) according to previously published procedures (Taylor et al., 2005; Taylor et al., 2009). Briefly, media was first removed from the axonal compartment of 'axotomized' experimental cultures and 'naive' control cultures and stored for future use. The axonal compartment of 'axotomized' cultures was aspirated until completely devoid of fluid, while the 'naive' cultures were not further manipulated. The stored culture media was then returned immediately to the axonal compartment for the duration of the culture time. Microfluidic devices with equivalent viable cell populations were randomly chosen for either axotomy or naïve control groups.

Cell viability assay

Dead cells were labeled using SYTOX Green (Invitrogen) at a final concentration of 1 µM and all cell nuclei were labeled with NucBlue Hoechst Stain (Invitrogen). Cells were incubated with SYTOX/Hoechst solution simultaneously in 1x Phosphate Buffered Saline (PBS) for 5 min at 37 °C, washed with PBS, and fixed with 4% paraformaldehyde (PFA) in PBS containing 40 mg/ml sucrose, 1 µM $MgCl_2$ and 0.1 µM $CaCl_2$ for 15 min at room temperature (RT). Coverslips were then rinsed three times with PBS and mounted onto the glass slide using Fluoromount G (Southern Biotech). SYTOX positive (Sytox+) cells were manually counted in ImageJ using sum projected z-stack confocal images. Percent cell viability was calculated using [(Hoechst - Sytox+) / Hoechst] * 100.

Retrograde labeling

Retrograde labeling was performed using either modified cholera toxin or rabies virus. Cholera Toxin Subunit B Alexa Fluor 488 (Thermo Fisher Scientific, C34775; 1 µg in 200 µl of neuronal culture media) was added to the axonal compartment of the microfluidic chamber and incubated for approximately 15 h at 37 °C. After 15 h of incubation, the axonal compartment media was removed, rinsed and replaced using fresh neuronal culture media. Cultures were immediately used for imaging or experimental manipulation.

G-deleted Rabies-mCherry (Wickersham et al., 2007a) (Salk Institute; $1x10^5$ viral units) in 50 µl conditioned media was added to the axonal compartment of each chamber and incubated for 2 h at 37 °C. Conditioned media was added back to the axonal compartments following two washes with fresh neuronal culture media. Chambers were maintained in 37 °C incubator for approximately 48 h until fluorescence expression was visible.

Immunocytochemistry

Cells were fixed with 4% paraformaldehyde in PBS containing 40 mg/ml sucrose, 1 µM $MgCl_2$ and 0.1 µM $CaCl_2$ then permeabilized in 0.25% Triton X-100 and blocked in 10% normal goat serum for 15 min each. Coverslips were incubated with anti-MAP2 (1:1000; Millipore # AB5622), anti-β-tubulin III (1:2000; Aves # TUJ) primary antibodies in 1% blocking solution for overnight at 4°C. Coverslips were then incubated with goat anti-rabbit or goat anti-mouse or anti-chicken secondary antibodies conjugated to Alexa-fluorophores (1:1000; Invitrogen) at RT for 1 h. Following PBS washes cells were counterstained with 71.5 µM 4',6-diamidino-2-phenylindole (DAPI) in PBS, washed again and coverslips were mounted onto glass slides with Fluoromount G (Southern Biotech).

Microgroove length analysis

Primary embryonic rat hippocampal neurons were cultured in microfluidic chambers with microgroove lengths of 150 µm, 450 µm and 900 µm, 2 chambers for each configuration. On DIV13 isolated axons and their associated somata were labeled with cholera toxin conjugated to AlexaFluor 488 as described above. On DIV14 after cholera toxin was washed away cells were fixed with 4% paraformaldehyde in PBS containing 40 mg/ml sucrose, 1 µM $MgCl_2$ and 0.1 µM $CaCl_2$, washed with PBS, counterstained with 71.5 µM DAPI and mounted onto glass slides with Fluoromount G (Southern Biotech). Imaging captured a region of each chamber measuring 2 mm wide by 1.7 mm long. The width of each chamber (2 mm) was visually divided into four equal regions measuring 0.5 mm wide by 1.7 mm long and DAPI nuclei and cholera toxin positive somata were manually counted in each region using the ImageJ plugin 'Cell Counter'.

RNA isolation

Total RNA from each of 3 axotomized chambers and 3 naive manipulated chambers (6 total samples) was isolated from the somatodendritic compartment of DIV14 cultures, 24 h after manipulation. RNA was collected from the entire somatodendritic compartment for gene expression analysis; thus, a fraction of neurons in the axotomized chambers were axotomized and the remaining fraction were uninjured (Fig. 3.1B). RNA was isolated using an RNAqueous-Micro Kit (Ambion) according to the manufacturer's instructions including DNase treatment, with modifications specific to accessing the microfluidic compartment (Taylor et al., 2009). Briefly, 50 µl lysis solution was added to one somatodendritic well and collected from the other somatodendritic well after solution flowed through the somatodendritic compartment. Lysate was added to 50 µl of fresh lysis solution and mixed by careful pipetting. Further RNA purification steps were performed according to the manufacturer's guidelines. Samples were stored at -80 °C until prepared for microarray gene expression.

Microarray analysis

Quantification of RNA integrity and concentration was confirmed with an Agilent TapeStation 2200 at the UNC Lineberger Comprehensive Cancer Center Genomics Core. Microarrays were processed at the UNC School of Medicine Functional Genomics Core using the Affymetrix GeneChip WT Plus Reagent Kit for cRNA amplification, cDNA synthesis, fragmenting and labeling. Samples were hybridized to Rat Gene 2.0 ST Arrays (Affymetrix). The Robust Multichip Analysis (RMA) algorithm was used for global background adjustment, quantile normalization and gene expression summarization between samples. This method is sensitive to small changes between samples without negatively affecting signal variance. Data analysis was performed with Affymetrix Expression Console software and Affymetrix Transcriptome Analysis Console v2.0 software to compare axotomized cultures to naive control samples using one-way between-subject ANOVA of RMA normalized intensities. Because a fraction of the harvested cells were uninjured in our axotomized samples, we used modest fold change values for defining our list of significantly changed transcripts (fold change absolute value ≥ 1.05 and ANOVA p-value < 0.05).

Raw microarray data of cortical layers V/VI of female Wistar rats subjected to either spinal cord transections at thoracic layer 8 or sham injury was downloaded from EMBL-EBI Array Express

(E-MTAB-794) (Jaerve et al., 2012). Four animals were used for each condition and samples were hybridized to Rat Gene 1.0 ST Arrays (Affymetrix). The microarray data was previously validated using qPCR. Data analysis was performed with Affymetrix Expression Console software and Affymetrix Transcriptome Analysis Console v2.0 software to compare cortical layers V/VI from injured to sham operated animals.

FM dye experiments and analysis

Cultures in microfluidic chambers at 24 h (DIV14), 48 h (DIV15), and 4 d (DIV17) after axotomy were loaded with lipophilic dye FM5-95 (Invitrogen) using KCl mediated depolarization as described previously (Taylor et al., 2013). Briefly, cultures were first incubated for 30 min with pre-warmed HEPES-buffered solution (HBS; 119 mM NaCl, 5 mM KCl, 2 mM $CaCl_2$, 2 mM $MgCl_2$, 30 mM glucose, 10 mM HEPES). Media was then replaced with FM dye loading solution containing 10 µM FM5-95, 20 µM AMPAR antagonist 6-cyano-7-nitroquinoxaline-2,3-dione disodium (CNQX; Tocris), 50 µM NMDAR antagonist D-(-)-2-amino-5-phosphonopentanoic acid (D-AP5; Tocris) in 90 mM KCl HBS for 1 min. The loading solution was replaced with HBS containing 10 µM FM5-95 for 1 min and later rinsed three times with a high-Mg^{2+}, low-Ca^{2+} solution (106 mM NaCl, 5 mM KCl, 0.5 mM $CaCl_2$, 10 mM $MgCl_2$, 30 mM glucose, 10 mM HEPES) containing 1 mM Advasep-7 (Biotium) to remove extracellular membrane-bound FM. Finally, cultures were washed in HBS containing 20 µM CNQX and 50 µM D-AP5 three times, 1 min each. Next, we stimulated the microfluidic chambers using extracellular electrodes by placing a positive and negative electrode in each well of the somatodendritic compartment.

Electrical stimulation was provided by an AD Instrument 2 Channel Stimulus Generator (STG4002) in current mode with an asymmetric waveform (-480 µA for 1 ms and +1600 µA for 0.3 ms) at 20 Hz for 600 pulses, approximately 1 min. The FM5-95 imaging was performed as described previously using a spinning disk confocal imaging system (Taylor et al., 2013). Z-stacks (31 slices) were captured every 15 s during the baseline (1 min), stimulation (1 min), and after stimulation (2 min) periods. This stimulation pattern was optimized for efficient FM unloading within these microfluidic chambers and the frequency is greater than typically used in open well dishes. At least 3 baseline

images were acquired before electrical stimulation. Sum projected confocal z-stacks were converted to 8-bit images and registered using TurboReg, an ImageJ plugin. We background subtracted the image stack using the image 3 min after stimulation began. Image stacks were thresholded to a pixel value of 15. FM puncta between 0.4 to 10 μm^2 were analyzed. We measured the intensity of each punctum in the whole field throughout all time-series. We normalized fluorescence intensity of each puncta to the frame before stimulation. Puncta with > 5% unloading immediately after the stimulation were used in the analysis as unloaded puncta.

In activity and transcription blocking experiments the FM5-95 unloading experiment were performed 48 h after axotomy and the intensity measurements of each punctum in the whole field and subsequent analysis of FM unloading kinetics was performed as described above.

Drug treatments

5,6-dichloro-1-β-D-ribofuranosyl-1H-benzimidazole (DRB; Sigma-Aldrich # D1916) was suspended in Dimethyl sulfoxide (DMSO) and applied to the somatodendritic compartment at a final concentration of 80 μM for 15 min prior to axotomy and 45 min after axotomy. Tetrodotoxin citrate (TTX; Tocris Bioscience # 1078) was suspended in HBS and applied to the somatodendritic compartment at a final concentration of 1 μM for 15 min prior to axotomy and 45 min after axotomy. Media stored from the axonal compartment prior to treatment was added back to the axonal compartment after treatment.

Microscopy

Fixed imaging, live imaging and FM kinetics imaging was performed using a CSU-X1 (Yokogawa) spinning disk confocal imaging unit configured for an Olympus IX81 microscope (Andor Revolution XD). Excitation for the spinning disk confocal imaging system was provided by 405 nm, 488 nm, 561 nm, and/or 640 nm lasers. The following bandpass emission filters (BrightLine, Semrock) were used: 447/60 nm (TRF447-060), 525/30 nm (TRF525-030), 607/36 nm (TR-F607-036), 685/40 nm (TR-F685-040). For FM imaging, the spinning disk confocal imaging system was used with

excitation at 561 nm and the 685/40 nm emission filter. We used 2x2 binning to reduce the laser intensity and acquisition time for each frame; each z-stack was obtained in approximately 5 s.

Statistics

Statistics were analyzed using GraphPad Prism 6. Unpaired two-tailed t-test was performed when comparing two independent groups. For FM unloading experiments and for comparing multiple groups, Two-way ANOVA and One-way ANOVA were used respectively followed by Bonferroni post-hoc test.

Data availability

The raw microarray data (CEL and CHP files) are available through the NCBI Gene Expression Omnibus under accession number GSE89407.

RESULTS

Fluidically isolated axons of embryonic rat hippocampal neurons can be injured without affecting cell viability

To investigate the effect of distal axotomy on cell viability, synaptic plasticity and gene expression we grew embryonic rat hippocampal neurons in 2-compartment axon-isolating microfluidic chambers with 900 µm microgrooves separating the compartments (Fig. 3.1A). Hippocampal tissue provided a consistently enriched population of pyramidal neurons (85-90% pyramidal) compared with similarly harvested cortical neurons. Neurons were plated in the somatodendritic compartment in the absence of exogenous growth or chemotactic factors. After 10 days *in vitro* (DIV) the axonal compartment was densely populated with neuron-specific class III β-tubulin (β-tubulin III, βtub) positive axons while the microtubule-associated protein 2 (MAP2) positive soma and dendrites were restricted to the somatodendritic compartment (Figure 3.1A). In this model system the somatodendritic compartment included the somata, dendrites and axons of neurons that did not extend into the axonal compartment (Figure 3.1B, grey neurons) as well as the somata and dendrites of neurons with axons extended into the isolated compartment (Fig. 3.1B, red neurons). The fluidic isolation of the

compartments allowed manipulation of the isolated axons without physically or chemically disrupting the somatodendritic compartment. To axotomize the isolated axons high speed airflow was applied to the axonal compartment for at least 60 seconds via a traditional tissue culture aspirator system (Taylor et al., 2005; Taylor et al., 2009). This manipulation completely ablated the axons within the compartment (Fig. 3.2A and 3.3C). Media was removed from the axons of naïve manipulated cultures for approximately 60 seconds, without aspiration air flow, then the media was returned to the compartment. Due to the enclosed design of the compartments the naïve axons remained surrounded by media during this control manipulation. These control, naïve cultures were exposed to minimal axonal stress and damage while controlling for the microforces associated with removing and recirculating the axonal media.

Figure 3.1

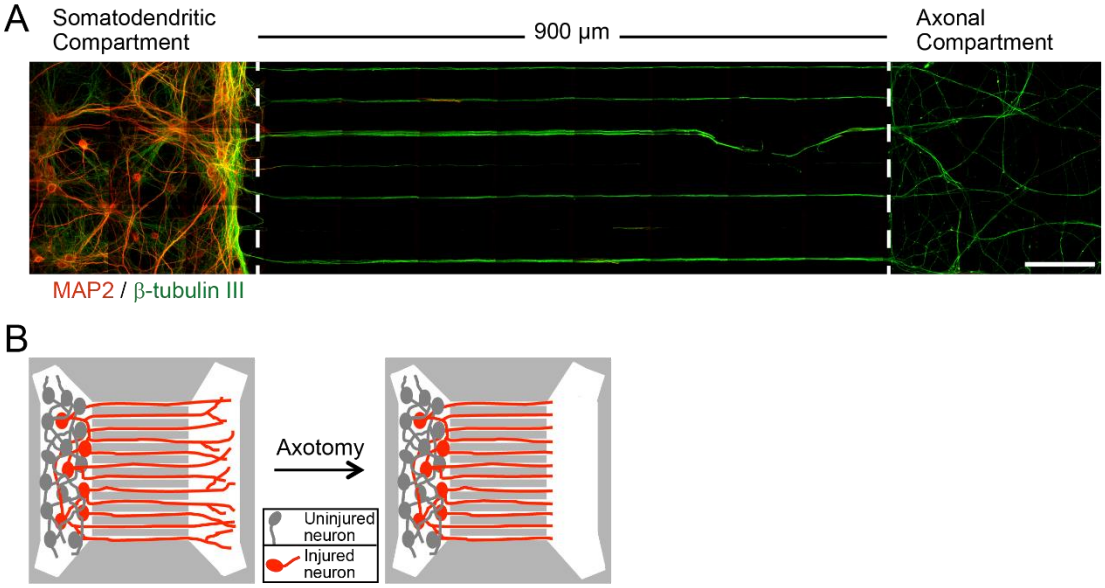

Figure. 3.1. Long projecting axons of rat hippocampal neurons grown in axon-isolating microfluidic chambers can be injured.
A. Representative montage image of fixed embryonic rat hippocampal neurons immunostained for somata and dendrites (MAP2, red) and axons (β-tubulin III, green), scale bar 100µm.
B. Diagram demonstrating axotomy of long projecting neurons and the mixed population of neurons that were injured (red) and uninjured (grey).

Previous work developing this *in vitro* axotomy model (Taylor et al., 2005; Taylor et al., 2009) but lacked the ability to track and label individual regenerating axons. To label the axons within the axonal compartment we applied recombinant Cholera toxin B subunit conjugated to Alexa Fluor 488 (Thermo Fisher Scientific, C34775) to the isolated axonal compartment. Cholera toxin B subunit binds to the pentasaccharide chain of ganglioside G_{M1} on the neuronal plasma membrane and is a common low-toxicity tool for *in vivo* retrograde tracing of neurons (Xu and Sudhof, 2013). Lateral diffusion of fluorescently labeled gangliosides within the plasma membrane lead to intense labeling of the somata in less than 24 h. We used live fluorescent imaging to identify the somata and axons before and 24 h after axotomy (Fig. 3.2A and 3.2B). Twenty-four hours after axotomy regeneration of fluorescently labeled axons was seen (Fig. 3.2A, arrowheads) while pseudo-DIC imaging revealed growth of axons that were not fluorescently labeled (Fig. 3.2A, arrows). Regeneration of injured axons suggested that axotomy in our *in vitro* system was not lethal. Further, gross cellular morphology was no different between directly injured neurons, labeled with Cholera toxin B subunit, and unlabeled uninjured neurons in the same culture 24 h after axotomy (Fig. 3.2A and 3.2B, Somata). Fluorescent imaging

settings were adjusted 24 h after axotomy to capture the faint regenerating axons leading to the appearance of increased fluorescence intensity of the somata and uninjured axons (compare fluorescent intensity of somata before and after manipulation in Fig. 3.2A and 3.2B and axons in Fig. 3.2B).

We directly evaluated the viability of cultures using a fluorescent nucleic acid stain impermeant to live cells allowing differential staining of nuclei of live and dead cells. Quantification of cell viability verified that neuron viability was very high in our microfluidic cultures and was no different between naïve and injured cultures 24 h (Fig. 3.2C) or 48 h (Fig. 3.2D) after axotomy similar to *in vivo* findings (Greer et al., 2012). Supporting the use of this approach, we previously found that axotomy performed within the microfluidic chambers induced rapid expression of the immediate early gene *c-fos*, as reported *in vivo* (Ikeda and Nakagawa, 1998; Taylor et al., 2005).

Figure 3.2

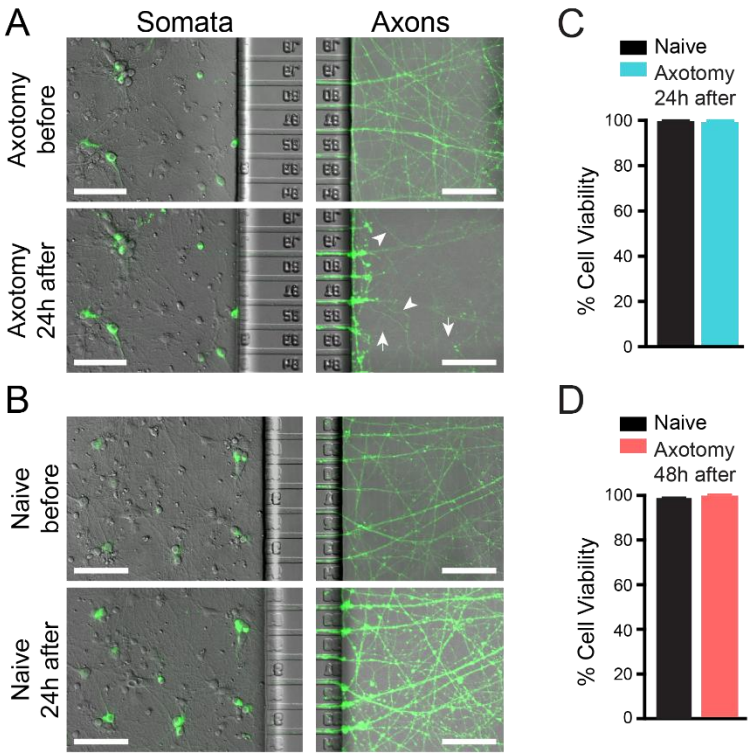

Figure. 3.2. Axons regenerated after axotomy and cell viability was unaffected.
Fluidically isolated axons and their somata were labeled with Cholera toxin conjugated to AlexaFluor 488 administered to the isolated axons (A, B).
A. Live imaging of somata and axons before and 24 hours (h) after axotomy. Arrows mark a representative non-fluorescent axon and arrowheads mark representative fluorescent regenerating axons, scale bars 100µm.
B. Live imaging of the somata and axons of naïve (uninjured) cultures before and 24h after the control manipulation.
C. Viability of naïve and axotomized cultures on DIV14, 24h after manipulation.
D. Viability of naïve and axotomized cultures on DIV15, 48h after manipulation.

Because the Cholera toxin imaging parameters had to be modified to capture the regenerating axons we sought an additional, brighter and more robust method to label the somata and axons that were directly injured. We chose to use a modified rabies virus carrying the fluorescent protein mCherry gene (Wickersham et al., 2007a). This method brightly labeled the somatodendritic arbor and axons of infected neurons within 48 h of viral treatment (Fig. 3.3A). Cultures infected with the modified rabies virus on DIV10 and imaged more than 48 hours later revealed that 80-85% of axons in the isolated compartment on DIV13 were positive for fluorescent protein. Live imaging of isolated axons before and immediately after axotomy showed the efficiency of our axotomy method (compare Fig. 3.3B and 3.3C). Repeated imaging of the regenerating axons in live cultures, 24 and 48 hours after axotomy,

showed that the regenerating axons, as expected, do not follow the same paths as the original axons (compare Fig. 3.3B, 3.3D and 3.3E). Additionally, these regenerated axons appear to create paths that are more jagged or irregular as compared to the original axon paths, potentially suggesting a change in growth cone function or cytoskeletal structure in regenerating hippocampal neuron axons.

Figure 3.3

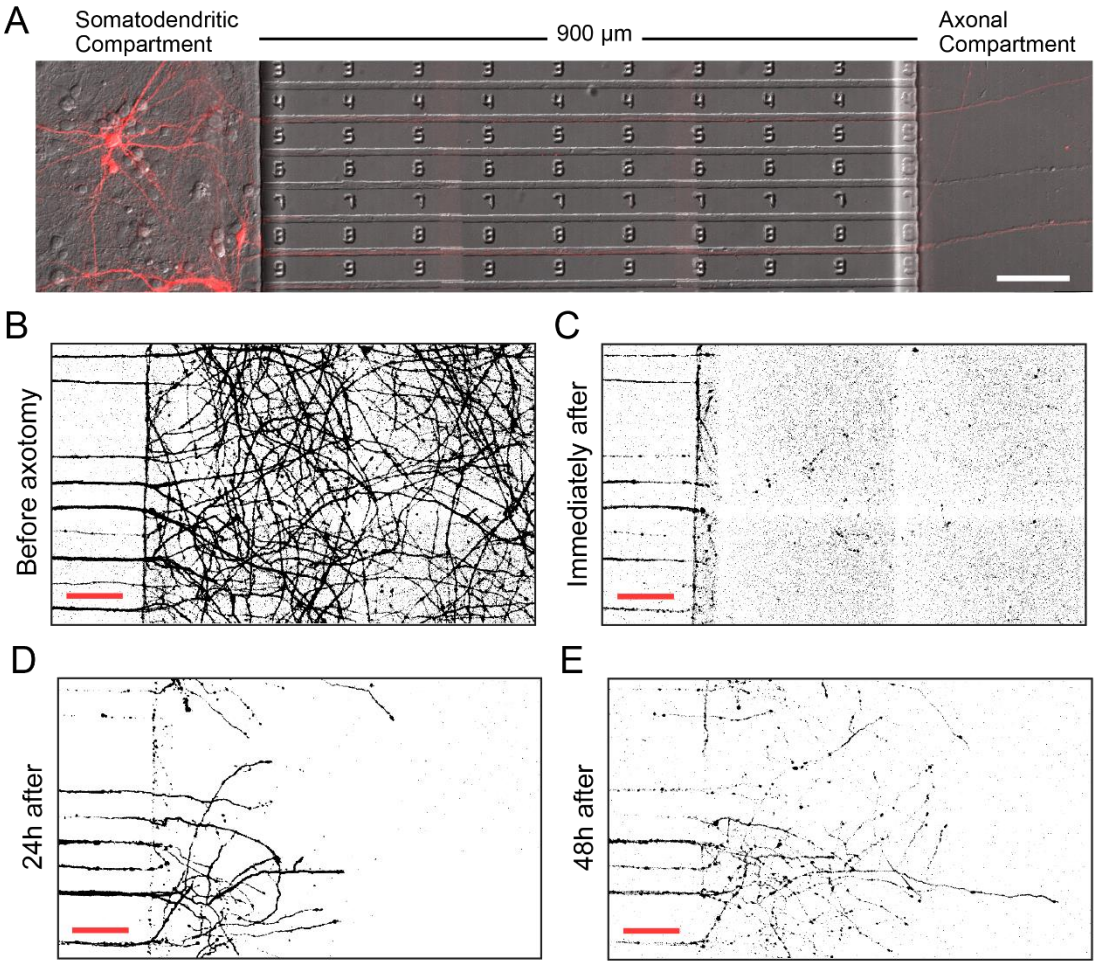

Figure. 3.3. Rabies virus carrying a fluorescent protein gene administered to the isolated axons allowed monitoring of the somatodendritic arbor and axons.
A. Representative live image montage of rabies virus treated neurons within a microfluidic culture chamber imaged 48h after viral infection, scale bar 100µm.
Repeated imaging of mCherry labeled axons regenerating following axotomy
B. A representative montage field of mCherry labeled axons on DIV13, prior to axotomy, scale bar 100µm.
C. The same axon field as in B imaged immediately after axotomy, scale bar 100µm.
D. The same axon field as in B imaged 24h after axotomy, scale bar 100µm.
E. The same axon field as in B imaged 48h after axotomy, scale bar 100µm.

Neurons with axons extending into the isolated compartment are typically close to the microgrooves

To determine the average percentage of neurons that had axons within the axonal compartment, and therefore were susceptible to axotomy, we again applied Alexa Fluor 488 conjugated recombinant Cholera toxin B subunit to the isolated axonal compartment, these axons were not injured. The cells were fixed, DAPI counterstained and imaged (Fig. 3.4A). For comparison we simultaneously evaluated neurons grown in two-compartment chambers with microgrooves of 900

µm, 450 µm or 150 µm. Only the microgroove length differed between these designs; all other dimensions of these chambers were identical, including compartment dimensions, number and spacing of microgrooves, as well as microgroove height and width. Equivalent numbers of cells were plated in all the chambers. The chambers with 150 µm microgrooves had statistically more neurons with fluidically isolated axons (approximately 10%) while there was no statistically significant difference between the chambers with 450 µm or 900 µm microgrooves (Fig. 3.4B**,** mean ± SEM: 150 µm: 0.1004 ± 0.001856; 450 µm: 0.05947 ± 0.004805; 900 µm: 0.04489 ± 0.001356).

Figure 3.4

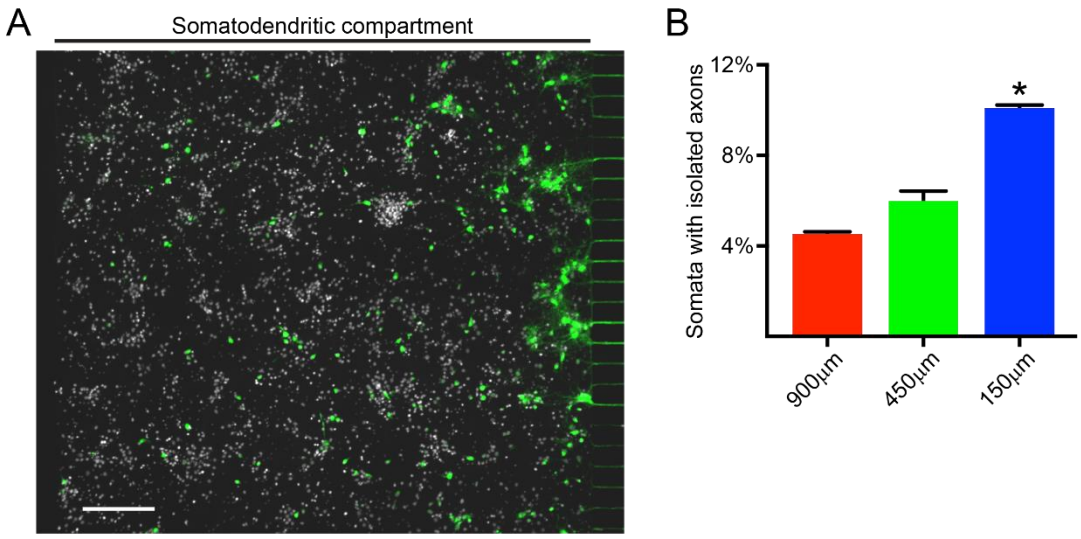

Figure. 3.4. The number of cells with isolated axons depended on microgroove length. **A.** Representative merged montage image of somatodendritic compartment with 150 µm long microgrooves oriented to the right. Somata with isolated axons were labeled with Cholera toxin conjugated to AlexaFluor 488 (green) and DAPI (white) was used to label all nuclei, scale bar 200µm. **B.** Quantification of the percent of DAPI labeled nuclei that were also positive for Cholera toxin in microfluidic chambers with different length microgrooves. Quantification field dimensions were approximately 2.0 mm x 1.7 mm, asterisks (*) indicates ANOVA with Tukey multiple comparisons test p-value < 0.01.

We were further interested in determining the probability that the axons of somata proximal to the microgrooves entered the isolated compartment versus whether the axons of somata distal to the microgrooves did so. To do this we visually divided the width of the somatic compartment, approximately 2 mm, into four equal regions of 0.5 mm x 1.7 mm (Fig. 3.5A). The most distal region was 1.5 mm to 2 mm from the microgrooves, the mid-distal region was 1.0 mm to 1.5 mm, the mid-proximal region was 0.5 mm to 1.0 mm and the most proximal region was 0 mm to 0.50 mm from the microgroove. We compared the regions within each microgroove length design and across designs (Fig. 3.5B). Surprisingly, there was no significant difference between the three microgroove designs in the most distal region from the microgrooves (region 1). Within each design there was no difference between the most distal region (region 1) and the mid-distal region (region 2) but between designs the mid-distal region of the 150 µm design had significantly more cells with axons in the isolated compartment than the 450 µm and 900 µm designs. The mid-proximal region (region 3) of the 900 µm design was not statistically different from the most distal or mid-distal regions but within the 450 µm

and 150 µm designs the mid-proximal region had significantly more cells with axons crossing the microgrooves. The most proximal region (region 4) within each design had the greatest number of soma with axons in the isolated compartment; the most proximal region is significantly different from all other regions within each design. Across designs the mid-proximal and most proximal regions of each design is significantly different from the others.

Figure 3.5

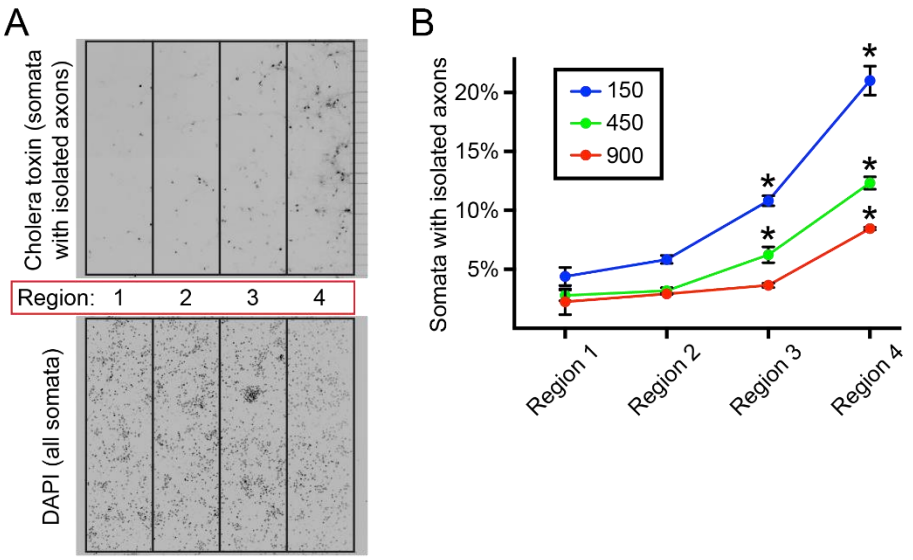

Figure. 3.5. The distribution of cells with isolated axons depended on microgroove length.
A. Separate greyscale images of the Cholera toxin and DAPI channels shown in A with the 4 regions outlined (most distal, mid-distal, mid-proximal and most proximal).
B. Quantification of the percent of DAPI labeled nuclei that were also positive for Cholera toxin in each region of the somatodendritic compartment of microfluidic chambers with different length microgrooves. The dimensions of each region were approximately 0.5 mm x 1.7 mm, asterisks (*) indicates ANOVA with Tukey multiple comparisons test p-value < 0.05 versus the immediate region more distal to the microgrooves.

Transcription is necessary for axotomy-induced functional changes

To evaluate how synapses are modified following distal axon injury, we next investigated whether presynaptic release properties were altered after axotomy. FM dyes, lipophilic styryl compounds, have been used in a variety of methods involving the plasma membrane and vesiculation, including eukaryotic cell endocytosis (Wiederkehr et al., 2000) and exocytosis (Mair et al., 1999). FM dyes have been applied to synaptically active neurons where the dye becomes internalized within recycling synaptic vesicles, intensely labeling the nerve terminals (Betz and Bewick, 1992; Betz and Angleson, 1998; Murthy and Stevens, 1998; Rea et al., 2004; Taylor et al., 2013). FM dyes are nontoxic, water soluble and virtually non-fluorescent in aqueous media. Their lipophilic nature allows them to insert into the cellular surface membrane where they become brightly fluorescent. FM puncta highly co-localize with synapsin1 presynaptic marker protein immunostaining. FM dyes provided us with a non-selective, unbiased method to label a majority of presynaptic terminals within the somatodendritic compartment (Gaffield and Betz, 2006; Taylor et al., 2013). FM5-95 is a slightly less

lipophilic analog of the red-fluorescent dye FM4-64 and can be easily removed from the cell membrane, minimizing background fluorescence, through repeated washes with Advasep-7, a sulfobutylated β-cyclodextrin derivative with higher affinity for FM dyes than the plasma membrane (Kay et al., 1999). Our FM loading method used a high concentration Potassium chloride solution (90 mM KCl) to rapidly stimulate synaptic vesicle cycling, exocytosis followed by endocytosis, after cells had been briefly incubated in an FM5-95 solution containing the antagonists CNQX (6-cyano-7-nitroquinoxaline-2,3-dione disodium, AMPA receptors) and D-AP5 (D-(-)-2-amino-5-phosphonopentanoic acid, NMDA receptors). We captured a representative field of FM puncta closest to the microgroove barrier region within the somatodendritic compartments at 60x magnification. This field was within the region where statistically the largest percentage of axotomized neurons were located, as determined in the previous section (Fig. 3.5B). We captured FM fluorescence to optically measure synaptic vesicle release before (Fig. 3.6A i and ii, Fig. 3.6B i and ii), during and after a 1 minute electrical field stimulation (Fig. 3.6A iii and Fig. 3.6B iii).

Twenty-four hours after axotomy there was no change in synaptic vesicle release kinetics as compared to naïve controls (Fig. 3.6C). In contrast, 48 h after axotomy synaptic vesicle release rate was significantly enhanced (Fig. 3.6D). The difference in presynaptic release rate persisted, though modestly, 4 days (d) after axotomy. Together, these data suggest a delayed and persistent increase in synaptic vesicle release rate following axotomy.

Figure 3.6

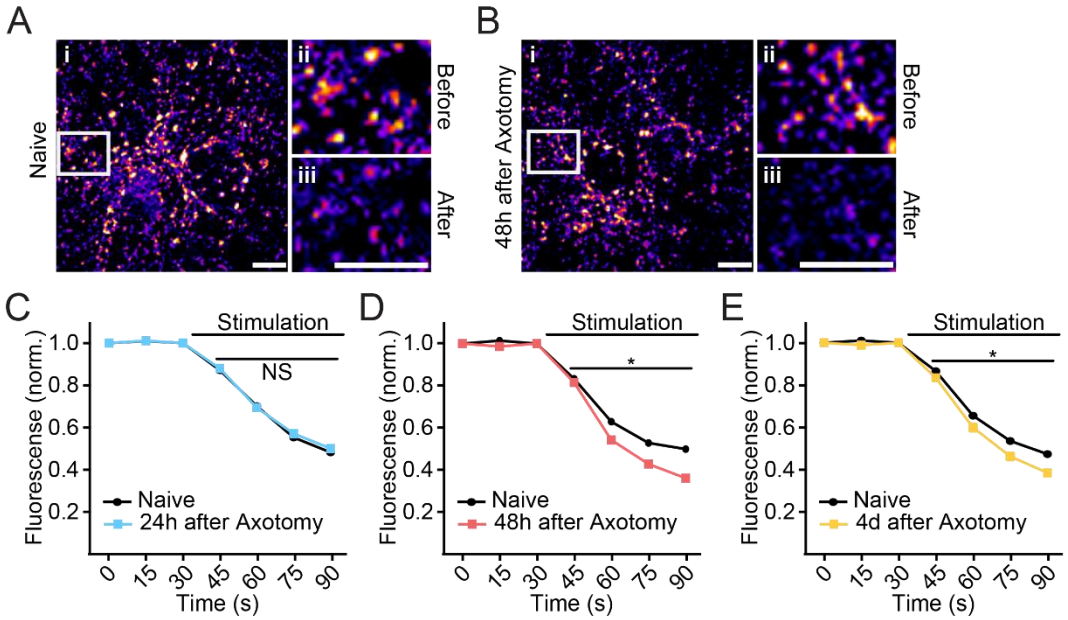

Figure. 3.6. Axotomy-induced hyper-excitability was present 48 hours after axotomy and persisted to 4 days after axotomy.
A. Representative images of FM5-95 labeled presynaptic terminals (FM puncta) proximal to the microgrooves within the somatodendritic compartment of a naïve culture on DIV15. Color look up table 'Fire'. (i) The whole field captured and evaluated for synaptic vesicle release kinetics, enlarged outlined region shows FM puncta before (ii) and after (iii) field stimulation (1 minute), scale bars 10µm.
B. Representative images of FM5-95 labeled presynaptic terminals (FM puncta) proximal to the microgrooves within the somatodendritic compartment of an axotomized culture on DIV15, 48 h after axotomy. Color look up table 'Fire'. (i) The whole field captured and evaluated for synaptic vesicle release kinetics, enlarged outlined region shows FM puncta before and after field stimulation (1 minute), scale bars 10µm.
C. FM unloading 24 h after axotomy (naive, n=782; axotomy, n=877; 4 chambers for each condition). NS, indicates no statistically significant difference between treatments, alpha = 0.05.
D. FM unloading 48 h after axotomy (naive, n=1,024; axotomy, n=1,015; 6 chambers for each condition). Asterisks (*) indicates two-way ANOVA with Bonferroni multiple comparison test p-value < 0.01 versus Naive.
E. FM unloading 4 days (d) after axotomy (naive, n=1,024; axotomy, n=1,015; 6 chambers for each condition). Asterisks (*) indicates two-way ANOVA with Bonferroni multiple comparison test p-value < 0.01 versus Naive.

Efficient axon regeneration requires signaling from the site of injury to the nucleus in multiple model systems (Rishal and Fainzilber, 2014), yet the signaling events required for synaptic remodeling following distal axotomy remain unclear. Breach of the axonal membrane following axon injury causes an influx of calcium and sodium ions into the intra-axonal space, potentially influencing signaling to the nucleus and gene expression. The retrograde axotomy signal could be chemical or molecular. Disruption of the axonal ion gradients could lead to back propagating action potentials which have the potential to initiate a cascade of events. Alternatively, the injury might activate local molecular

signaling events, such as local translation, changes in activity of cytoskeletal motor proteins or ion-dependent enzymes that communicate the injury to the cell body. To determine whether synaptic activity during axotomy, possibly caused by disruption of ion gradients following breach of the plasma membrane, was involved in the hyper-excitability seen 48 h after axotomy we treated the somatodendritic compartment with tetrodotoxin (TTX) 15 min prior to, during and 45 min after axotomy. Tetrodotoxin reversibly binds voltage-gated sodium channels preventing action potentials. Somatodendritic action potential blockade with TTX at the time of axotomy did not affect changes in presynaptic release (Fig. 3.7A). Next, we investigated whether injury-induced transcription was required for the presynaptic changes seen at 48 h. We treated the somatodendritic compartment with the reversible transcriptional blocker DRB 15 min prior to axotomy and removed the drug 45 minutes later. We found that blocking transcription during this brief time was sufficient to prevent the axotomy-induced hyper-excitability at 48 h compared with similarly treated naive chambers (Fig. 3.7B). We conclude that the transcriptional response rapidly initiated following distal axotomy, but not local synaptic activity during axotomy, is a critical mediator of the delayed changes in presynaptic release properties.

Figure 3.7

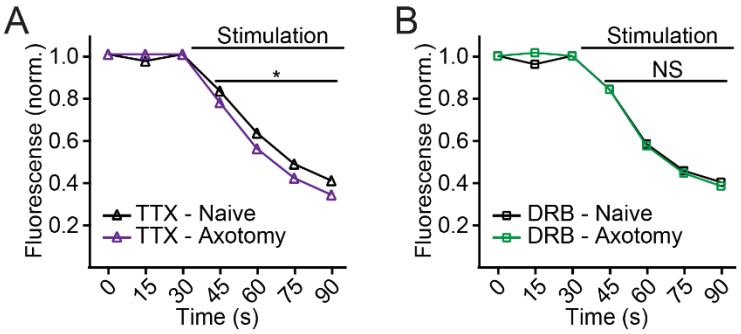

Figure. 3.7. Hyper-excitability is dependent on transcription not action potentials at the time of axotomy.
A. FM5-95 unloading curves following application of TTX. Approximately 200 puncta were analyzed per chamber; 4 individual chambers were analyzed for each condition across two independent experiments. The same trend was observed in each pair of experiments. Asterisks (*) indicates two-way ANOVA with Bonferroni multiple comparison test p-value < 0.01 versus Naive.
B. FM5-95 unloading following application of DRB. Approximately 200 puncta were analyzed per chamber; 4 individual chambers were analyzed per condition across two independent experiments. Two-way ANOVA with Bonferroni multiple comparison test, alpha = 0.05, NS indicates no statistically significant difference between treatments.

Microarray analysis suggests possible mechanisms of injury-induced plasticity

To identify differentially expressed transcripts that might mediate axotomy-induced synaptic plasticity within a therapeutically-relevant time window we performed microarray analysis 24 h after axotomy. Total RNA was collected from the somatodendritic compartment of three axotomized and three naïve cultures and submitted to the UNC Lineberger Comprehensive Cancer Center Genomics Core. RNA integrity was evaluated by TapeStation gel and fluorescence intensity traces (Fig. 3.8A and 3.8B). Consistently strong ribosomal RNA banding (Fig. 3.8A) and peaks (Fig. 3.8B), at approximately 1500 nt and 5000 nt, and a minor amount of degraded RNA confirmed the integrity of the RNA. In addition, the TapeStation reports an objective, robust and reproducible measurement of RNA degradation, the RNA integrity number equivalent (RIN^e), on a linear scale from 1 (fully degraded) to 10 (no degradation). Our samples ranged from RIN^e 9.2 to 9.7.

RNA samples were evaluated by microarray at the UNC School of Medicine Functional Genomics Core. Raw microarray probe fluorescence data was automatically normalized to on-chip Affymetrix controls. We evaluated the distribution of probe cell intensity across all six samples (Fig. 3.8C) to confirm that each microarray dataset was reliable. The Robust Multichip Analysis (RMA) algorithm was used for global background adjustment, quantile normalization and gene expression

summarization between replicate samples. This method is sensitive to small changes between samples without negatively affecting signal variance. Following RMA we re-evaluated the distribution of the probe intensity (Fig. 3.8D) finding an equivalent distribution within and between our treatment groups. Lastly, Pearson's correlation analysis of gene expression (Fig. 3.8E) suggested a modest amount of differential gene expression between our samples. Taken together, these data reassured us that our gene expression data was reliable and suggested that we would find only a few genes that were differentially expressed following axotomy.

Figure 3.8

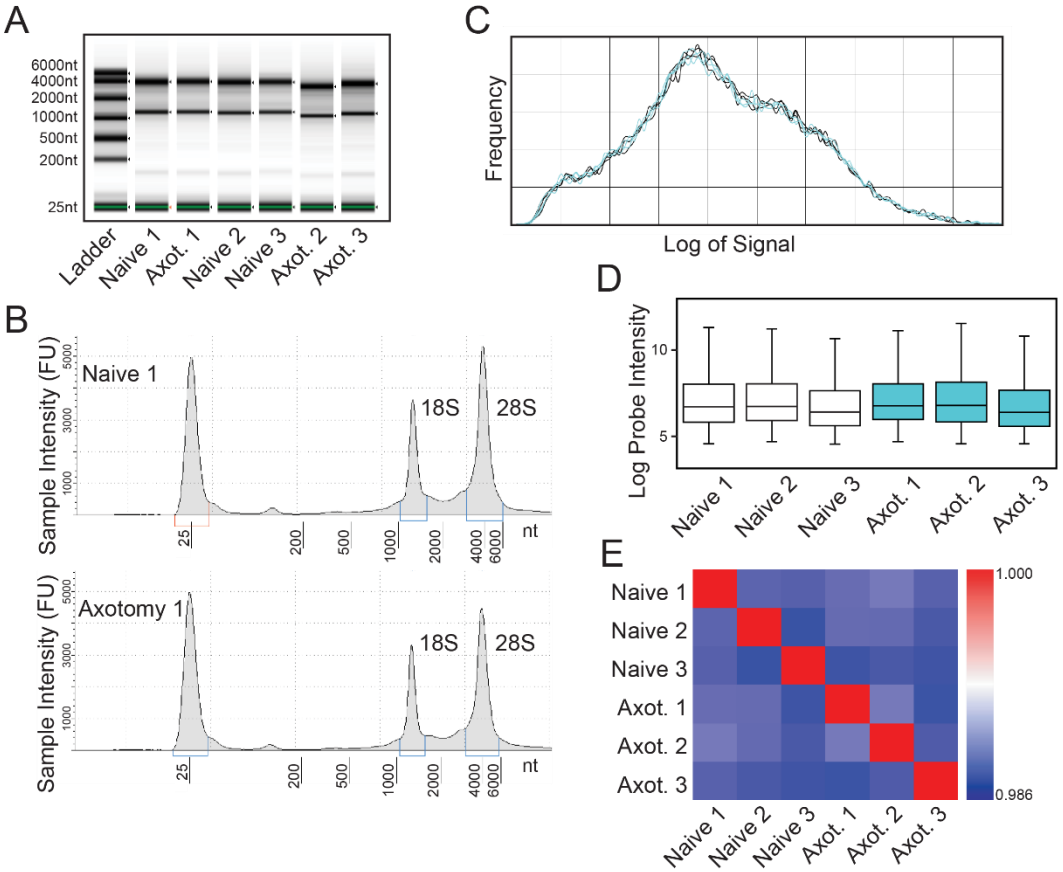

Figure. 3.8. RNA quality assessment and verification of microarray quality controls.
A. Image of ScreenTape gel from TapeStation RNA quality assessment of triplicate naïve and axotomy (Axot.) RNA samples, standard ladder is included.
B. Fluorescence intensity traces of ScreenTape lanes from "Naïve 1" and "Axotomy 1" samples plotted versus nucleotide length as determined by the ladder. Clearly defined 18S and 28S bands in the gel (A) and peaks in the traces (B) indicate high quality RNA samples.
C. Histogram of microarray probe cell intensity prior to RMA analysis, plotted as frequency of signal versus signal intensity (log scale) for all naive (black) and axotomy (blue) arrays.
D. Box-and-whiskers plot of the probe cell intensity (log scale) for each of the triplicate naïve (white) and axotomy (Axot., blue) arrays following RMA analysis.
E. Pearson's correlation of normalized expression signal after analysis of triplicate naïve and axotomy (Axot.) arrays. Indicator to the right demonstrates degree of correlation between samples.

The lack of a drastic change in the transcriptional profile 24 h after axotomy was not completely unexpected having determined that in these cultures approximately 4.5% of the cells were directly injured (Fig. 3.4B). To account for this fact we set a low threshold for differential gene expression, 5% change in expression (± 0.05 fold change) with ANOVA p-value < 0.05 (Fig. 3.9A). This threshold resulted in 1059 differentially expressed probes representing 639 known genes. DAVID Gene Functional Classification (Huang da et al., 2009a; Huang da et al., 2009b) revealed that genes

in ‘synaptic function’, ‘calcium binding’, ‘neuron projections’ and ‘cell cycle’ were significantly enriched in the differentially expressed genes. We evaluated whether the genes in these categories tended to increase or decrease in expression following axotomy and found that they were equally distributed, except for ‘cell cycle’ genes which were predominantly increased (Fig. 3.9B). ‘Synaptic function’ and ‘calcium binding’ genes as the top differentially expressed categories suggests that the transcription dependent hyper-excitability might be directly mediated through changes in expression of synaptic proteins and calcium-dependent enzymes which can modify synaptic proteins.

Figure 3.9

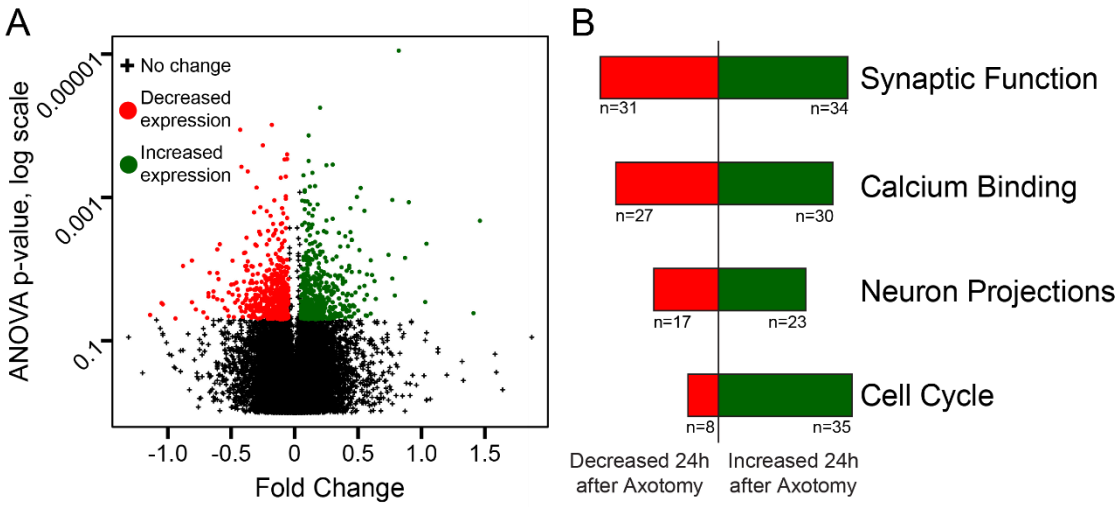

Figure. 3.9. Differential gene expression 24 hours after axotomy.
A. Volcano plot of gene expression fold change (linear, x-axis) versus ANOVA p-value (log, y-axis). Threshold for significantly changed gene expression was set at 0.05 with ANOVA p-value < 0.05. Unchanged probes are black (n = 29370), probes with significantly decreased expression are red (n = 521) and probes with significantly increased expression are green (n = 538).
B. Top DAVID gene ontology categories of differentially expressed genes. Number of genes with decreased expression in each category represented by red bars. Number of genes with increased expression in each category represented by green bars.

Differential gene expression following in vitro axotomy resembles that of young rats 24 hours after spinal cord injury

Finally, we wanted to determine if gene expression in our *in vitro* axotomy model was similar to gene expression following *in vivo* spinal cord injury (Jaerve et al., 2012). In this *in vivo* model the corticospinal tract (CST) of young and old rats (2- and 22-months old, respectively) was injured, by dorsal spinal cord hemisection. The sensorimotor cortex layer V, which contained the somata of primary motor neurons projecting their axons to the corticospinal tract, was collected 1, 7 and 35 days post operation (DPO) for microarray gene expression analysis. They verified that the correct cortical region was collected using DiI delivered to the injury site as a retrograde tracer. This region not only contained the somata of directly injured neurons but also those of uninjured neurons and astrocytes, oligodendrocytes and microglia.

We hypothesized that our differential expression data from embryonic rat hippocampal neurons 24 h after axotomy would most closely resemble the differential expression of young rats 1 DPO. The *in vivo* data and our *in vitro* data were measured using different microarray chip platforms

so a direct comparison was not possible. To overcome this we determined the comparable probe sets from the two microarray platforms (19991 probe sets) and rank scored the gene expression fold change for each dataset from lowest to highest, this controlled for different scales of gene expression across experiments. We analyzed the fold change rank correlation of our axotomy induced differential gene expression with that of the six datasets generated by Jaerve *et al* (Fig. 3.10). The Spearman correlation r value quantitatively reports the correlation between two datasets from -1 (negatively correlated) to 1 (positively correlated), an r value of 0 indicates no correlation. As predicted, our data had the highest Spearman correlation r value with the data from young rats 1 DPO. Unexpectedly, the second highest correlation was with the data from old rats 1 DPO. Also, our data was significantly positively correlated with the young rats 35 DPO but not young rats 7 DPO. To confirm that these correlation values represented true correlation we compared 5 randomly generated dataset to the *in vitro* and *in vivo* data, the resulting r values ranged from 0.020 to -0.015 with an average of 0.0015. This confirms a true correlation between these *in vitro* and *in vivo* models. A similar correlation pattern was obtained when we evaluated 'fold change' not 'rank scored fold change'. These results suggest that the early time course of gene expression changes within our *in vitro* axotomy model broadly recapitulated those seen *in vivo* in the first 24 h after corticospinal tract injury.

Figure 3.10

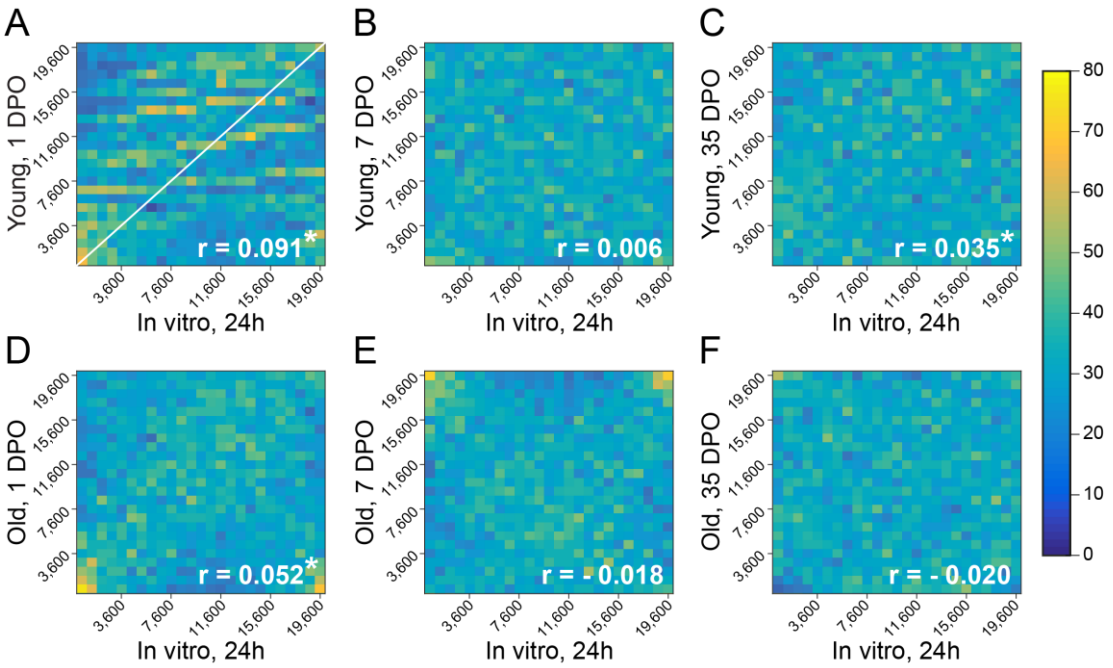

Figure. 3.10. Comparison of ranked gene expression fold change from *in vitro* axotomy model and published *in vivo* corticospinal tract injury model.
Bivariate histograms of the 19991 microarray probes sets common between our in vitro axotomy data and in vivo injury data generated by Jaerve et al, 2012. Dorsal spinal cord hemisection operation was performed on young (2 months old) and old (22 months old) rats and gene expression in the sensorimotor cortex layer V was evaluated at 3 time points. XY scatter data was binned 25 x 25 and coloring corresponds to the number of probes in each bin, according to scale on far right. Two-tailed Spearman correlation of ranked expression, r value quantifies the correlation, asterisks (*) indicates two-tailed p-value < 0.0001.
A. Ranked correlation between 24 hour in vitro axotomy and injured young rats (2 months old) 1 day post operation (DPO). White diagonal line marks 1:1 correspondence of ranked expression, note how the bins with more probes (tinted orange and yellow as opposed to blue and purple) roughly follow this diagonal indicating correlation. Asterisks (*) indicates two-tailed p-value < 0.0001.
B. Ranked correlation between 24 hour in vitro axotomy and injured young rats (2 months old) 7 days post operation (DPO). Note that there are few orange-yellow bins and no clustering around the diagonal.
C. Ranked correlation between 24 hour in vitro axotomy and injured young rats (2 months old) 35 days post operation (DPO). Note that there are no bright yellow bins but there is clustering toward the diagonal of orange-yellow bins. Asterisks (*) indicates two-tailed p-value < 0.0001.
D. Ranked correlation between 24 hour in vitro axotomy and injured old rats (22 months old) 1 day post operation (DPO). There are bright yellow bins and clustering along the diagonal demonstrating statistically significant correlation between the datasets. Asterisks (*) indicates two-tailed p-value < 0.0001.
E. Ranked correlation between 24 hour in vitro axotomy and injured old rats (22 months old) 7 day post operation (DPO). Correlation r value is not statistically significant.
F. Ranked correlation between 24 hour in vitro axotomy and injured old rats (22 months old) 35 day post operation (DPO). Correlation r value is not statistically significant.

DISCUSSION

Significance

While axon regeneration following injury is extensively studied, much less is known about how proximal neurons within the mammalian brain are affected following axonal damage (Canty et al., 2013) and more specifically how synapses onto injured neurons are remodeled. We used a model system to enable the study the cellular mechanisms of synaptic remodeling following axon injury; this model recapitulated several hallmarks of neurons subjected to axonal injury *in vivo*, including axon regeneration and retrograde hyper-excitability (Nudo and Milliken, 1996; Nudo, 2013; Takechi et al., 2014). Axotomy-induced transcriptional changes in this *in vitro* model are also consistent with *in vivo* findings (Jaerve et al., 2012; Urban et al., 2012). Because of the ability to separate neuronal compartments, this tool facilitates the investigation of axotomy-induced retrograde signaling intrinsic to neurons and the resulting effects to interneuronal communication.

Our results demonstrate that axon regeneration occurs autonomously and viability and gross morphology of axotomized neurons is normal. Regeneration of axons within the peripheral nervous system (PNS) depends on axon-to-soma signaling, multiple transcription factor pathways and epigenetic mechanisms (Loh et al., 2017; Wang et al., 2017; Weng et al., 2017) but PNS neurons have a higher capacity for axon regeneration than CNS neurons and autonomous activation of these mechanisms appear to be uniquely to the PNS. It has been proposed that exogenous activation of these regenerative mechanisms or those involved in CNS axon growth and neurite extension might facilitate CNS axon regeneration (Patel et al., 2017; Venkatesh and Blackmore, 2016).

The changes in presynaptic plasticity that we saw, and have been characterized *in vivo* (Nudo and Milliken, 1996; Nudo, 2013; Takechi et al., 2014), required the activation of a transcriptional response within the first 45 m after axotomy. This is consistent with axonal injury signaling in other non-CNS model systems (Rishal and Fainzilber, 2014). Laser axotomy of *in vitro* peripheral neurons laser axotomy induced local calcium influx that back-propagated to the nucleus to induce a transcriptional response that was necessary for axon regeneration (Cho et al., 2013). The localized influx of calcium may be a priming effect for axonal translation of signaling complexes (Chierzi et al.,

2005) or retrograde transport of pre-existing signaling complexes required to initiate transcription (Rishal and Fainzilber, 2014). Further, our TTX results suggests that any disorganized or random spiking of axotomized neurons was not a major contributor to the changes in presynaptic function observed 48 h after axotomy.

Our microarray results suggest that the presynaptic functional changes might depend on molecular remodeling of the synapse through altered expression of 'synaptic function' transcripts and 'calcium binding' proteins. Axon regeneration and synaptic plasticity might be facilitated through transcriptional changes of mRNAs associated with 'neuron projections'. Cyclin-dependent kinase 5 (Cdk5) and it's activator (p35/p25), canonical cell cycle proteins, have been shown to have neuron-specific cell cycle-independent functions in synaptic plasticity and Alzheimer-like pathology (Seo et al., 2014; Sheng et al., 2016). Many DNA repair proteins and pathways, commonly classified as 'cell cycle', are associated with neurodevelopmental or neurodegenerative diseases. Rad51, a central component in homologous recombination during double strand break repair, distributes from the perinuclear region to the axon following Netrin-1 bath application and regulates axon branching stimulated by Netrin-1 (Glendining et al., 2017). Mutations associated with Amyotrophic Lateral Sclerosis have been shown to reduce the prevention or repair of normal transcription-associated DNA damage (Hill et al., 2016) or generate amounts of DNA damage that are lethal to neurons (Farg et al., 2017). Additionally, single nucleotide polymorphism variants in two base excision repair genes significantly increase the risk of Parkinson's disease following environmental exposure to pesticides (Sanders et al., 2017). The enrichment of 'cell cycle' genes in our differentially expressed transcripts could be involved in the synaptic plasticity changes seen at 48 h or, speculatively, in responding to DNA damage induced by axon injury.

Finally, our demonstration that gene expression in our *in vitro* model system broadly correlates with gene expression following *in vivo* injury supports the conclusion that our simple, robust and reliable axotomy model is biologically relevant and helpful tool for evaluating neuronal gene expression and response following axon injury. While the correlation r values were low we are confident they represent a true similarity between the gene expression profiles. Low r values potentially result from the cellular heterogeneity of the two systems. Our *in vitro* data included a large

population of uninjured neurons while the *in vivo* data encompassed multiple cell types, including injured and uninjured neurons, astrocytes, oligodendrocytes and microglia, each with a potentially unique response to the stress of injury.

Axonal damage within the CNS occurs in multiple disorders and diseases, but little is known about the overall impact on cortical circuit function. Our findings and model system have broader applicability beyond spinal cord injury to conditions where axonal damage is prevalent such as traumatic brain injury, Alzheimer's disease, and multiple sclerosis.

Possible improvements

We modified two retrograde tracing methods, fluorescently labeled Cholera toxin subunit B and a modified rabies virus delivering a fluorescent protein gene, to identify the somata directly injured by *in vitro* axotomy. Both of these methods had unique strengths and weaknesses. The greatest strength of Cholera toxin labeling was that cells could be imaged or axotomized immediately after treatment. Additionally, all Cholera toxin labeled axons were equivalently fluorescent initially. Unfortunately, there was variability in the somata labeling intensity and labeling was isolated to the cell body with very little dendritic labeling. Second, the fluorescence intensity of the Cholera toxin labeling decreased over time; photobleaching during imaging, dilution of the label during membrane expansion associated with axon regeneration and recycling of toxin bound gangliosides likely all contributed to this.

A drawback of rabies virus was that mCherry expression was not visible until around 48 h after viral treatment. Further, at 48 h only 80-85% of the axons in the isolated compartment were fluorescently labeled. This could be due to axons entering the compartment after the viral treatment, resistance of these axons to the virus or a slower course of viral infection and gene expression such that mCherry had not reached the threshold for imaging. Additionally, the time course of fluorescent protein accumulation required for imaging was inconsistent between neurons. In each culture cells were brightly fluorescent after 48 h. As we imaged the same cultures over the course of a four days a few more cells became fluorescent raising the question whether these neurons were different from the cells that were fluorescent at 48 h after infection. This difference in fluorescent protein expression

could be due to temporal variations in the course of events between viral infection and fluorescent protein accumulation or, more concerning, it could suggest trans-synaptic viral transmission. The glycoprotein, genetically removed in these G-deleted viruses, is required for receptor binding and membrane fusion and this viral genotype has been characterized to be transmission incompetent without a helper virus carrying the glycoprotein gene (Wickersham et al., 2007b). The greatest benefits of the rabies virus method were that the fluorescent protein was present throughout the neuron, including the dendrites and dendritic spines, facilitating very detailed morphological evaluation of the injured cells and the fluorescent signal did not fade over time or with repeated imaging.

CHAPTER FOUR: FUTURE DIRECTIONS

Many of the major challenges associated with investigating intra-axonal events are limitations of scale; while axons are long their volume is small making them difficult to visually and physically isolate *in vivo* from the surrounding cells. *In vitro* isolation of axons is easier, especially using specially designed axon-isolating culture chambers, but the yield of material for biochemical analysis is extremely low. Pooling or amplifying samples prior to analysis can compensate for low yield but these manipulations can introduce background noise. Novel microfluidic chamber configurations could be designed to increase axon yield. As technological advances make it easier to isolate and evaluate axons some of the most interesting questions to address include the regulation and specific location of translation within axons, a deeper understanding of bidirectional axon-to-glia communication, a deeper understanding of the widespread effect of axon injury, especially in the CNS, and the extent to which 'model' organisms model human neurons.

Novel microfluidic chamber to increase axon yield

In the current symmetric microfluidic chamber configuration (Fig. 4.1A) the vast majority of the isolated axon come from neurons closest to the microgrooves such that very few of the neurons have isolated axon (Fig. 3.4B and Fig. 3.5B). Factors contributing to the probability that an axon reaches the fluidically isolated compartment include the probability that the axon enters a microgroove, which is a random event, and the potential maximum axon length of that neuron. Neuron classes have different length axons *in vivo*, for example inhibitory interneurons of the hippocampus have short axons while excitatory neurons have significantly longer axons. Tissue samples enriched for neurons with short axons will always have fewer fluidically isolated axons than samples enriched for neurons with the capacity to extend long axons.

To increase the yield of axons and the percentage of cells with isolated axons I propose a novel asymmetric compartment design (Fig. 4.1B) based on the quantitative analysis of isolated axons

in the existing symmetric design. In this design the somata compartment is half the width of the original design and twice as long (1 mm by 14 mm). These dimensions maintain the surface area and volume of the compartment so the same number of somata can be seeded into the ‘Somata compartment’ in this design as the original to maintain cell density. The neurons in the new design are distributed closer the microgrooves, effectively increasing the number of axons that will enter the microgrooves, to increase axon yield and the percentage of somata with isolated axons. The axon compartment remains 2 mm to provide a large surface area for axon growth. I predict in a chamber with 150 µm microgrooves approximately 20% of the embryonic rat hippocampal derived neurons would have fluidically isolated axons, with 450 µm microgrooves approximately 12% and in a 900 µm microgroove configuration more than 7%. This would significantly increase axon yield as well as the percentage of somata that could be evaluated following axon manipulation

Figure 4.1

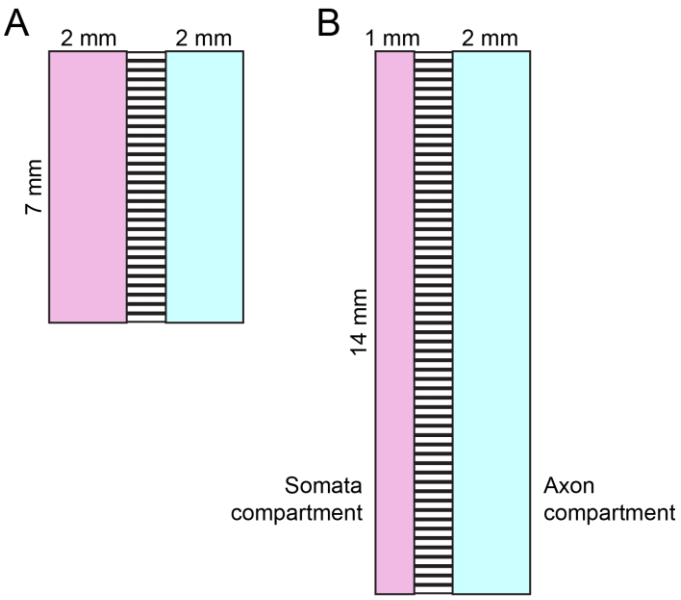

Figure. 4.1. A novel asymmetric microfluidic chamber design to maximize axon growth.
A. Current symmetric microfluidic chamber configuration. Two identical microfluidic chambers are separated by over 150 microgrooves, somata can be plated in either chamber and axons extend into the opposite chamber.
B. Proposed novel asymmetric microfluidic chamber. Somata are specifically plated in the narrow 'Somata compartment' which is separated from the 'Axon compartment' by over 300 microgrooves. This design should facilitate the isolation of significantly more axons from significantly more neurons

Zooming in on the axonal transcriptome

Are there quantitative or qualitative differences in the axonal transcriptome along the length of the axon? Is RNA equally distributed along the axon or is it clustered, potentially with translational machinery, increasing the local concentration of components necessary for translation? RNA-FISH puncta for specific transcripts appear to be almost randomly distributed along the axon, with clustering at presynaptic terminals (Taylor et al., 2013) and enrichment at growth cones (Yao et al., 2006). More broadly, polyA RNA-FISH for total mRNA demonstrated a difference between the axon portion close to the soma and distal axon regions (Bassell et al., 1994) though translationally silent mRNAs frequently have very short polyA tails (Jain and Parker, 2013).

Many of the tools necessary to address these broad questions *in vitro* are available. Transgenic cells or animals can be used to study specific mRNAs and their proteins within live axons but broad questions require broader tools. Selective RNA dyes compatible with live cell imaging have been developed (Li et al., 2006) and SYTO RNASelect dye is commercially available (Thermo Fisher

Scientific). These stains could reveal the distribution of RNA within fluidically isolated axons *in vitro*. The isolated axons could be treated directly or, potentially, RNA transport could be visualized by treating the fluidically isolated somata and imaging the axon compartment. To visualize changes in the distribution of axonal RNA during synaptogenesis inert presynapse-inducing microspheres (Lucido et al., 2009) can be added in following RNA labeling within the somata or axons.

An alternative to this synaptogenesis model system is the use of co-culture assays that support synaptogenesis (Biederer and Scheiffele, 2007). Cell adhesion molecule 1 (SynCAM) is a brain-specific protein that functions as a cell adhesion molecule at the synapse (Biederer et al., 2002). Exogenous expression of SynCAM in non-neuronal cells, such as HEK 293 cells, co-cultured with hippocampal neurons is sufficient to induce synapse initiation and maturation (Biederer et al., 2002). A microfluidic chamber design with one compartment enclosed in PDMS, for the neuron somata, connected by microgrooves to an open compartment not enclosed in PDMS could be used for such co-culture experiments. Dissociated neurons would be plated in the enclosed compartment and grown for 7 to 10 d to allow axons to extend into the open compartment. HEK 293 cells expressing SynCAM would be added at low density to the isolated axons and RNA localization dynamics could be observed by live microscopy. Axonal RNA could be labeled prior to adding the HEK 293 cells to observe redistribution of RNA during synaptogenesis and synapse maturation or added to the somata coincident with adding the HEK 293 cells to observe RNA transport during these events. While the SYTO RNASelect dye can be visualized with standard fluorescein (FITC) filters microscopy equipment capable of detecting dim signal at high magnification would be necessary. Post-imaging processing could be applied to differentiate the signal from noise as well, such as algorithms correcting for point spread function.

Stimulus driven changes in local translation

There are clear examples of stimulus-driven axonal translation, such as in synaptic plasticity. Are maintenance functions, for example synthesis of mitochondrial proteins, constitutive or stimulus-driven? Of the whole axonal transcriptome which mRNAs are constitutively translated and which transition from translationally silent to active to meet the demand for new proteins?

Polysome profiling, to differentiate actively translating mRNAs from translationally silent mRNAs (Zuccotti and Modelska, 2016), of the axonal transcriptome would provide an informative window into the regulation of intra-axonal translation in multiple contexts. This technique uses sucrose gradients to enrich for actively translating ribosomes and their bound mRNA. Ribosomal RNA is then preferentially degraded and the remaining mRNAs are sequenced. It requires a significant amount of starting material so careful optimization of methods to pool and/ or amplify axonal ribosome-associated mRNA, as well as deconvolution of the sequencing results, would be necessary. This technique could be applied to microfluidically isolated axons *in vitro* treated with neurotrophic factors.

An alternative method to investigate actively translated mRNAs, the translatome, in the context of synaptic plasticity could use the cre-mediated RiboTag allele (Sanz et al., 2009) specifically expressed in the presynaptic neuron of the CA3-CA1 hippocampal synapse. The promoter for the α subunit of Ca^{2+}/calmodulin-dependent protein kinase II (CAMK2A) is specific to the CA3 neuron in the hippocampus (Xu et al., 2000; Zakharenko et al., 2003). The hippocampal sub-region containing the CA3 axons can be dissected and evaluated before and after LTP induction in organotypical hippocampal slice cultures (Kang et al., 1997), a form of plasticity at this synapse that is dependent on presynaptic translation (Kang and Schuman, 1996). The differentially translated mRNAs following the induction of LTP would suggest specific ways the local proteome changes with LTP. This information could suggest specific mRNA targets to investigate in the context of LTP or inform mechanistic studies of the signaling cascade regulating plasticity-inducing translation.

Axon-glia communication

Glia-to-axon RNA transport has only been investigated in the mammalian PNS and Schwann cells in the context of injury and regeneration. Is glia-to-axon RNA transport limited to injury signaling in the PNS, where axon regeneration is common? Does glia-to-axon RNA transport explain why PNS axon regeneration occurs while CNS axon regeneration, where oligodendrocytes are the local glial cells, does not occur? Further, current work of axon injury signaling focuses on axon-to-soma signaling, should axon injury signaling focus on axon-to-glia signaling molecules and mechanisms too?

The axon-to-glia distance is significantly shorter than the axon-to-soma distance suggesting that glial cells are poised to have a more rapid local response. Visually and physically separating the axon from the neuron somata *in vivo* is easier than separating the axon from the surrounding glia. Combining genetic tools with super-resolution microscopy or immuno-EM might allow differentiation of neuron-derived ribosomes and oligodendrocyte-derived ribosomes in the mature CNS.

Multiple genetic mouse tools exist to specifically express transgenes in oligodendrocytes. Recombinant adeno-associated viral (rAAV) vectors with the human myelin associated glycoprotein (MAG) promoter are specific for oligodendrocytes (von Jonquieres et al., 2016). The myelin basic protein (MBP) promoter can be used to drive exogenous gene expression in oligodendrocytes of transgenic mice (Goujet-Zalc et al., 1993) or delivered by rAAV (Chen et al., 1999). Neuron specific transgene expression can be controlled with the synapsin 1 promoter (Schoch et al., 1996) or an rAAV carrying the cytomegalovirus (CMV) immediate early promoter (Chen et al., 1999). *In vivo* expression of a neuron-specific myc-tagged ribosomal protein L4 and an oligodendrocyte specific HA-tagged ribosomal protein L4 followed by super-resolution microscopy or immune-EM for the peptide tags in axons of the CNS could suggest whether glia-to-axon ribosome transport occurs in the uninjured adult CNS and the relative contribution of ribosomes from the soma versus the surrounding oligodendrocytes.

Secondary axon injury signaling

Much of the *in vitro* mechanical axon injury work has focused on the neuron-intrinsic response to the initial primary axon injury but there is clear evidence of progressive long-term secondary loss of function, far from the injury site, that follow neural network pathways. The complex primary injury involves neurons, glia, and blood vessels, with immediate small scale hemorrhage and hypoxia. Some aspects of the *in vivo* injury response are beneficial and necessary to repair cerebral circulation while other aspects lead to widespread functional changes within the brain. These primary and secondary injuries in the CNS, following stroke and blunt trauma to the brain and spine, contribute to the disability and mortality of these conditions. Currently, we do not understand the molecular events and

biochemical messengers of the secondary injuries well enough to develop targeted pharmacological therapeutics.

A more refined view of the transcriptional events following distal axotomy might lead to a better treatment course following brain and spinal cord injury. In this era of significant advances in single-cell molecular biology, including proteomics and DNA and RNA sequencing, we could directly evaluate injured neurons separate from their uninjured neighbors. Our simple methods of labeling injured neurons using Cholera toxin or G-deleted rabies virus could be coupled with laser capture microdissection (LCM) to evaluate transcription factor occupancy, by DNA immunoprecipitation methods, immediately following axotomy, the transcriptional timeframe we identified as critical for altered synaptic plasticity 48 h later. In addition, we could evaluate *de novo* transcription using nuclear run-on assay techniques in the primary injured neurons and the secondary neurons. Neuron labeling coupled with LCM could be used to investigate injury-induced epigenetic remodeling, which has been studied in PNS neurons but not CNS neurons (Loh et al., 2017; Weng et al., 2017).

While the focus of this work was not on CNS axon regeneration we are poised to build on previously published work evaluating mRNAs within regenerating axons (Taylor et al., 2009). Identification of local molecular mechanisms facilitating CNS axon regeneration and pharmacological manipulation of regeneration have significant therapeutic value for rehabilitation following spinal cord and brain injuries. Our model system, using enriched neuronal preparations and axon-isolating microfluidic chambers, is more reproducible and cost effective than *in vivo* injury models for reductionist mechanistic studies and drug screens.

Human stem cell derived neurons and axon function

As in all biomedical research fields, there is the question of similarity between humans and the common mammalian model organisms. Human axons tend to be longer that the axons of model organisms, does the increase in axon-to-soma distance necessitate a significantly different reliance on local translation? Axon localized ATF4 mRNA, implicated in Alzheimer's Aβ peptide toxicity signaling (Baleriola et al., 2014), has been verified in post-mortem human brain tissue from healthy adults and Alzheimer's disease patients (Baleriola et al., 2015) but there are many obstacles to obtaining human

samples and culturing human neurons. Researchers are turning to neurons derived *in vitro* from human stem cells as an additional model system.

While derivative, it is important to confirm that key findings in rodent axons are conserved in human axons. Verifying that axonal translation is necessary for axon guidance, response to neurotrophins, axon maintenance and injury signaling in hESC-neurons will begin to reveal similarities and differences between the model systems. Stem cell derived neurons are synaptically active but whether they have the capacity for synaptic plasticity has not been established. With a better understanding of the functional limitations and strengths of *in vitro* differentiated and matured human neurons their research utility will be clearer.

The ability to generate patient-derived induced pluripotent stem cells and differentiate these cells to neurons within axon isolating microfluidic chambers will facilitate studying axon function in complex genetic diseases such as schizophrenia and autism spectrum disorders. CRISPR-mediated engineered stem cells, such as targeted deletion of RNA binding proteins associated with neurological diseases, applied to our system would provide further insight into axonal mRNA trafficking and local translation in human neurons. Mechanistic examination of translation within human axons has the potential to reveal human specific axonal mRNAs and mechanisms in disease and normal neuron function.

Closing thoughts

Many of the traits that make us uniquely human physically originate in our neural networks. Our language skills, social skills, external and internal perception, motor skills, thoughts, memories and our consciousness itself are all encoded in our brain. These exquisite traits make us what we are as a species and who we are as individuals. Brain injury as well as neurodevelopmental and neurodegenerative diseases are financially costly to diagnose and treat but the true costs are how these conditions can negatively affect our most valuable qualities. The benefits to mankind of research to better understand our complex nervous system in health and disease could lie in restoring these functions.

APPENDIX A: hESC-NEURON EXPRESSION OF CELL TYPE SPECIFIC MARKERS

Soma average expression signal, log2 (Exp) of markers for neural stem cells, mature neurons, astrocytes and oligodendrocytes used for Figure 2.4A, sorted alphabetically by gene name.

NEURAL STEM CELL		**MATURE NEURON**		**ASTROCYTE**		**OLIGODENDROCYTE**	
Gene	**Exp**	**Gene**	**Exp**	**Gene**	**Exp**	**Gene**	**Exp**
BUB1	5.29	CALB1	6.05	ACOT11	4.68	ADAMTS4	5.24
BUB1B	5.61	CRH	4.45	ACSBG1	4.76	BCAS1	5.55
CRMP1	4.62	DCX	9.19	ALDH1L1	4.78	CLDN11	5.17
CYP2D6	4.83	DLX1	6.36	ALDOC	6.9	CPM	4.3
CYP2E1	4.45	ENO2	6.04	AQP4	4.37	ELOVL7	5.08
DRD2	5.58	EPHA7	8.01	ATP1A2	5.49	ENPP6	4.27
DRD4	5.09	GABRA1	5.16	BMPR1B	5.21	ERBB3	4.71
GSTM1	6.51	GABRA5	5.69	CHRDL1	6.22	EVI2A	4.1
GSTM3	5.42	GABRG2	5.27	DCN	4.87	FA2H	4.88
KIF20A	4.39	GDA	5.35	DIO2	4.34	GAL3ST1	6.41
LIPC	4.49	GLRA2	6.19	F3	4.77	GPR62	4.9
LPL	5.32	GPR88	6.05	FZD2	6.25	GSN	5.09
NEUROG2	4.7	HS3ST2	5.21	GFAP	5.55	IL23A	5.33
OGG1	5.6	HTR2C	4.24	GJB6	4.77	MAG	4.51
PAX6	5.61	MAL2	6.35	HAPLN1	3.87	MAL	5.74
PSMA2	4.88	MAP2	9.59	MERTK	4.24	MBP	4.91
SEMA4G	5.57	MEF2C	6.63	MLC1	5.65	MOBP	4.95
SEMA6C	5.38	MYT1L	6.91	NFIX	6.43	MOG	3.22
SOX1	5.77	NCAM1	7.85	PAPSS2	5.63	OLIG1	5.18

SRGAP1	6.01	NEFM	9.92	PLA2G7	4.95	OLIG2	5.47
XRCC1	6.14	NEUROD6	4.55	PPP1R3G	5.22	PDGFRA	4.44
		NOV	5.52	PRODH	4.72	PLA2G4A	4.93
		NPAS4	4.71	RFX4	8.98	PLEKHH1	5.44
		NTS	6.15	SLC14A1	4.24	PLP1	6.6
		PCSK2	5.4	SLC15A2	5.22	PLXNB3	5.02
		PGM2L1	8.72	SLC1A1	4.04	PPP1R14A	5.16
		PLCXD3	4.93	SLC1A2	7.06	PRKCQ	4.07
		PRDM8	5.38	SLC1A3	7.93	SGK2	5.37
		SATB2	5.16	SLC25A18	4.89	SOX10	5.71
		SCG2	8.4	SLC39A12	4.39	SRPK3	5.05
		SLA	5.36	SLC4A4	6.91	TSPAN2	7.46
		SLC12A5	6.1	TLR3	4.09		
		SLC17A6	5.2	TTPA	4.55		
		SNAP25	7.85				
		SSTR2	5.69				
		STMN2	10.54				
		SYT1	7.68				
		TUBB3	6.14				
		VIP	4.6				

REFERENCES

Alvarez, J., Giuditta, A., and Koenig, E. (2000). Protein synthesis in axons and terminals: significance for maintenance, plasticity and regulation of phenotype. With a critique of slow transport theory. Prog. Neurobiol. 62, 1-62.

Andreassi, C., Zimmermann, C., Mitter, R., Fusco, S., De Vita, S., Saiardi, A., and Riccio, A. (2010). An NGF-responsive element targets myo-inositol monophosphatase-1 mRNA to sympathetic neuron axons. Nat. Neurosci. 13, 291-301.

Aschrafi, A., Schwechter, A.D., Mameza, M.G., Natera-Naranjo, O., Gioio, A.E., and Kaplan, B.B. (2008). MicroRNA-338 regulates local cytochrome c oxidase IV mRNA levels and oxidative phosphorylation in the axons of sympathetic neurons. J. Neurosci. 28, 12581-12590.

Baleriola, J., Jean, Y., Troy, C., and Hengst, U. (2015). Detection of Axonally Localized mRNAs in Brain Sections Using High-Resolution In Situ Hybridization. J. Vis. Exp. (100):e52799. doi, e52799.

Baleriola, J., Walker, C.A., Jean, Y.Y., Crary, J.F., Troy, C.M., Nagy, P.L., and Hengst, U. (2014). Axonally synthesized ATF4 transmits a neurodegenerative signal across brain regions. Cell 158, 1159-1172.

Bamji, S.X., Rico, B., Kimes, N., and Reichardt, L.F. (2006). BDNF mobilizes synaptic vesicles and enhances synapse formation by disrupting cadherin-beta-catenin interactions. J. Cell Biol. 174, 289-299.

Bamji, S.X., Shimazu, K., Kimes, N., Huelsken, J., Birchmeier, W., Lu, B., and Reichardt, L.F. (2003). Role of beta-catenin in synaptic vesicle localization and presynaptic assembly. Neuron 40, 719-731.

Baronchelli, S., La Spada, A., Conforti, P., Redaelli, S., Dalpra, L., De Blasio, P., Cattaneo, E., and Biunno, I. (2015). Investigating DNA methylation dynamics and safety of human embryonic stem cell differentiation towards striatal neurons. Stem Cells Dev.

Barrientos, R.M., O'Reilly, R.C., and Rudy, J.W. (2002). Memory for context is impaired by injecting anisomycin into dorsal hippocampus following context exploration. Behav. Brain Res. 134, 299-306.

Bassell, G.J., Singer, R.H., and Kosik, K.S. (1994). Association of poly(A) mRNA with microtubules in cultured neurons. Neuron 12, 571-582.

Benech, C., Sotelo, J.R.,Jr, Menendez, J., and Correa-Luna, R. (1982). Autoradiographic study of RNA and protein synthesis in sectioned peripheral nerves. Exp. Neurol. 76, 72-82.

Ben-Yaakov, K., Dagan, S.Y., Segal-Ruder, Y., Shalem, O., Vuppalanchi, D., Willis, D.E., Yudin, D., Rishal, I., Rother, F., Bader, M.*, et al.* (2012). Axonal transcription factors signal retrogradely in lesioned peripheral nerve. EMBO J. 31, 1350-1363.

Betz, W.J., and Angleson, J.K. (1998). The synaptic vesicle cycle. Annu. Rev. Physiol. 60, 347-363.

Betz, W.J., and Bewick, G.S. (1992). Optical analysis of synaptic vesicle recycling at the frog neuromuscular junction. Science 255, 200-203.

Biederer, T., Sara, Y., Mozhayeva, M., Atasoy, D., Liu, X., Kavalali, E.T., and Sudhof, T.C. (2002). SynCAM, a synaptic adhesion molecule that drives synapse assembly. Science 297, 1525-1531.

Biederer, T., and Scheiffele, P. (2007). Mixed-culture assays for analyzing neuronal synapse formation. Nat. Protoc. 2, 670-676.

Biewenga, J.E., Schrama, L.H., and Gispen, W.H. (1996). Presynaptic phosphoprotein B-50/GAP-43 in neuronal and synaptic plasticity. Acta Biochim. Pol. 43, 327-338.

Bisbal, M., Wojnacki, J., Peretti, D., Ropolo, A., Sesma, J., Jausoro, I., and Caceres, A. (2009). KIF4 mediates anterograde translocation and positioning of ribosomal constituents to axons. J. Biol. Chem. 284, 9489-9497.

Cahoy, J.D., Emery, B., Kaushal, A., Foo, L.C., Zamanian, J.L., Christopherson, K.S., Xing, Y., Lubischer, J.L., Krieg, P.A., Krupenko, S.A., Thompson, W.J., and Barres, B.A. (2008). A transcriptome database for astrocytes, neurons, and oligodendrocytes: a new resource for understanding brain development and function. J. Neurosci. 28, 264-278.

Cajigas, I.J., Tushev, G., Will, T.J., tom Dieck, S., Fuerst, N., and Schuman, E.M. (2012). The local transcriptome in the synaptic neuropil revealed by deep sequencing and high-resolution imaging. Neuron 74, 453-466.

Calabresi, P., Maj, R., Pisani, A., Mercuri, N.B., and Bernardi, G. (1992). Long-term synaptic depression in the striatum: physiological and pharmacological characterization. J. Neurosci. 12, 4224-4233.

Calliari, A., Farias, J., Puppo, A., Canclini, L., Mercer, J.A., Munroe, D., Sotelo, J.R., and Sotelo-Silveira, J.R. (2014). Myosin Va associates with mRNA in ribonucleoprotein particles present in myelinated peripheral axons and in the central nervous system. Dev. Neurobiol. 74, 382-396.

Calliari, A., Sotelo-Silveira, J., Costa, M.C., Nogueira, J., Cameron, L.C., Kun, A., Benech, J., and Sotelo, J.R. (2002). Myosin Va is locally synthesized following nerve injury. Cell Motil. Cytoskeleton 51, 169-176.

Campenot, R.B. (1977). Local control of neurite development by nerve growth factor. Proc. Natl. Acad. Sci. U. S. A. 74, 4516-4519.

Canty, A.J., Teles-Grilo Ruivo, L.M., Nesarajah, C., Song, S., Jackson, J.S., Little, G.E., and De Paola, V. (2013). Synaptic elimination and protection after minimal injury depend on cell type and their prelesion structural dynamics in the adult cerebral cortex. J. Neurosci. 33, 10374-10383.

Cautain, B., Hill, R., de Pedro, N., and Link, W. (2015). Components and regulation of nuclear transport processes. FEBS J. 282, 445-462.

Chen, H., McCarty, D.M., Bruce, A.T., and Suzuki, K. (1999). Oligodendrocyte-specific gene expression in mouse brain: use of a myelin-forming cell type-specific promoter in an adeno-associated virus. J. Neurosci. Res. 55, 504-513.

Chierzi, S., Ratto, G.M., Verma, P., and Fawcett, J.W. (2005). The ability of axons to regenerate their growth cones depends on axonal type and age, and is regulated by calcium, cAMP and ERK. Eur. J. Neurosci. 21, 2051-2062.

Cho, Y., Sloutsky, R., Naegle, K.M., and Cavalli, V. (2013). Injury-induced HDAC5 nuclear export is essential for axon regeneration. Cell 155, 894-908.

Choi, S., and Lovinger, D.M. (1997). Decreased probability of neurotransmitter release underlies striatal long-term depression and postnatal development of corticostriatal synapses. Proc. Natl. Acad. Sci. U. S. A. 94, 2665-2670.

Colak, D., Ji, S.J., Porse, B.T., and Jaffrey, S.R. (2013). Regulation of axon guidance by compartmentalized nonsense-mediated mRNA decay. Cell 153, 1252-1265.

Collin, C., Vicario-Abejon, C., Rubio, M.E., Wenthold, R.J., McKay, R.D., and Segal, M. (2001). Neurotrophins act at presynaptic terminals to activate synapses among cultured hippocampal neurons. Eur. J. Neurosci. 13, 1273-1282.

Court, F.A., and Alvarez, J. (2005). Local regulation of the axonal phenotype, a case of merotrophism. Biol. Res. 38, 365-374.

Court, F.A., Hendriks, W.T., MacGillavry, H.D., Alvarez, J., and van Minnen, J. (2008). Schwann cell to axon transfer of ribosomes: toward a novel understanding of the role of glia in the nervous system. J. Neurosci. 28, 11024-11029.

Court, F.A., Midha, R., Cisterna, B.A., Grochmal, J., Shakhbazau, A., Hendriks, W.T., and van Minnen, J. (2011). Morphological evidence for a transport of ribosomes from Schwann cells to regenerating axons. Glia 59, 1529-1539.

Cox, L.J., Hengst, U., Gurskaya, N.G., Lukyanov, K.A., and Jaffrey, S.R. (2008). Intra-axonal translation and retrograde trafficking of CREB promotes neuronal survival. Nat. Cell Biol. 10, 149-159.

Dillon, C., and Goda, Y. (2005). The actin cytoskeleton: integrating form and function at the synapse. Annu. Rev. Neurosci. 28, 25-55.

Ding, M.C., Wang, Q., Lo, E.H., and Stanley, G.B. (2011). Cortical excitation and inhibition following focal traumatic brain injury. J. Neurosci. 31, 14085-14094.

Donnelly, C.J., Fainzilber, M., and Twiss, J.L. (2010). Subcellular communication through RNA transport and localized protein synthesis. Traffic 11, 1498-1505.

Donnelly, C.J., Park, M., Spillane, M., Yoo, S., Pacheco, A., Gomes, C., Vuppalanchi, D., McDonald, M., Kim, H.H., Merianda, T.T., Gallo, G., and Twiss, J.L. (2013). Axonally synthesized beta-actin and GAP-43 proteins support distinct modes of axonal growth. J. Neurosci. 33, 3311-3322.

Doron-Mandel, E., Fainzilber, M., and Terenzio, M. (2015). Growth control mechanisms in neuronal regeneration. FEBS Lett. 589, 1669-1677.

Duan, L., Peng, C.Y., Pan, L., and Kessler, J.A. (2015). Human pluripotent stem cell-derived radial glia recapitulate developmental events and provide real-time access to cortical neurons and astrocytes. Stem Cells Transl. Med. 4, 437-447.

Eng, H., Lund, K., and Campenot, R.B. (1999). Synthesis of beta-tubulin, actin, and other proteins in axons of sympathetic neurons in compartmented cultures. J. Neurosci. 19, 1-9.

Eyman, M., Cefaliello, C., Ferrara, E., De Stefano, R., Lavina, Z.S., Crispino, M., Squillace, A., van Minnen, J., Kaplan, B.B., and Giuditta, A. (2007). Local synthesis of axonal and presynaptic RNA in squid model systems. Eur. J. Neurosci. 25, 341-350.

Farg, M.A., Konopka, A., Ying Soo, K., Ito, D., and Atkin, J.D. (2017). The DNA damage response (DDR) is induced by the C9orf72 repeat expansion in Amyotrophic Lateral Sclerosis. Hum. Mol. Genet.

Frost, S.B., Barbay, S., Friel, K.M., Plautz, E.J., and Nudo, R.J. (2003). Reorganization of remote cortical regions after ischemic brain injury: a potential substrate for stroke recovery. J. Neurophysiol. 89, 3205-3214.

Gaffield, M.A., and Betz, W.J. (2006). Imaging synaptic vesicle exocytosis and endocytosis with FM dyes. Nat. Protoc. 1, 2916-2921.

Gambetti, P., Autilio-Gambetti, L., Shafer, B., and Pfaff, L.D. (1973). Quantitative autoradiographic study of labeled RNA in rabbit optic nerve after intraocular injection of (3H)uridine. J. Cell Biol. 59, 677-684.

Garesse, R., and Vallejo, C.G. (2001). Animal mitochondrial biogenesis and function: a regulatory cross-talk between two genomes. Gene 263, 1-16.

Genheden, M., Kenney, J.W., Johnston, H.E., Manousopoulou, A., Garbis, S.D., and Proud, C.G. (2015). BDNF stimulation of protein synthesis in cortical neurons requires the MAP kinase-interacting kinase MNK1. J. Neurosci. 35, 972-984.

Gioio, A.E., Eyman, M., Zhang, H., Lavina, Z.S., Giuditta, A., and Kaplan, B.B. (2001). Local synthesis of nuclear-encoded mitochondrial proteins in the presynaptic nerve terminal. J. Neurosci. Res. 64, 447-453.

Glendining, K.A., Markie, D., Gardner, R.J., Franz, E.A., Robertson, S.P., and Jasoni, C.L. (2017). A novel role for the DNA repair gene Rad51 in Netrin-1 signalling. Sci. Rep. 7, 39823.

Goldman, J.S., Ashour, M.A., Magdesian, M.H., Tritsch, N.X., Harris, S.N., Christofi, N., Chemali, R., Stern, Y.E., Thompson-Steckel, G., Gris, P.*, et al.* (2013). Netrin-1 promotes excitatory synaptogenesis between cortical neurons by initiating synapse assembly. J. Neurosci. 33, 17278-17289.

Goujet-Zalc, C., Babinet, C., Monge, M., Timsit, S., Cabon, F., Gansmuller, A., Miura, M., Sanchez, M., Pournin, S., and Mikoshiba, K. (1993). The proximal region of the MBP gene promoter is sufficient to induce oligodendroglial-specific expression in transgenic mice. Eur. J. Neurosci. 5, 624-632.

Gowda, M., Jantasuriyarat, C., Dean, R.A., and Wang, G.L. (2004). Robust-LongSAGE (RL-SAGE): a substantially improved LongSAGE method for gene discovery and transcriptome analysis. Plant Physiol. 134, 890-897.

Greer, J.E., Povlishock, J.T., and Jacobs, K.M. (2012). Electrophysiological abnormalities in both axotomized and nonaxotomized pyramidal neurons following mild traumatic brain injury. J. Neurosci. 32, 6682-6687.

Gumy, L.F., Yeo, G.S., Tung, Y.C., Zivraj, K.H., Willis, D., Coppola, G., Lam, B.Y., Twiss, J.L., Holt, C.E., and Fawcett, J.W. (2011). Transcriptome analysis of embryonic and adult sensory axons reveals changes in mRNA repertoire localization. RNA 17, 85-98.

Hanz, S., Perlson, E., Willis, D., Zheng, J.Q., Massarwa, R., Huerta, J.J., Koltzenburg, M., Kohler, M., van-Minnen, J., Twiss, J.L., and Fainzilber, M. (2003). Axoplasmic importins enable retrograde injury signaling in lesioned nerve. Neuron 40, 1095-1104.

Hengst, U., Cox, L.J., Macosko, E.Z., and Jaffrey, S.R. (2006). Functional and selective RNA interference in developing axons and growth cones. J. Neurosci. 26, 5727-5732.

Hill, S.J., Mordes, D.A., Cameron, L.A., Neuberg, D.S., Landini, S., Eggan, K., and Livingston, D.M. (2016). Two familial ALS proteins function in prevention/repair of transcription-associated DNA damage. Proc. Natl. Acad. Sci. U. S. A. 113, E7701-E7709.

Hillefors, M., Gioio, A.E., Mameza, M.G., and Kaplan, B.B. (2007). Axon viability and mitochondrial function are dependent on local protein synthesis in sympathetic neurons. Cell. Mol. Neurobiol. 27, 701-716.

Holt, C.E., and Schuman, E.M. (2013). The central dogma decentralized: new perspectives on RNA function and local translation in neurons. Neuron 80, 648-657.

Hsiao, K., Bozdagi, O., and Benson, D.L. (2014). Axonal cap-dependent translation regulates presynaptic p35. Dev. Neurobiol. 74, 351-364.

Hsu, W.L., Chung, H.W., Wu, C.Y., Wu, H.I., Lee, Y.T., Chen, E.C., Fang, W., and Chang, Y.C. (2015). Glutamate Stimulates Local Protein Synthesis in the Axons of Rat Cortical Neurons by Activating AMPA Receptors and Metabotropic Glutamate Receptors. J. Biol. Chem.

Hu, W., He, Y., Xiong, Y., Lu, H., Chen, H., Hou, L., Qiu, Z., Fang, Y., and Zhang, S. (2015). Derivation, Expansion, and Motor Neuron Differentiation of Human-Induced Pluripotent Stem Cells with Non-Integrating Episomal Vectors and a Defined Xenogeneic-free Culture System. Mol. Neurobiol.

Huang da, W., Sherman, B.T., and Lempicki, R.A. (2009a). Bioinformatics enrichment tools: paths toward the comprehensive functional analysis of large gene lists. Nucleic Acids Res. 37, 1-13.

Huang da, W., Sherman, B.T., and Lempicki, R.A. (2009b). Systematic and integrative analysis of large gene lists using DAVID bioinformatics resources. Nat. Protoc. 4, 44-57.

Ikeda, S., and Nakagawa, S. (1998). Spinal cord transection induced c-fos protein in the rat motor cortex. Brain Res. 792, 164-167.

Ivins, K.J., Bui, E.T., and Cotman, C.W. (1998). Beta-amyloid induces local neurite degeneration in cultured hippocampal neurons: evidence for neuritic apoptosis. Neurobiol. Dis. 5, 365-378.

Jacobs, K.M., and Donoghue, J.P. (1991). Reshaping the cortical motor map by unmasking latent intracortical connections. Science 251, 944-947.

Jaerve, A., Kruse, F., Malik, K., Hartung, H.P., and Muller, H.W. (2012). Age-dependent modulation of cortical transcriptomes in spinal cord injury and repair. PLoS One 7, e49812.

Jain, S., and Parker, R. (2013). The discovery and analysis of P Bodies. Adv. Exp. Med. Biol. 768, 23-43.

Jung, H., and Holt, C.E. (2011). Local translation of mRNAs in neural development. Wiley Interdiscip. Rev. RNA 2, 153-165.

Jung, H., O'Hare, C.M., and Holt, C.E. (2011). Translational regulation in growth cones. Curr. Opin. Genet. Dev. 21, 458-464.

Kaech, S., and Banker, G. (2006). Culturing hippocampal neurons. Nat. Protoc. 1, 2406-2415.

Kang, H., and Schuman, E.M. (1996). A requirement for local protein synthesis in neurotrophin-induced hippocampal synaptic plasticity. Science 273, 1402-1406.

Kang, H., Welcher, A.A., Shelton, D., and Schuman, E.M. (1997). Neurotrophins and time: different roles for TrkB signaling in hippocampal long-term potentiation. Neuron 19, 653-664.

Kar, A.N., Sun, C.Y., Reichard, K., Gervasi, N.M., Pickel, J., Nakazawa, K., Gioio, A.E., and Kaplan, B.B. (2014). Dysregulation of the axonal trafficking of nuclear-encoded mitochondrial mRNA alters neuronal mitochondrial activity and mouse behavior. Dev. Neurobiol. 74, 333-350.

Katsumoto, T., Mitsushima, A., and Kurimura, T. (1990). The role of the vimentin intermediate filaments in rat 3Y1 cells elucidated by immunoelectron microscopy and computer-graphic reconstruction. Biol. Cell 68, 139-146.

Kay, A.R., Alfonso, A., Alford, S., Cline, H.T., Holgado, A.M., Sakmann, B., Snitsarev, V.A., Stricker, T.P., Takahashi, M., and Wu, L.G. (1999). Imaging synaptic activity in intact brain and slices with FM1-43 in C. elegans, lamprey, and rat. Neuron 24, 809-817.

Kelly, A., Mullany, P.M., and Lynch, M.A. (2000). Protein synthesis in entorhinal cortex and long-term potentiation in dentate gyrus. Hippocampus 10, 431-437.

Kim, B.G., Dai, H.N., McAtee, M., Vicini, S., and Bregman, B.S. (2006). Remodeling of synaptic structures in the motor cortex following spinal cord injury. Exp. Neurol. 198, 401-415.

Kisiel, M., McKenzie, K., and Stewart, B. (2014). Localization and mobility of synaptic vesicles in Myosin VI mutants of Drosophila. PLoS One 9, e102988.

Koenig, E., and Martin, R. (1996). Cortical plaque-like structures identify ribosome-containing domains in the Mauthner cell axon. J. Neurosci. 16, 1400-1411.

Koenig, E., Martin, R., Titmus, M., and Sotelo-Silveira, J.R. (2000). Cryptic peripheral ribosomal domains distributed intermittently along mammalian myelinated axons. J. Neurosci. 20, 8390-8400.

Kondrashov, N., Pusic, A., Stumpf, C.R., Shimizu, K., Hsieh, A.C., Xue, S., Ishijima, J., Shiroishi, T., and Barna, M. (2011). Ribosome-mediated specificity in Hox mRNA translation and vertebrate tissue patterning. Cell 145, 383-397.

Korte, M., Griesbeck, O., Gravel, C., Carroll, P., Staiger, V., Thoenen, H., and Bonhoeffer, T. (1996a). Virus-mediated gene transfer into hippocampal CA1 region restores long-term potentiation in brain-derived neurotrophic factor mutant mice. Proc. Natl. Acad. Sci. U. S. A. 93, 12547-12552.

Korte, M., Staiger, V., Griesbeck, O., Thoenen, H., and Bonhoeffer, T. (1996b). The involvement of brain-derived neurotrophic factor in hippocampal long-term potentiation revealed by gene targeting experiments. J. Physiol. Paris 90, 157-164.

Lafon, M. (2005). Rabies virus receptors. J. Neurovirol. 11, 82-87.

Lankford, K.L., Waxman, S.G., and Kocsis, J.D. (1998). Mechanisms of enhancement of neurite regeneration in vitro following a conditioning sciatic nerve lesion. J. Comp. Neurol. 391, 11-29.

Levi-Montalcini, R. (1987). The nerve growth factor 35 years later. Science 237, 1154-1162.

Levi-Montalcini, R., and Hamburger, V. (1951). Selective growth stimulating effects of mouse sarcoma on the sensory and sympathetic nervous system of the chick embryo. J. Exp. Zool. 116, 321-361.

Levi-Montalcini, R., Meyer, H., and Hamburger, V. (1954). In vitro experiments on the effects of mouse sarcomas 180 and 37 on the spinal and sympathetic ganglia of the chick embryo. Cancer Res. 14, 49-57.

Li, Q., Kim, Y., Namm, J., Kulkarni, A., Rosania, G.R., Ahn, Y.H., and Chang, Y.T. (2006). RNA-selective, live cell imaging probes for studying nuclear structure and function. Chem. Biol. 13, 615-623.

Li, X.J., Zhang, X., Johnson, M.A., Wang, Z.B., Lavaute, T., and Zhang, S.C. (2009). Coordination of sonic hedgehog and Wnt signaling determines ventral and dorsal telencephalic neuron types from human embryonic stem cells. Development 136, 4055-4063.

Li, Y.X., Xu, Y., Ju, D., Lester, H.A., Davidson, N., and Schuman, E.M. (1998). Expression of a dominant negative TrkB receptor, T1, reveals a requirement for presynaptic signaling in BDNF-induced synaptic potentiation in cultured hippocampal neurons. Proc. Natl. Acad. Sci. U. S. A. 95, 10884-10889.

Loh, Y.E., Koemeter-Cox, A., Finelli, M.J., Shen, L., Friedel, R.H., and Zou, H. (2017). Comprehensive mapping of 5-hydroxymethylcytosine epigenetic dynamics in axon regeneration. Epigenetics 12, 77-92.

Lu, J., Zhong, X., Liu, H., Hao, L., Huang, C.T., Sherafat, M.A., Jones, J., Ayala, M., Li, L., and Zhang, S.C. (2016). Generation of serotonin neurons from human pluripotent stem cells. Nat. Biotechnol. 34, 89-94.

Lucido, A.L., Suarez Sanchez, F., Thostrup, P., Kwiatkowski, A.V., Leal-Ortiz, S., Gopalakrishnan, G., Liazoghli, D., Belkaid, W., Lennox, R.B., Grutter, P., Garner, C.C., and Colman, D.R. (2009). Rapid assembly of functional presynaptic boutons triggered by adhesive contacts. J. Neurosci. 29, 12449-12466.

Lunn, E.R., Perry, V.H., Brown, M.C., Rosen, H., and Gordon, S. (1989). Absence of Wallerian Degeneration does not Hinder Regeneration in Peripheral Nerve. Eur. J. Neurosci. 1, 27-33.

Lyles, V., Zhao, Y., and Martin, K.C. (2006). Synapse formation and mRNA localization in cultured Aplysia neurons. Neuron 49, 349-356.

Mair, N., Haller, T., and Dietl, P. (1999). Exocytosis in alveolar type II cells revealed by cell capacitance and fluorescence measurements. Am. J. Physiol. 276, L376-82.

Meiri, N., and Rosenblum, K. (1998). Lateral ventricle injection of the protein synthesis inhibitor anisomycin impairs long-term memory in a spatial memory task. Brain Res. 789, 48-55.

Merianda, T.T., Coleman, J., Kim, H.H., Kumar Sahoo, P., Gomes, C., Brito-Vargas, P., Rauvala, H., Blesch, A., Yoo, S., and Twiss, J.L. (2015). Axonal amphoterin mRNA is regulated by translational control and enhances axon outgrowth. J. Neurosci. 35, 5693-5706.

Merianda, T.T., Lin, A.C., Lam, J.S., Vuppalanchi, D., Willis, D.E., Karin, N., Holt, C.E., and Twiss, J.L. (2009). A functional equivalent of endoplasmic reticulum and Golgi in axons for secretion of locally synthesized proteins. Mol. Cell. Neurosci. 40, 128-142.

Merianda, T.T., and Twiss, J.L. (2013). Peripheral nerve axons contain machinery for co-translational secretion of axonally-generated proteins. Neurosci. Bull. 29, 493-500.

Michaelevski, I., Medzihradszky, K.F., Lynn, A., Burlingame, A.L., and Fainzilber, M. (2010). Axonal transport proteomics reveals mobilization of translation machinery to the lesion site in injured sciatic nerve. Mol. Cell. Proteomics 9, 976-987.

Miller, J.D., Ganat, Y.M., Kishinevsky, S., Bowman, R.L., Liu, B., Tu, E.Y., Mandal, P.K., Vera, E., Shim, J.W., Kriks, S.*, et al.* (2013). Human iPSC-based modeling of late-onset disease via progerin-induced aging. Cell. Stem Cell. 13, 691-705.

Minichiello, L., Calella, A.M., Medina, D.L., Bonhoeffer, T., Klein, R., and Korte, M. (2002). Mechanism of TrkB-mediated hippocampal long-term potentiation. Neuron 36, 121-137.

Minichiello, L., Korte, M., Wolfer, D., Kuhn, R., Unsicker, K., Cestari, V., Rossi-Arnaud, C., Lipp, H.P., Bonhoeffer, T., and Klein, R. (1999). Essential role for TrkB receptors in hippocampus-mediated learning. Neuron 24, 401-414.

Minis, A., Dahary, D., Manor, O., Leshkowitz, D., Pilpel, Y., and Yaron, A. (2014). Subcellular transcriptomics-dissection of the mRNA composition in the axonal compartment of sensory neurons. Dev. Neurobiol. 74, 365-381.

Moretti, F., Rolando, C., Winker, M., Ivanek, R., Rodriguez, J., Von Kriegsheim, A., Taylor, V., Bustin, M., and Pertz, O. (2015). Growth Cone Localization of the mRNA Encoding the Chromatin Regulator HMGN5 Modulates Neurite Outgrowth. Mol. Cell. Biol. 35, 2035-2050.

Murthy, V.N., and Stevens, C.F. (1998). Synaptic vesicles retain their identity through the endocytic cycle. Nature 392, 497-501.

Nakatomi, H., Kuriu, T., Okabe, S., Yamamoto, S., Hatano, O., Kawahara, N., Tamura, A., Kirino, T., and Nakafuku, M. (2002). Regeneration of hippocampal pyramidal neurons after ischemic brain injury by recruitment of endogenous neural progenitors. Cell 110, 429-441.

Natera-Naranjo, O., Aschrafi, A., Gioio, A.E., and Kaplan, B.B. (2010). Identification and quantitative analyses of microRNAs located in the distal axons of sympathetic neurons. RNA 16, 1516-1529.

Niedringhaus, M., Dumitru, R., Mabb, A.M., Wang, Y., Philpot, B.D., Allbritton, N.L., and Taylor, A.M. (2015). Transferable neuronal mini-cultures to accelerate screening in primary and induced pluripotent stem cell-derived neurons. Sci. Rep. 5, 8353.

Nudo, R.J. (2013). Recovery after brain injury: mechanisms and principles. Front. Hum. Neurosci. 7, 887.

Nudo, R.J., and Milliken, G.W. (1996). Reorganization of movement representations in primary motor cortex following focal ischemic infarcts in adult squirrel monkeys. J. Neurophysiol. 75, 2144-2149.

Oudega, M., and Perez, M.A. (2012). Corticospinal reorganization after spinal cord injury. J. Physiol. 590, 3647-3663.

Patel, A.K., Park, K.K., and Hackam, A.S. (2017). Wnt signaling promotes axonal regeneration following optic nerve injury in the mouse. Neuroscience 343, 372-383.

Patterson, S.L., Abel, T., Deuel, T.A., Martin, K.C., Rose, J.C., and Kandel, E.R. (1996). Recombinant BDNF rescues deficits in basal synaptic transmission and hippocampal LTP in BDNF knockout mice. Neuron 16, 1137-1145.

Perlson, E., Hanz, S., Ben-Yaakov, K., Segal-Ruder, Y., Seger, R., and Fainzilber, M. (2005). Vimentin-dependent spatial translocation of an activated MAP kinase in injured nerve. Neuron 45, 715-726.

Perry, R.B., Doron-Mandel, E., Iavnilovitch, E., Rishal, I., Dagan, S.Y., Tsoory, M., Coppola, G., McDonald, M.K., Gomes, C., Geschwind, D.H., *et al.* (2012). Subcellular knockout of importin beta1 perturbs axonal retrograde signaling. Neuron 75, 294-305.

Preibisch, S., Saalfeld, S., and Tomancak, P. (2009). Globally optimal stitching of tiled 3D microscopic image acquisitions. Bioinformatics 25, 1463-1465.

Rea, R., Li, J., Dharia, A., Levitan, E.S., Sterling, P., and Kramer, R.H. (2004). Streamlined synaptic vesicle cycle in cone photoreceptor terminals. Neuron 41, 755-766.

Reddington, A.E., Rosser, A.E., and Dunnett, S.B. (2014). Differentiation of pluripotent stem cells into striatal projection neurons: a pure MSN fate may not be sufficient. Front. Cell. Neurosci. 8, 398.

Rezaul, K., Wu, L., Mayya, V., Hwang, S.I., and Han, D. (2005). A systematic characterization of mitochondrial proteome from human T leukemia cells. Mol. Cell. Proteomics 4, 169-181.

Rishal, I., and Fainzilber, M. (2014). Axon-soma communication in neuronal injury. Nat. Rev. Neurosci. 15, 32-42.

Sachdeva, R., Farrell, K., McMullen, M.K., Twiss, J.L., and Houle, J.D. (2016). Dynamic Changes in Local Protein Synthetic Machinery in Regenerating Central Nervous System Axons after Spinal Cord Injury. Neural Plast. 2016, 4087254.

Sagal, J., Zhan, X., Xu, J., Tilghman, J., Karuppagounder, S.S., Chen, L., Dawson, V.L., Dawson, T.M., Laterra, J., and Ying, M. (2014). Proneural transcription factor Atoh1 drives highly efficient differentiation of human pluripotent stem cells into dopaminergic neurons. Stem Cells Transl. Med. 3, 888-898.

Sanders, L.H., Paul, K.C., Howlett, E.H., Lawal, H., Boppana, S., Bronstein, J.M., Ritz, B., and Greenamyre, J.T. (2017). Base excision repair variants and pesticide exposure increase Parkinson's disease risk. Toxicol. Sci.

Sanz, E., Yang, L., Su, T., Morris, D.R., McKnight, G.S., and Amieux, P.S. (2009). Cell-type-specific isolation of ribosome-associated mRNA from complex tissues. Proc. Natl. Acad. Sci. U. S. A. 106, 13939-13944.

Schoch, S., Cibelli, G., and Thiel, G. (1996). Neuron-specific gene expression of synapsin I. Major role of a negative regulatory mechanism. J. Biol. Chem. 271, 3317-3323.

Searle, A.G. (1952). A lethal allele of dilute in the house mouse. Heredity 6, 395-401.

Seo, J., Giusti-Rodriguez, P., Zhou, Y., Rudenko, A., Cho, S., Ota, K.T., Park, C., Patzke, H., Madabhushi, R., Pan, L.*, et al.* (2014). Activity-dependent p25 generation regulates synaptic plasticity and Abeta-induced cognitive impairment. Cell 157, 486-498.

Sheng, Y., Zhang, L., Su, S.C., Tsai, L.H., and Julius Zhu, J. (2016). Cdk5 is a New Rapid Synaptic Homeostasis Regulator Capable of Initiating the Early Alzheimer-Like Pathology. Cereb. Cortex 26, 2937-2951.

Shigeoka, T., Jung, H., Jung, J., Turner-Bridger, B., Ohk, J., Lin, J.Q., Amieux, P.S., and Holt, C.E. (2016). Dynamic Axonal Translation in Developing and Mature Visual Circuits. Cell 166, 181-192.

Shirao, T., and Gonzalez-Billault, C. (2013). Actin filaments and microtubules in dendritic spines. J. Neurochem. 126, 155-164.

Singer, M., and Green, M.R. (1968). Autoradiographic studies of uridine incorporation in peripheral nerve of the newt, Triturus. J. Morphol. 124, 321-344.

Sotelo, J.R., Canclini, L., Kun, A., Sotelo-Silveira, J.R., Xu, L., Wallrabe, H., Calliari, A., Rosso, G., Cal, K., and Mercer, J.A. (2013). Myosin-Va-dependent cell-to-cell transfer of RNA from Schwann cells to axons. PLoS One 8, e61905.

Stein, J.L., de la Torre-Ubieta, L., Tian, Y., Parikshak, N.N., Hernandez, I.A., Marchetto, M.C., Baker, D.K., Lu, D., Hinman, C.R., Lowe, J.K.*, et al.* (2014). A quantitative framework to evaluate modeling of cortical development by neural stem cells. Neuron 83, 69-86.

Stella, N. (2009). Endocannabinoid signaling in microglial cells. Neuropharmacology 56 Suppl 1, 244-253.

Takechi, U., Matsunaga, K., Nakanishi, R., Yamanaga, H., Murayama, N., Mafune, K., and Tsuji, S. (2014). Longitudinal changes of motor cortical excitability and transcallosal inhibition after subcortical stroke. Clin. Neurophysiol. 125, 2055-2069.

Taylor, A.M., Berchtold, N.C., Perreau, V.M., Tu, C.H., Li Jeon, N., and Cotman, C.W. (2009). Axonal mRNA in uninjured and regenerating cortical mammalian axons. J. Neurosci. 29, 4697-4707.

Taylor, A.M., Blurton-Jones, M., Rhee, S.W., Cribbs, D.H., Cotman, C.W., and Jeon, N.L. (2005). A microfluidic culture platform for CNS axonal injury, regeneration and transport. Nat. Methods 2, 599-605.

Taylor, A.M., Rhee, S.W., Tu, C.H., Cribbs, D.H., Cotman, C.W., and Jeon, N.L. (2003). Microfluidic Multicompartment Device for Neuroscience Research. Langmuir 19, 1551-1556.

Taylor, A.M., Wu, J., Tai, H.C., and Schuman, E.M. (2013). Axonal translation of beta-catenin regulates synaptic vesicle dynamics. J. Neurosci. 33, 5584-5589.

Tcherkezian, J., Brittis, P.A., Thomas, F., Roux, P.P., and Flanagan, J.G. (2010). Transmembrane receptor DCC associates with protein synthesis machinery and regulates translation. Cell 141, 632-644.

Todd, K.J., Serrano, A., Lacaille, J.C., and Robitaille, R. (2006). Glial cells in synaptic plasticity. J. Physiol. Paris 99, 75-83.

Twiss, J.L., Smith, D.S., Chang, B., and Shooter, E.M. (2000). Translational control of ribosomal protein L4 mRNA is required for rapid neurite regeneration. Neurobiol. Dis. 7, 416-428.

Urban, E.T.,3rd, Bury, S.D., Barbay, H.S., Guggenmos, D.J., Dong, Y., and Nudo, R.J. (2012). Gene expression changes of interconnected spared cortical neurons 7 days after ischemic infarct of the primary motor cortex in the rat. Mol. Cell. Biochem. 369, 267-286.

van de Leemput, J., Boles, N.C., Kiehl, T.R., Corneo, B., Lederman, P., Menon, V., Lee, C., Martinez, R.A., Levi, B.P., Thompson, C.L.*, et al.* (2014). CORTECON: a temporal transcriptome analysis of in vitro human cerebral cortex development from human embryonic stem cells. Neuron 83, 51-68.

Venkatesh, I., and Blackmore, M.G. (2016). Selecting optimal combinations of transcription factors to promote axon regeneration: Why mechanisms matter. Neurosci. Lett.

Vicario-Abejon, C. (2004). Long-term culture of hippocampal neurons. Curr. Protoc. Neurosci. Chapter 3, Unit 3.2.

Vicario-Abejon, C., Collin, C., McKay, R.D., and Segal, M. (1998). Neurotrophins induce formation of functional excitatory and inhibitory synapses between cultured hippocampal neurons. J. Neurosci. 18, 7256-7271.

Villegas, R., Martinez, N.W., Lillo, J., Pihan, P., Hernandez, D., Twiss, J.L., and Court, F.A. (2014). Calcium release from intra-axonal endoplasmic reticulum leads to axon degeneration through mitochondrial dysfunction. J. Neurosci. 34, 7179-7189.

von Jonquieres, G., Frohlich, D., Klugmann, C.B., Wen, X., Harasta, A.E., Ramkumar, R., Spencer, Z.H., Housley, G.D., and Klugmann, M. (2016). Recombinant Human Myelin-Associated Glycoprotein Promoter Drives Selective AAV-Mediated Transgene Expression in Oligodendrocytes. Front. Mol. Neurosci. 9, 13.

Wang, L.F., Huang, S.B., Zhao, H.D., Liu, C.J., Yao, L., and Shen, Y.Q. (2017). Activating transcription factor 3 promotes spinal cord regeneration of adult zebrafish. Biochem. Biophys. Res. Commun.

Wang, S.H., Ostlund, S.B., Nader, K., and Balleine, B.W. (2005). Consolidation and reconsolidation of incentive learning in the amygdala. J. Neurosci. 25, 830-835.

Wang, W., van Niekerk, E., Willis, D.E., and Twiss, J.L. (2007). RNA transport and localized protein synthesis in neurological disorders and neural repair. Dev. Neurobiol. 67, 1166-1182.

Welshhans, K., and Bassell, G.J. (2011). Netrin-1-induced local beta-actin synthesis and growth cone guidance requires zipcode binding protein 1. J. Neurosci. 31, 9800-9813.

Weng, Y.L., An, R., Cassin, J., Joseph, J., Mi, R., Wang, C., Zhong, C., Jin, S.G., Pfeifer, G.P., Bellacosa, A.*, et al.* (2017). An Intrinsic Epigenetic Barrier for Functional Axon Regeneration. Neuron 94, 337-346.e6.

Wickersham, I.R., Finke, S., Conzelmann, K.K., and Callaway, E.M. (2007a). Retrograde neuronal tracing with a deletion-mutant rabies virus. Nat. Methods 4, 47-49.

Wickersham, I.R., Lyon, D.C., Barnard, R.J., Mori, T., Finke, S., Conzelmann, K.K., Young, J.A., and Callaway, E.M. (2007b). Monosynaptic restriction of transsynaptic tracing from single, genetically targeted neurons. Neuron 53, 639-647.

Wiederkehr, A., Avaro, S., Prescianotto-Baschong, C., Haguenauer-Tsapis, R., and Riezman, H. (2000). The F-box protein Rcy1p is involved in endocytic membrane traffic and recycling out of an early endosome in Saccharomyces cerevisiae. J. Cell Biol. 149, 397-410.

Will, B., Galani, R., Kelche, C., and Rosenzweig, M.R. (2004). Recovery from brain injury in animals: relative efficacy of environmental enrichment, physical exercise or formal training (1990-2002). Prog. Neurobiol. 72, 167-182.

Willis, D.E., van Niekerk, E.A., Sasaki, Y., Mesngon, M., Merianda, T.T., Williams, G.G., Kendall, M., Smith, D.S., Bassell, G.J., and Twiss, J.L. (2007). Extracellular stimuli specifically regulate localized levels of individual neuronal mRNAs. J. Cell Biol. 178, 965-980.

Wolf, M., Zimmermann, A.M., Gorlich, A., Gurniak, C.B., Sassoe-Pognetto, M., Friauf, E., Witke, W., and Rust, M.B. (2015). ADF/Cofilin Controls Synaptic Actin Dynamics and Regulates Synaptic Vesicle Mobilization and Exocytosis. Cereb. Cortex 25, 2863-2875.

Wu, K.Y., Hengst, U., Cox, L.J., Macosko, E.Z., Jeromin, A., Urquhart, E.R., and Jaffrey, S.R. (2005). Local translation of RhoA regulates growth cone collapse. Nature 436, 1020-1024.

Xu, B., Gottschalk, W., Chow, A., Wilson, R.I., Schnell, E., Zang, K., Wang, D., Nicoll, R.A., Lu, B., and Reichardt, L.F. (2000). The role of brain-derived neurotrophic factor receptors in the mature hippocampus: modulation of long-term potentiation through a presynaptic mechanism involving TrkB. J. Neurosci. 20, 6888-6897.

Xu, W., and Sudhof, T.C. (2013). A neural circuit for memory specificity and generalization. Science 339, 1290-1295.

Yao, J., Sasaki, Y., Wen, Z., Bassell, G.J., and Zheng, J.Q. (2006). An essential role for beta-actin mRNA localization and translation in Ca2+-dependent growth cone guidance. Nat. Neurosci. 9, 1265-1273.

Yin, H.H., Davis, M.I., Ronesi, J.A., and Lovinger, D.M. (2006). The role of protein synthesis in striatal long-term depression. J. Neurosci. 26, 11811-11820.

Yoon, B.C., Jung, H., Dwivedy, A., O'Hare, C.M., Zivraj, K.H., and Holt, C.E. (2012). Local translation of extranuclear lamin B promotes axon maintenance. Cell 148, 752-764.

Younts, T.J., Monday, H.R., Dudok, B., Klein, M.E., Jordan, B.A., Katona, I., and Castillo, P.E. (2016). Presynaptic Protein Synthesis Is Required for Long-Term Plasticity of GABA Release. Neuron 92, 479-492.

Yuan, S., and Burrell, B.D. (2013). Endocannabinoid-dependent long-term depression in a nociceptive synapse requires coordinated presynaptic and postsynaptic transcription and translation. J. Neurosci. 33, 4349-4358.

Yudin, D., Hanz, S., Yoo, S., Iavnilovitch, E., Willis, D., Gradus, T., Vuppalanchi, D., Segal-Ruder, Y., Ben-Yaakov, K., Hieda, M.*, et al.* (2008). Localized regulation of axonal RanGTPase controls retrograde injury signaling in peripheral nerve. Neuron 59, 241-252.

Zakharenko, S.S., Patterson, S.L., Dragatsis, I., Zeitlin, S.O., Siegelbaum, S.A., Kandel, E.R., and Morozov, A. (2003). Presynaptic BDNF required for a presynaptic but not postsynaptic component of LTP at hippocampal CA1-CA3 synapses. Neuron 39, 975-990.

Zeng, H., Guo, M., Martins-Taylor, K., Wang, X., Zhang, Z., Park, J.W., Zhan, S., Kronenberg, M.S., Lichtler, A., Liu, H.X.*, et al.* (2010). Specification of region-specific neurons including forebrain glutamatergic neurons from human induced pluripotent stem cells. PLoS One 5, e11853.

Zheng, J.Q., Kelly, T.K., Chang, B., Ryazantsev, S., Rajasekaran, A.K., Martin, K.C., and Twiss, J.L. (2001). A functional role for intra-axonal protein synthesis during axonal regeneration from adult sensory neurons. J. Neurosci. 21, 9291-9303.

Zivraj, K.H., Tung, Y.C., Piper, M., Gumy, L., Fawcett, J.W., Yeo, G.S., and Holt, C.E. (2010). Subcellular profiling reveals distinct and developmentally regulated repertoire of growth cone mRNAs. J. Neurosci. 30, 15464-15478.

Zuccotti, P., and Modelska, A. (2016). Studying the Translatome with Polysome Profiling. Methods Mol. Biol. 1358, 59-69.

Zweifel, L.S., Kuruvilla, R., and Ginty, D.D. (2005). Functions and mechanisms of retrograde neurotrophin signalling. Nat. Rev. Neurosci. 6, 615-625.